Multiply-and-Forward and Phase-Forward Two Way Relays

by

Huai Tan

M.Eng., National University of Singapore, 2002

B.Sc. (Hons.), National University of Singapore, 2000

Thesis Submitted in Partial Fulfillment
of the Requirements for the Degree of

Doctor of Philosophy

in the
School of Engineering Science
Faculty of Applied Sciences

SIMON FRASER UNIVERSITY
Spring 2015

APPROVAL

Name: Huai Tan

Degree: Doctor of Philosophy

Title: Multiply-and-Forward and Phase-Forward Two Way Relays

Examining Committee: **Chair**: Dr. Rodney Vaughan, Professor

---

Dr. Paul Ho,
Professor, Senior Supervisor

Dr. Jie Liang,
Associate Professor, Supervisor

Dr. Shawn Stapleton,
Professor, SFU Examiner

Dr. Abu Sesay,
Professor, External Examiner, University of Calgary

Date Approved: April 16, 2015

Partial Copyright Licence

Abstract

Relay/cooperative communication has been an active area of research in the past few years. In most of the investigations, the amplifiers used in the system are assumed to be linear. In this thesis, we first investigate the effect of amplifier non-linearity has on the bit-error-rate (BER) of a two-way cooperative communication system that employs linear modulation and amplify-and-forward (AF). It was found that irreducible error floor arises, caused by the inter-modulation effect with non-linear amplification and the subsequent imperfect self-interference cancellation. As a result of this finding, we propose two signal forwarding techniques that offer MPSK modulations immunity against non-linear amplifier distortion. The first technique, termed *multiply-and-forward* (MF), scales the product of the two received signals at the relay for downlink transmission. The second technique, termed *phase-forward* (PF), has a similar product structure, except that the amplitude information in the product signal is discarded. We show that both schemes do not exhibit the irreducible error characteristic found in AF when the amplifier is non-linear. The PF scheme, in particular, can attain a BER lower than that of AF even when the amplifier is linear. The conclusion is reached that MF and PF are suitable signal forwarding strategies for two-way cooperative communication in the presence of amplifier non-linearity, with PF being the more robust of the two.

Due to the multiplicative nature of the MF and PF, self-informantion cancellation becomes simple when differential modulation is used in the two-way cooperative relay system. With differential modulation, there is no explicit channel state information (CSI) estimation and and this leads to a saving of pilot symbol overhead. In the second and third parts of this thesis proposal, we extend the MF and PF protocols to DPSK and CPFSK modulations. Specifically, we demonstrate that the proposed forwarding methods has low computational complexity at the relay as well as simple self-information cancellation at the receiver in the last phase of the cooperative communication.

Based on the results we have obtained on the new relay forwarding protocols, we can see that the MF and PF are two promising forwarding techniques and they worth further study and refinement.

Acknowledgments

I am indebted to many for their help and support during my PhD program at SFU. It is my honor to take this opportunity to express my gratitude.

First and foremost, I am deeply thankful to my senior supervisor Prof. Paul Ho, who admitted me into the PhD program that I had longed for. It is not easy to express my gratitude towards him in a few words. He has consistently devoted excellence mentoring, endless encouragement, great patience and countless support during my entire graduate studies, while at the same time giving me space and freedom in my research. He has continuously supported my graduate study financially and has provided opportunities to exchange ideas with the research community in academic conferences. Prof. Paul leads by inspiration. He has not only inspired new ideas in my mind, but has also inspired me to see and think in the big picture. I will have lifetime benefits by learning from him.

I would like to thank Prof. Jie Liang for being my supervisor and providing valuable comments on my research work. He taught me multirate signal processing, and I was impressed by his intuitive interpretation on matrix maneuvers. I was even more so by how he can explain a complex subject in a clear and simple manner. His class has opened a door to extended my knowledge base to advanced signal processing. I am also grateful to his help on my future career.

I would like to thank my internal examiner Prof. Shawn Stapleton for accepting to take part in my examining committee. His constructive comments and questions has improved the contents of my thesis and has helped me to connect my research to practice. I am also grateful to his warm encouragement that gave me confidence.

I would like to express my sincere appreciation towards my external examiner Prof. Abu Sesay for accepting to take part in my examining committee and taking the burden of traveling to SFU from Calgary just to attend my thesis defense despite his tight schedule at

University of Calgary. His insightful questions and comments has contributed to the depth and quality of my thesis.

I am truly grateful to Prof. Rodney Vaughan who has kindly served as the chair of my examining committee during his busy spring term. I appreciate his valuable contribution on my thesis and his advice on career development.

It has been my privilege to know and work with a highly selected group of students from the Sierra Wireless Mobile Communications Laboratory at SFU. I would like to thank my fellow labmates and engineering science classmates for their warmth, discussions, support and friendship, in particular, Qi Yang, Phoenix Yuan, Rio Li, Ying Chen, Dr. Jane Xing Yun, Dr. Jinyun Ren, Dr. Mehdi Seyfi, Dr. Maryam Dehghani Estarki, Dr. Milad Amir Toutounchian, Dr. Seyed Alireza Banani, and Dr. Yu Gao.

I also want to express my gratitude towards the ENSC general office staff, especially Raj and Pilar. They have always responded to my requests promptly and have provided many administrative supports. I would like to thank Bryan from the computer helpdesk team of Faculty of Applied Sciences for his timely support that resolves my computer issues.

Finally, I would like to thank my parents and my wife Qi Luo for their love, encouragement and care that have accompanied me along the way.

List of Symbols

$\mathrm{G}_{p,q}^{m,n}(\cdot)$	Meijer G function
$A(\cdot)$	AM-AM distortion of an amplifier
B	Bandwidth of a signal
D	Decision variable
G	Relay gain
$J_v(\cdot)$	Bessels's function of the first kind of order v
$K_v(\cdot)$	Modified Bessels's function of the second kind of order v
N_0	Additive white Gaussian noise power spectral density
P_e	Error probability
$Pr\{A\}$	Probability of event A
R	Relay terminal
S_i	Source node i
T	Symbol duration
X	Represents a random variable
$\Phi(\cdot)$	AM-PM distortion of an amplifier
$\Phi_X(\cdot)$	Characteristic function of random variable X
$\Re(\,\cdot\,)$	Real operator
$\bar{\gamma}_{ij}$	Average SNR on the link from node i to j
$\mathbb{E}[\,\cdot\,]$	Expectation operator
γ_{ij}	Instantaneous SNR on thelink from node i to j
$\hat{s}$	Detected symbol
$\mathcal{CN}(0,\sigma^2)$	Circularly symmetric complex Gaussian with zero mean and variance σ^2
σ_{ij}^2	The variance of the fading gain g_{ij}
$\tilde{s}_R$	Distorted transmitted relay signal

$\tilde{y}$	Received signal after self-interference cancellation
$\mathbf{I}$	Identity matrix
$\mathbf{X}$	Represents a matrix
$\mathbf{x}$	Represents a vector
$\{\cdot\}^*$	Complex conjungate
$\{\cdot\}^H$	Hermitian transpose
$\{\cdot\}^T$	Transpose
d	Data symbol of DPSK or CPFSK modulation
f_d	Maximum Doppler frequency
g_{ij}	Fading channel gain on the link from node i to j
h	Modulation index
n_{ij}	Noise at the receiver on the link from node i to j
$p(x)$	Probability density function of random variable X
s_i	Transmitted symbol from node i
$x(t)$	Continuous time signal at time instant t
$x[k]$	Discrete time signal at time index k
y_{ij}	Received signal on the link from node i to j
$\lvert\cdot\rvert$	Absolute value
$\lvert\lvert\cdot\rvert\rvert$	Determinant of a matrix

List of Acronyms

ADC	Analog to Digital Converter
AF	Amplify-and-Forward
AGC	Automatic Gain Control
AM-AM	Amplitude to amplitude distortion
AM-PM	Amplitude to phase distortion
ANC	Analog Network Coding
AoF	Amount of Fading
AWGN	Additive White Gaussian Noise
BER	Bit Error Rate
CCDF	Complementary Cumulative Density Function
CF	Characteristic Function
CMAD	Complex Multiply and Add
CPFSK	Continuous Phase Frequency Shift Keying
CRC	Cyclic Redundancy Code
CSI	Channel State Information
dB	decibel
DDSTC	Differential Distributed Space Time Coding
DF	Decode-and-Forward
DNF	Denoise-and-Forward
DPF	Decode-and-Phase-Forward
DPSK	Differential Phase Shift Keying
DSF	Decode-Superposition-Forward
DSTC	Distributed Space Time Coding
DXF	Decode-XOR-Forward

IBO	Input Back-off
LPA	Linear Power Amplifier
LPF	Low Pass Filter
MF	Multiply-and-Forward
MGF	Moment Generating Function
MIMO	Multiple Input Multiple Output
ML	Maximum Likelihood
MRC	Maximal Ratio Combining
MSK	Mimimum Shift Keying
NLPA	Non-linear Power Amplifier
OFDM	Orthogonal Frequency Division Modulation
PAPR	Peak to Average Power Ratio
PDF	Probability Density Function
PF	Phase-Forward
PSD	Power Spectrum Density
PSK	Phase Shift Keying
QAM	Quadrature Amplitude Modulation
RV	Random Variable
SNR	Signal to Noise Ratio
SQNR	Signal to Quantization Noise Ratio
SQRC	Square Root Raised Cosine

Contents

List of Tables

List of Figures

Chapter 1

Thesis Overview

Cooperative transmission, a distributed signaling technique built upon relay communication, has been recognized as an effective way to increase network coverage and reduce outage. Two-way relaying techniques have gained much attention in recent years. A common signal forwarding scheme proposed in these two-way relaying protocols is amplify-and-forward (AF), which can be considered as analog network coding (ANC), whereby the signal sent by the relay is a a linear combination of the signals it receives from the two sources. In comparison to the decode-and-forward (DF) method, the AF relay has cost effective implementation complexity by bypassing the signal regeneration process.

1.1 Literature Review

Cooperative transmission [1, 2, 3, 4], which is based on relay forwarding [5], is a cost effective way to combat fading because it creates a virtual multiple-input-multiple-output (MIMO) communication channel without resorting to mounting antenna arrays at individual nodes. In addition to spatial diversity from cooperative relaying [3], the adoption of relays can also help to improve network coverage [6, 7], e.g. providing coverage at the edge of a cell where a coverage hole often presents. Active development has been carried out to adopt cooperative relays in the wireless communications industry. For instance, the third generation partnership project (3GPP) has included relaying technologies in its long term evolution (LTE) standardization [8, 9].

Earlier researches on cooperative transmission focus on one-way relaying with AF and DF protocols [4, 10, 11]. Orthogonal time-slots are employed by the source and the relay

to allow the destination node to obtain independent faded copies of the same message for combining purpose [4, 10]. The creation of these orthogonal time slots reduces the throughput of the system [12]. For example, the so-called Protocol II in [2] has a throughput of 1/N message/slot, where N is the number of relays in the system.

To improve the transmission efficiency of cooperative communication, two-way relaying is proposed [13, 14, 15, 16, 17]. For example in [17], a two-way relay network where two users exchange information with the assistance of an intermediate relay node was considered. Commonly adopted two-way relay protocols include two-phase two-way relay and three-phase two-way relay are considered. Both schemes offer an improved transmission efficiency over their one-way relay counterpart. The two-phase two-way relay system starts with a multiple access phase, where two user terminals transmit simultaneously to the relay, and then followed by a broadcast phase, where the relay broadcasts a processed signal back to both the user terminals. The two-phase two-way relay doubles the transmission efficiency compared to that of one-way relaying. On the other hand, in a three-phase two-way relay system, the aforementioned multiple access phase is decomposed into two phases, where each of the user terminal transmits at a time. This approach allows the reception of direct path signals for half duplex transceivers. It thus can provide a diversity effect and leads to a better bit-error-rate (BER) performance.

The relay forwarding schemes can be broadly categorized into regenerative and non-regenerative relays. A regenerative relay first demodulates the received signals and then regenerates the transmitted relay signal based on the decision made. From an implementation point of view, the signal transmitted by the regenerative relay shares the same power characteristics and can thus be amplified using the same type of power amplifiers used at source terminals. On the other hand, a non-regenerative relay does not involve decision making and the relay combines the received signals according to analog network code. Since the relay eliminates decision making, the computation complexity is much simpler than the regenerative relays. However, non-regenerative relay techniques such as AF may experience very large amplitude fluctuation. The implication is that AF relay, which has limited instantaneous power in practice, either the highly dynamic transmitted signal will experience non-linear signal distortion, or a linear power amplifier with wide enough linear region must be used at the relay. The former situation can lead to system performance degradation. The latter case, though avoids the non-linearity, will add hardware cost on

the relay and decrease the power efficiency of the relay. Hence the design of relay forwarding techniques should take into consideration different aspects of implementation to achieve a good balance between implementation complexity, performance and cost. We want the relay to have simple computation but at the same time we want the relay can reliably work as it is intended. Further, the system performance, especially the BER performance, should not be compromised.

1.2 Objective

The main objective of this thesis is to develop cooperative relay techniques capable of coping with power amplifier non-linearity that exists in practical power amplifiers. At the same time, we aim to design protocols that have low computational complexity at both the relay and user terminals. The new protocols should also demonstrate good performance compared to the AF cooperative relay.

1.3 Organization and Contributions

In this thesis, we propose multiplication based non-regenerative signal forwarding schemes that share similar implementation complexity as AF but offers immunity against non-linear amplifier distortion at the relay.

In Chapter 2, two new forwarding schemes, i.e. MF and PF, are formulated around MPSK modulation. Based on our findings, the proposed relay protocols using MPSK modulation offer good resistance to power amplifier nonlinearity. The MF protocol shows little performance degradation when the relay power amplifier is limited by a maximum instantaneous power output. The PF protocol, sharing similar instantaneous power distribution as a PSK signal, can use the same type of the power amplifier as the user terminals. Further, the PF protocol exhibits better BER performance compared with AF relay, especially when the source to relay link quality improves. Analytical results are developed for the two proposed protocols, which include a unified BER lower bound for both the MF and AF relays and a lower bound for the PF relay. Furthermore, diversity order analysis is performed to show that both MF and PF relays can fully exploit the diversity order available to the system.

In Chapter 3, the MF protocol is extended to MDPSK modulation. In the two-way relay literature, differential modulation receives much less adoption compared to coherent modulation such as PSK and QAM. A major challenge is the difficulty in self-information cancellation because of the lack of accurate CSI at the receivers, especially when fading is not static. However, due to the multiplicative nature of the MF protocol, self-interference cancellation becomes straightforward for a two-way relay employing DPSK modulation. The performance of DPSK modulated MF three-phase two-way relay is studied analytically under static fading environment. Based on the analysis, we also demonstrate that full diversity order is achieved. The relay system is further verified via simulation under both static and time varying fading for both linear and non-linear power amplifiers. Similar to the PSK MF relay, the DPSK MF relay is insensitive to power amplifier nonlinearity.

In Chapter 4, we further apply the PF protocol to continuous phase frequency shift keying (CPFSK) and compared it against DF based forwarding strategies. For both forwarding protocols, the signals transmitted at the relay have a constant envelope, which allows the choice of highly power efficient non-linear amplifiers at the relay. Exact BER analysis of the protocols presented in this chapter are derived and verified via simulation. Results indicate that the PF relaying approach leads to a more reliable relaying system.

Finally, Chapter 5 summarizes the research finding on the proposed two-way relay forwarding protocols. We also layouts future research direction.

Chapter 2

Coherent Multiply-and-Forward and Phase-Forward

2.1 Introduction

Currently research on cooperative communication systems often assumes linear power amplifier at the relay. This assumption, especially for the non-regenerative relays [18, 19, 20], may require the power amplifier to be linear over a large range due to signal fluctuations. In practice though, most amplifiers used in wireless transmission are often non-linear (or only linear within a certain operating range), either because of cost consideration or because of a power-efficiency concern. The highly power-efficient Class C-type amplifiers is a very good example. When the amplifier is non-linear, one has to take into consideration the relay signal's peak power when evaluating the performance of the underlying cooperative communication system. This is particularly important for the AF protocol because the forwarded signal can vary over a wide range around its mean amplitude level, owing to the fading fluctuation in the source to relay links, which are also referred to as uplinks in this thesis. Current research work that involves power amplifier non-linearity has mainly layed on the one-way relay networks. In [21], the authors proposed a variable power scaling factor that can be used to limit the peak power of a one-way AF relay. Further studies on the distribution of the instantaneous power of the AF relay in [22, 23] reveals that even in the case of one-way relaying whereby the relay's received signal involves only one uplink fading process, the peak-to-average power ratio (PAPR) [24, 25] of an AF relay can be very large. Consequently, power amplifier non-linearity is a practical issue that AF relays have to face.

Effects of such non-linearity on the performance of relay networks are mostly carried out for one-way AF OFDM systems [26, 27, 28, 29]. There seems to be limited techniques available to cope with the high PAPR of the AF relay signals. In [30], a peak power efficient one-way relay using a hard limiter is proposed for punctured convolutional coded star-QAM. However, the adoption of channel coding reduces the transmission efficiency.

Currently, little attention has been paid to two-way cooperative communication systems that are resistant to power amplifier non-linearity. Similar to one-way relaying (if not worse), the performance of AF can be severely degraded in a two-way relaying system if the power amplifier at the relay is non-linear. This can be intuitively understood by considering the signal broadcasted by the relay is of the form $G \cdot (g_{1R}(t)s_1(t) + g_{2R}(t)s_2(t))$, where g_{1R} and g_{2R} denote the uplink channel gains, $s_1(t)$ and $s_2(t)$ the users' data signals, and G a fixed scaling factor. If this signal is transmitted through a non-linear power amplifier (NLPA), the received signal will comprise of a series of inter-modulation products. As a result, a source node will not be able to cancel out its own signal completely. The residual self-interference will lead to an irreducible error floor that cannot be lowered even with very large transmit power. In this chapter, we first propose a multiply-and-forward (MF) technique for two-way relaying that is insensitive to NLPA distortion when used with PSK modulations. While this technique can avoid an irreducible error floor when the amplifier at the relay is non-linear, its performance with a linear power amplifier (LPA) is slightly worse than AF. As such, we propose a second technique known as phase-forward (PF) [31] that can outperform both AF and MF irrespectively of the type of amplifiers. As the reader will discover, PF is essentially MF with self-induced hard-limiting. The technique was first considered for one-way cooperative communication as a mean to keep the signal forwarded by the relay constant envelope when the source itself employs constant envelope CPFSK modulation [31].

This chapter is organized as follows. We first review in Section 2.2 the basic signal structures of a two-way three-phase cooperative communication system that employs AF. The BER of this baseline system, with LPA and NLPA, is evaluated via simulation. The idea of MF is then introduced in Section 2.3 as a mean to alleviate the distortion introduced by a NLPA at the relay. We show that MF is superior to AF when the amplifier in non-linear. When the amplifier is linear though, MF suffers a degradation when compared to AF. This motivates us to introduce in Section 2.4 the idea of phase-fowrad (PF) as a technique

to achieve good performance in both cases of LPF and NLPA. The relationship between MF and PF is outlined in this section. Finally, a conclusion of this chapter is provided in Section 2.5.

2.2 AF in the Presence of Non-linear Amplifier Distortion

We consider two-way three-phase cooperative communication whereby two source nodes (or users), S_1 and S_2, exchange information with the help of a relay R; refer to Figure 2.1. We focus on three-phase cooperation because, as opposed to two-phase, it can provide a second-order diversity effect. All the nodes in the communication network in Figure 2.1 have single antenna and half duplex transceivers. The modulation format adopted by both users is coherent M-ary phase shift keying (MPSK). While we recognize this modulation format is not as power-efficient as its QAM counterpart when the amplifier is linear, we will demonstrate that MPSK, when used in conjunction with the proposed MF and PF relaying strategies, offers immunity towards non-linear amplifier distortion. In contrast, QAM with a dense constellation is almost unusable when the amplifier used in AF is non-linear. Finally, all the links in the system are assumed to exhibit Rayleigh flat fading and additive white Gaussian noise (AWGN) with power spectral density N_0. Note that throughout this thesis, the notation $\mathcal{CN}(0, \sigma^2)$ refers to a complex Gaussian random variable with zero mean and variance σ^2 in both its real and imaginary parts. All the fading and noise processes are assumed statistically independent. For simplicitly, perfect channel state information (CSI) is assumed available at the receiver for self-interference cancellation and data detection. Techniques for estimating the channel gains in cooperative/relay communication systems based on embedded pilot symbols can be found in [32, 33].

Our baseline system is one that employs AF at the relay. In addition to being one of the most frequently used benchmarks in the literature, AF has similar implementation complexity as the proposed MF and PF techniques (refer to Section 2.4.3) and all three techniques do not require intermediate decisions to be made at the relay. A decode-and-forward (DF) relay, on the other hand, makes intermediate decisions. This leads to an increased implementation complexity at the relay because channel estimation must be performed before data detection can take place. Furthermore, data detection is a form of quantization which may lead to a loss in performance when compared to AF. The user terminals in Figure 2.1

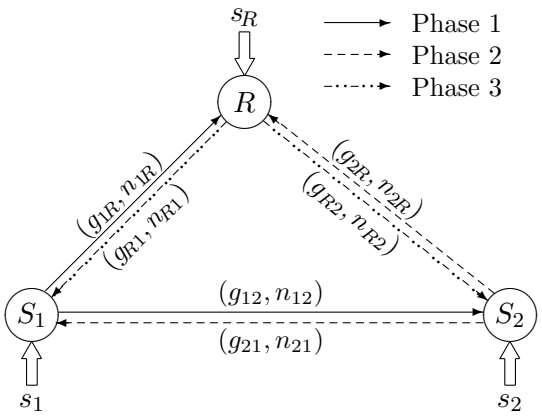

Figure 2.1: System model of the three phase two-way cooperative communication system.

transmit their complex MPSK symbols, s_i, $i \in \{1, 2\}$, in Phase 1 and 2 respectively, using a common square root raised cosine (SQRC) pulse shape. The data symbols have a mean square value of one and the SQRC pulse itself has unit energy. The transmitted uplink signals are subjected to fading and noise. The relay adds the two received uplink waveforms, scales the sum by a constant gain, amplifies and broadcasts the resultant signal back to the two users. The receiver of each user first filters its received signal using a matched filter and then samples the matched filter's output to generate the required decision statistics. Figure 2.2 (a) depicts the trasmitting and receiving operations in the relay to source path, or downlink, where $s_R(t)$ represents the forwarded signal, and $G(\cdot)$ represents the amplifier used at the relay. Because of the nature of AF, $s_R(t)$ is a superposition of symbol-spaced SQRC pulses, just like the source signals transmitted by the users. This structure is depicted on the left-hand side of the diagram with $s_R[k]$ being the equivalent discrete-time symbols.

2.2.1 Baseline System - AF with LPA at all the Nodes

When all the amplifiers in the system are linear, we can describe the operations in the entire AF system using an equivalent one-shot discrete-time model. This stems from the fact that the received downlink signal in AF is a superposition of SQRC pulses.

During the first phase of communication, the source node S_1 broadcasts its data symbol s_1 to both node S_2 and the relay R, where s_1 is a unit-amplitude MPSK symbol taken from

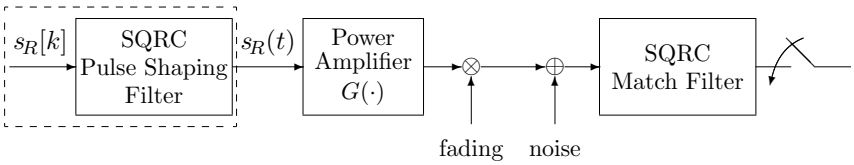

(a) Orignal downlink model.

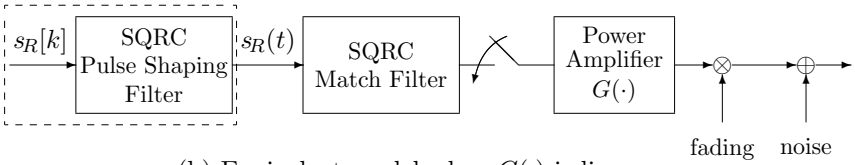

(b) Equivalent model when $G(\cdot)$ is linear

Figure 2.2: Downlink models with the forwarded signal described as a superposition of symbol-spaced SQRC pulses.

the set $X = \{e^{j\frac{2\pi(k-1)}{M}}\}_{k=1}^{M}$. The average power of the data symbols is defined as

$$P_s = \frac{1}{2}\mathbb{E}\big[|s_1|^2\big] = \frac{1}{2}, \tag{2.1}$$

where $\mathbb{E}[\,\cdot\,]$ is the expectation operator. Assuming the linear amplifier used at the source has a gain of 1, then the equivalent discrete-time received signals at R and S_2 are

$$y_{1R} = g_{1R}s_1 + n_{1R} \tag{2.2}$$

and

$$y_{12} = g_{12}s_1 + n_{12}, \tag{2.3}$$

where $n_{1R} = \mathcal{CN}(0, N_0)$ and $n_{12} = \mathcal{CN}(0, N_0)$ are complex AWGNs at R and S_2, $g_{1R} = \mathcal{CN}(0, \sigma_{1R}^2)$ and $g_{12} = \mathcal{CN}(0, \sigma_{12}^2)$ represent the Rayleigh fading in the $S_1 \to R$ and $S_1 \to S_2$ links, and $\bar{\gamma}_{1R} = \sigma_{1R}^2/N_0$ and $\bar{\gamma}_{12} = \sigma_{12}^2/N_0$ are the corresponding average link signal-to-noise ratios (SNRs).

Similarly, in the second phase of transmission, node S_2 broadcasts its data symbol s_2 to S_1 and R using a linear amplifier. The equivalent discrete-time received signals at R and S_1 are

$$y_{2R} = g_{2R}s_2 + n_{2R} \tag{2.4}$$

and

$$y_{21} = g_{21}s_2 + n_{21}, \tag{2.5}$$

where $n_{2R} = \mathcal{CN}(0, N_0)$ and $n_{21} = \mathcal{CN}(0, N_0)$ are complex AWGNs at R and S_1, $g_{2R} = \mathcal{CN}(0, \sigma_{2R}^2)$ and $g_{21} = \mathcal{CN}(0, \sigma_{21}^2)$ represent the Rayleigh fading in the $S_2 \to R$ and $S_2 \to S_1$ links, and $\bar{\gamma}_{2R} = \sigma_{2R}^2/N_0$ and $\bar{\gamma}_{21} = \sigma_{21}^2/N_0$ are the corresponding average link SNRs.

Upon receiving both y_{1R} and y_{2R}, an AF relay scales the sum of the two signals by a constant G_{AF} to form the forwarded symbol s_R in Phase 3 of the AF protocol:

$$s_R = G_{AF}(y_{1R} + y_{2R}) = |s_R|e^{j\theta_R}, \tag{2.6}$$

where $|s_R|$ and θ_R are the amplitude and phase of s_R, respectively. The scaling factor G_{AF} is chosen such that the average power of s_R is 1/2, the same as that of the source symbols; refer to (2.1). This requires

$$G_{AF} = \frac{1}{\sqrt{2\left(\bar{\gamma}_{1R} + \bar{\gamma}_{2R} + 2\right) N_0}}. \tag{2.7}$$

Under the assumption of a linear amplifier at the relay, the received symbol at node S_1 is

$$\begin{aligned} y_{R1} =& g_{R1}s_R + n_{R1} \\ =& \underbrace{G_{AF}g_{R1}g_{2R}s_2}_{desired\ signal} + \underbrace{G_{AF}g_{R1}g_{1R}s_1}_{self-interference} \\ &+ \underbrace{G_{AF}g_{R1}(n_{1R} + n_{2R}) + n_{R1}}_{composite\ noise\ term}, \end{aligned} \quad \text{(AF-LPA)} \tag{2.8}$$

where $g_{R1} = \mathcal{CN}(0, \sigma_{R1}^2)$ and $n_{R1} = \mathcal{CN}(0, N_0)$ are the fading and noise terms in the $R \rightarrow S_1$ link, and $\bar{\gamma}_{R1} = \sigma_{R1}^2/N_0$ is the corresponding link SNR. The first term in the above equation is the desired signal, the second term is self-interference, and the last term is a composite noise term. Since perfect CSI is assumed in this chapter, i.e. all the g_{ij}'s, $i, j \in \{1, 2, R\}$, are known, the self-interference term in (2.8) can be removed by the receiver at S_1. As for the composite noise term,

$$N = G_{AF}g_{R1}(n_{1R} + n_{2R}) + n_{R1}, \quad \text{(AF-LPA)} \tag{2.9}$$

it is complex Gaussian with zero mean and variance $\sigma_N^2 = (2G_{AF}^2|g_{R1}|^2 + 1)N_0$ when conditioned on g_{R1}. After self-interference cancellation, the effective signal becomes

$$\begin{aligned} \tilde{y}_{R1} &= y_{R1} - G_{AF}g_{R1}g_{1R}s_1 \\ &= G_{AF}g_{R1}g_{2R}s_2 + N, \end{aligned} \quad \text{(AF-LPA)} \tag{2.10}$$

which can then be combined with the direct path's received signal y_{21} in (2.5) using maximal ratio combining (MRC) [34] to form the final decision variable

$$D = \frac{g_{21}^* y_{21}}{N_0} + \frac{G_{AF}g_{2R}^* g_{R1}^*}{(2G_{AF}^2|g_{R1}|^2 + 1)N_0}\tilde{y}_{R1}. \quad \text{(AF)} \tag{2.11}$$

The decision rule is

$$\hat{s}_2 = \underbrace{\arg\max}_{k=1,2,\ldots,M} \{2\Re(Dx_k^*)\}, \tag{2.12}$$

where the x_k's are points in the MPSK signal constellation, and $\Re(\cdot)$ is the real operator. The instantaneous SNR of the decision statistics in (2.11) is

$$\gamma_{AF} = \frac{|g_{21}|^2}{N_0} + \frac{G_{AF}^2 |g_{2R}|^2 |g_{R1}|^2}{(2G_{AF}^2 |g_{R1}|^2 + 1)N_0}. \tag{2.13}$$

2.2.2 Non-linear Power Amplifier

The AF strategy described in (2.6) and (2.7) has the attribute of being simple – there is no need for signal detection and regeneration at the relay. However, it suffers from one drawback – the peak power of the forwarded symbol s_R is, strictly speaking, infinite. This stems from the fact that individual components of this signal are complex Gaussian processes, which can assume very large values. What this means in practice is that occasionally, the amplitude of the forwarded signal s_R will go beyond the linear operating range of a "real-world" power amplifier, creating non-linear distortion. If the amplifier is fixed, we can choose to mitigate this non-linear distortion through input back-off (IBO) or through signal pre-distortion [35]. Both techniques have their drawbacks, for example IBO reduces the SNR in the decision statistics while signal pre-distortion leads to additional transceiver complexity. Alternatively, if the amplifier's non-linearity is known to the receiver, then in principle, a new decision rule can be devised to deal with the non-linearity. However, it is doubtful how the entire input-output characteristics of a non-linear amplifier can be measured accurately and conveyed effectively by the relay without sacrificing downlink data throughput (as in the case of pilot-assisted estimation). Even if the non-linear characteristic is known exactly at the receiver, any signal compression that takes place inside the amplifier will lead to a loss of information, rendering a non-linear distortion compensating receiver not very effective. A good example is clipping – detailed information on the input signal amplitude is lost when it is beyond the clipping threshold.

Over the years, a number of popular models have been developed to describe non-linear power amplification, for example, the Saleh model [36], the Ghorbanian model [37] and the Rapp model [38]. Of the three, the Rapp model is specifically developed for solid-sate power amplifiers, the type of amplifiers commonly used in wireless communications. Given that solid state power amplifiers have very small phase distortion, the AM-PM distortion

in the Rapp model is often set to zero, as in [39, 40, 41]. In this investigation, we adopt the clipping model (a.k.a a soft limiter), which is a special case of the Rapp model when the smoothness factor goes to infinity. With the clipping model, there is no AM-PM distortion (as in [39, 40]), and the input-output relationship of the NLPA can be expressed as:

$$\tilde{s}_R(t) = \begin{cases} s_R(t), & |s_R(t)| \leq V, \\ V e^{j\theta_R(t)}, & |s_R(t)| > V. \end{cases} \tag{2.14}$$

where the input $s_R = |s_R| e^{j\theta_R}$ is the forwarded symbol in (2.6) and V is the clipping level. From hereon, we will refer to $\rho = V^2/2$ as the saturation power level of a NLPA.

For the non-linear amplifiers considered in this investigation, we assume the clipping level is chosen such that the instantaneous power of the transmitted uplink signals will not exceed the saturation level by a certain percentage of time. This information can be extracted from the complementary cumulative density function (CCDF) of the instantaneous power [24, 25] of the uplink source signals. Figure 2.3 shows the CCDFs of the instantaneous power of BPSK, 16PSK, and 16QAM (the first group of curves on the left). The results are based on a square-root raised cosine pulse with a roll-off factor of 0.5. In the cases of BPSK and 16PSK, it is observed that 99.99 percent of the times, the instantaneous power is at most 3.2 dB and 2.7 dB above the average power of the two signals, respectively. For 16QAM, the figure increases to 4.7 dB. If the NLPAs used for transmitting these modulations have saturation power levels set according to these instantaneous power values, it means only 0.0001 fraction of the times will the amplifiers be operating in their non-linear regions. This translates to practically no non-linear distortion. All the NLPAs considered in this study are assumed to meet the 0.0001 CCDF requirement. As such, the source signals are essentially free from non-linear distortion.

What would happen when the same NLPA is used at the relay to transmit an AF signal? To answer this question, we include in Figure 2.3 the CCDF of the forwarded signal of an AF relay (the middle set of curves), as well as those of the proposed MF (the right-hand set of curves) and PF schemes (same set of curves as the source signals). Without loss of generality, all three links in the cooperative communication network are assumed to have the same average SNR at 20 dB. Details of the signal structures in MF and PF will be provided in Sections 2.3 and 2.4 respectively. In the mean time, we can see from the figure that AF has very large instantaneous power. As an example, with BPSK modulation at the source terminals, the CCDF of the instantaneous power of the forwarded signal is 0.0001 at

11 dB above the average power, a staggering 7.8 dB increase over that of the source BPSK signals. This means that if AF were to be used, highly linear and expensive power amplifiers must be used, not only at the relay, but also at the source nodes, since all nodes have equal opportunity to function as a relay. If a NLPA with a saturation power level of 3.2 dB is used instead, then according to the figure, 10 percent of the times the power amplifier will be operating in its non-linear region, generating substantial distortion. In contrast, if PF is used at the relay, we see from the figure that the instantaneous power distribution of the forwarded signal is unchanged from that of the source signals, suggesting minimal non-linear distortion. It should be pointed out that while MF has an even higher instantaneous power than AF, it is not sensitive to non-linear amplifier distortion because of the way the relay signal is constructed from the received uplink signals and the way self-interference is being cancelled. Detailed discussion will be provided in the next section. It is worth noting that the CCDF's of the PAPR of the forwarded signals at the relay generally do not correspond to a complex Gaussian signal. This means in the event of non-linear distortion at the relay, the Bussgang Theorem [42] cannot be used to quantify the distortion, as in the case of multi-carrier systems [43, 44].

When the non-linearly amplified downlink signal arrives at the source, it is matched filter and sampled, just like that described in the previous subsection. However, because of the non-linearity in the downlink, Eqn. (2.8) no longer represents the structure of the received samples. Instead, each received sample is now made up of a series of intermodulation products. The best a user can do in this circumstance is to (make an attempt to) cancel out the linear component of its self interference as per (2.10), perform signal combining according to (2.11), and make decision as per (2.12). As will be shown in the next section, the higher order interference terms that remain in the decision statistics will have a dramatic effect on the performance of the AF protocol.

2.2.3 BER Performance

The BER performance of the AF protocol with a LPA has been studied considerably in the literature; see for example [18, 19, 20]. In this section, we provide a BER analysis that is applicable to both AF and the proposed MF scheme in Section 2.3. The analysis is valid for a LPA and is based on the discrete-time signal model in Section 2.2. To gain some quick insight, let's ignore the noise terms n_{1R} and n_{2R} at the relay (high SNR approximation).

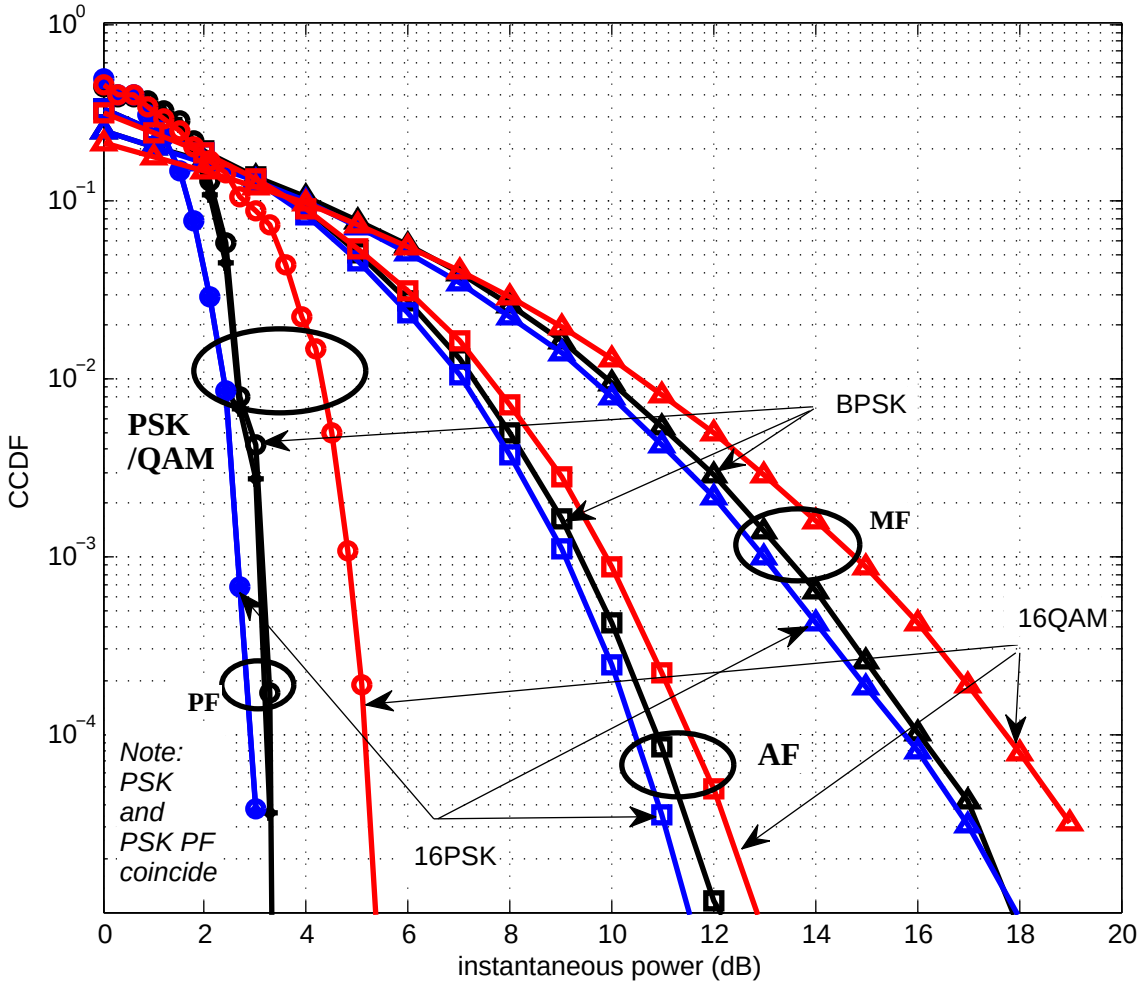

Figure 2.3: CCDF of the PAPR of PSK and the relay's transmitted signal.

The received signal in (2.10) becomes

$$\hat{y}_{R1} = G_{AF} g_{R1} g_{2R} s_2 + n_{R1}. \qquad \text{(AF-LPA)} \quad (2.15)$$

If this is the structure of the downlink signal, then the combining rule that yields the largest SNR is

$$D_{Bound}^{LPA} = \frac{g_{21}^* y_{21}}{N_0} + \frac{G_{AF} g_{2R}^* g_{R1}^* \hat{y}_{R1}}{N_0}, \qquad \text{(AF-LPA)} \quad (2.16)$$

and the corresponding instantaneous SNR is

$$\gamma_{AF}^{LPA} = \frac{|g_{21}|^2}{N_0} + \frac{|G_{AF} g_{R1} g_{2R}|^2}{N_0}. \qquad (2.17)$$

Note that (2.17) represents an upper bound on the SNR in the decision variable. The SNR that can be achieved in practice using the actual combining rule in (2.11) will be less. For BPSK modulation at the source, according to the BER analysis in Appendix A, the average BER of AF with a LPA is bounded by (2A.12) with $n = 2$, $\lambda^2 = \sigma_{2R}^2 \sigma_{R1}^2$. This analytical result for a LPA, along with the simulation results[1] for a NLPA, are shown in Figure 2.4. In the case of NLPA, different saturation power levels are considered. Specifically, a curve label "AF, $\rho = X$ dB" in the figure refers to the case which a NLPA with a saturation power level of $10log_{10}(V^2/2) = X$ dB is used at the relay. The reason why only simulation results are provided in the NLPA case is because the two downlink models in Figure 2.2 (a) and Figure 2.2 (b) are no longer equivalent. Consequently, we can no longer capture all the signal and amplifier characteristics using a symbol-space discrete-time model. The BER analysis would become very difficult, if not impossible, to perform. In the simulations, all the three links in the system are assumed to be equally strong. SQRC pulse with unit energy and a roll-off factor of 0.5 is adopted and eight samples per symbol is used to approximate the received waveform at the relay. We focus on in-band distortion as out-of-band distortion is out of the scope of this thesis. Hence, there is no further attempt to filter out the out-of-band distortion. As mentioned in the previous section, the steps outlined in (2.8), (2.10) and (2.11) are used to arrive at the decisions on the transmitted symbols, irrespective of the type of amplifiers. As seen from the figure, the lower bound on the BER of AF with a LPA obtained from (2A.12) closely matches that obtained from simulation. As expected, the lower the saturation level of the NLPA, the higher the BER. In particular, at a saturation

[1]Key simulation parameters are summarized in Appendix A.

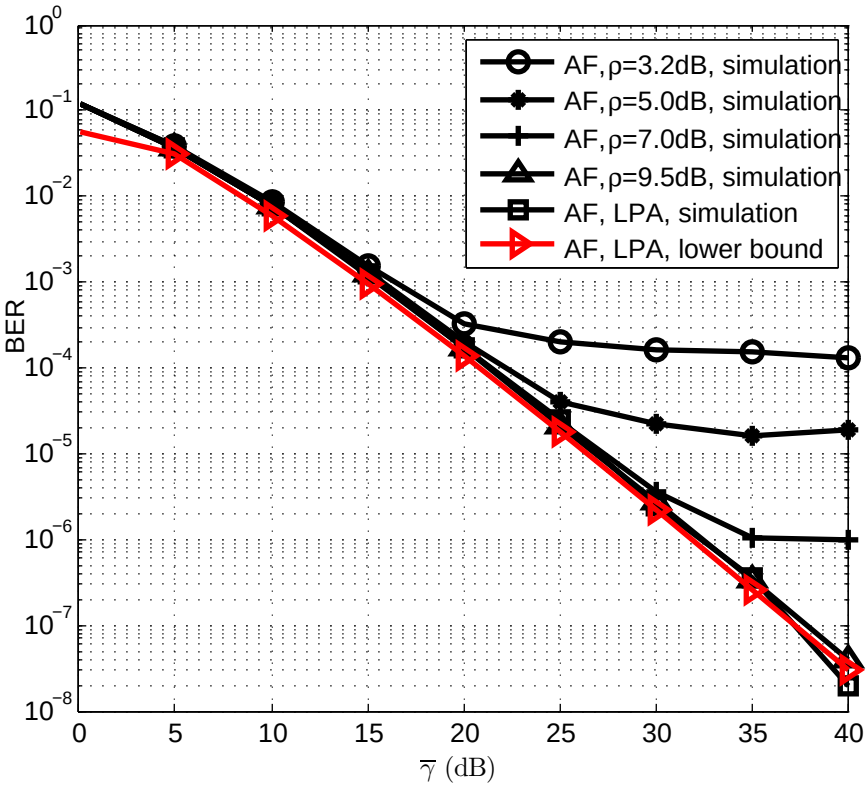

Figure 2.4: BER of AF with BPSK modulation as a function of the common link-SNR $\bar{\gamma} = \bar{\gamma}_{1R} = \bar{\gamma}_{2R} = \bar{\gamma}_{R1} = \bar{\gamma}_{21}$.

power level of 3.2 dB, an irreducible error floor of 1.5×10^{-4} is observed. In contrast, when the saturation power level is 9.5 dB, there is no irreducible error floor. These BER results appear to be consistent with those CCDF results shown earlier in Figure 2.3.

2.3 Multiply and Forward

Given the problems of AF when subjected to NLPA distortion, we explore in this section a relay strategy that offers immunity to such distortion. Instead of forwarding the sum of the received signals in Phase 1 and 2, the relay in the proposed system forwards the product of the two received signals. We term this new relay method multiply-and-forward (MF).

A MF relay operates as follows. During Phase 1 and 2 of the protocol, users S_1 and S_2 transmit their respective data to the relay using PSK modulations and SQRC pulse shaping. The relay filters the two received signals using a matched filter, samples the matched filter's output at the symbol rate, and multiplies the corresponding samples of the two received signals to form a product symbol sequence. After amplitude scaling, the product symbol sequence is then fed to a linear modulator to generate the forwarded signal. It should be emphasized that the bandwidth of the forwarded signal is identical to that of the uplink signals because multiplication is done in the digital domain via sampling and remodulation. The product samples used to construct the remodulated signal contain sufficient information required to detect the product data symbols $s_1 s_2$ at the users terminals. We choose not to make any individual decisions on s_1 and s_2 at the relay (i.e. adopting a DF approach) because this would lead to a loss of information and hence a degraded BER performance. Beside, data detection requires channel estimation and it is preferrable to have this task performed instead at the user terminals.

We describe next the detailed signal structure of this MF protocol. In the discussion, it is assumed that the amplifiers used at the source terminals to transmit the uplink signals follow the clipping model. However, the saturation levels of these amplifiers are high enough so that the source signals will experience negligible distortion. As demonstrated earlier, a saturation level of 3.2 dB above the average power level is sufficient for this purpose when PSK modulations are considered. With such an amplifier, the matched filter output of an MF relay for S_1's data symbol s_1 is simply given by (2.2). This equation can be rewritten

as

$$\begin{aligned} y_{1R} &= g_{1R}s_1 + n_{1R} \\ &\stackrel{a}{=} (g_{1R} + n_{1R})s_1 \\ &\stackrel{b}{=} e^{j\psi_{1R}}(a_{1R} + n_{1R})s_1 \\ &= b_{1R}e^{j\phi_{1R}}e^{j\psi_{1R}}s_1, \end{aligned} \tag{2.18}$$

where a_{1R} and ψ_{1R} are the amplitude and phase of g_{1R}, and b_{1R} and ϕ_{1R} are the amplitude and phase of $(a_{1R}+n_{1R})$. Note that Equality (a) in the above equation is obtained from the observation that statistically, $n_{1R}s_1$ and n_{1R} are identical. This stems from the fact that n_{1R} is complex Gaussian with uniform phase, and s_1 is a unit-amplitude PSK symbol. A similar manipulation has been applied to the analysis of the BER of DPSK; see for example [45]. Similarly, Equality (b) is obtained by absorbing the fading phase ψ_{1R} into the term n_{1R} in Equality (a). Analogous to (2.18), the received sample at the relay's matched filter output for S_2's data symbol s_2 can be written as

$$\begin{aligned} y_{2R} &= g_{2R}s_2 + n_{2R} \\ &= (g_{2R} + n_{2R})s_2 \\ &= e^{j\psi_{2R}}(a_{2R} + n_{2R})s_2 \\ &= b_{2R}e^{j\phi_{2R}}e^{j\psi_{2R}}s_2, \end{aligned} \tag{2.19}$$

where a_{2R} and ψ_{2R} are the amplitude and phase of g_{2R}, and b_{2R} and ϕ_{2R} are the amplitude and phase of $(a_{2R}+n_{2R})$. Now let us multiply the signals in (2.18) and (2.19) together and scale the product by a scaling factor G_{MF} to form the forwarded symbol

$$\begin{aligned} s_R &= G_{MF}y_{1R}y_{2R} \\ &\equiv G_{MF}b_{1R}b_{2R}e^{j\phi_{1R}}e^{j\psi_{1R}}e^{j\phi_{2R}}e^{j\psi_{2R}}s_1s_2, \quad \text{(MF)} \end{aligned} \tag{2.20}$$

where G_{MF} is chosen such that the average power of s_R is $1/2$, the same as that of the source symbols; see (2.1). This requires

$$G_{MF} = \frac{1}{2N_0\sqrt{(\bar{\gamma}_{1R}+1)(\bar{\gamma}_{2R}+1)}}. \tag{2.21}$$

The sequence of symbols in (2.20) obtained at different sampling times is fed to a linear modulator that uses the same pulse shape and symbol rate as those used at the user terminals. The resultant modulated signal is sent over the downlink to the two users.

2.3.1 Linear Power Amplifier at the Relay

With a LPA at the relay, the signal received at node S_1 in Phase 3 (after matched filtering and sampling) can be written as

$$\begin{aligned} y_{R1} =& g_{R1}s_R + n_{R1} \\ =& G_{MF}g_{R1}(g_{1R} + n_{1R})(g_{2R} + n_{2R})s_1 s_2 \\ &+ n_{R1}. \qquad \text{(MF-LPA)} \end{aligned} \tag{2.22}$$

After de-rotating y_{R1} by s_1^* and ignoring the product noise term, which is negligibly small compared to other product terms at high SNR's, we obtain the observation

$$\begin{aligned} \tilde{y}_{R1} =& y_{R1}s_1^* \\ \approx& \underbrace{G_{MF}g_{R1}g_{1R}g_{2R}s_2}_{desired\ signal} + \underbrace{G_{MF}g_{R1}(g_{1R}n_{2R} + g_{2R}n_{1R})s_2 + n_{R1}}_{composite\ noise}, \qquad \text{(MF-LPA)} \end{aligned} \tag{2.23}$$

where the composite noise term $N = G_{MF}g_{R1}(g_{1R}n_{2R} + g_{2R}n_{1R})s_2 + n_{R1}$ has a variance of $\sigma_N^2 = (G_{MF}^2|g_{R1}|^2(|g_{1R}|^2 + |g_{2R}|^2) + 1)N_0$. After combining $\tilde{y}_{R1}$ with the direct path signal y_{21} in (2.5) using MRC, the receiver at S_1 obtains the decision variable

$$D = \frac{g_{21}^* y_{21}}{N_0} + \frac{G_{MF}g_{R1}^* g_{1R}^* g_{2R}^*}{(G_{MF}^2|g_{R1}|^2(|g_{1R}|^2 + |g_{2R}|^2) + 1)N_0}\tilde{y}_{R1}. \qquad \text{(MF)} \tag{2.24}$$

The data symbol s_2 of user S_2 is then detected according to (2.12). The instantaneous SNR of the decision variable in (2.24) is

$$\gamma_{MF} = \frac{|g_{21}|^2}{N_0} + \frac{G_{MF}^2|g_{R1}|^2|g_{1R}|^2|g_{2R}|^2}{(G_{MF}^2|g_{R1}|^2(|g_{1R}|^2 + |g_{2R}|^2) + 1)N_0}. \tag{2.25}$$

2.3.2 Non-linear Power Amplifier at the Relay

With a non-linear amplifier at the relay, it is strictly speaking not accurate to describe the received signal at S_1 using the discrete-time model in (2.22)-(2.24). This stems from the fact that matched filtering and sampling of a faded, non-linearly amplified signal comprising of a superposition of SQRC pulses is not the same as introducing fading and non-linear distortion to the output samples of a matched filter; compare Figure 2.2 (a) and 2.2 (b). Nonetheless, we will employ the discrete-time non-linear model to help us explain intuitively why the proposed MF scheme can mitigate non-linear amplifier distortion. The claim will be verified via waveform level simulation in the next subsection.

Assuming a non-linear amplifier with amplitude and phase responses of $A(x)$ and $\Phi(x)$ respectively, where x is the input signal magnitude. This means after amplification, the relay symbol in (2.20) become

$$\tilde{s}_R = \underbrace{A(G_{MF}b_{1R}b_{2R})}_{\substack{unknown\\ amplitude\\ distortion}} \underbrace{e^{j\Phi(G_{MF}b_{1R}b_{2R})}e^{j(\phi_{1R}+\phi_{2R})}}_{\substack{unknown\\ phase\\ distortion}} \underbrace{e^{j(\psi_{1R}+\psi_{2R})}}_{\substack{known\\ phase\\ distortion}} s_1 s_2. \tag{2.26}$$

The corresponding received signal at node S_1 is $y_{R1} = g_{R1}\tilde{s}_R + n_{R1}$, which after multiplication by $\exp(-j(\psi_{1R}+\psi_{2R}))s_1^*$, generates the decision variable

$$\tilde{y}_{R1} = g_{R1}A(G_{MF}b_{1R}b_{2R})e^{j\Phi(G_{MF}b_{1R}b_{2R})}e^{j(\phi_{1R}+\phi_{2R})}s_2 + n_{R1}. \quad \text{(MF)} \tag{2.27}$$

Given that s_2 is an MPSK symbol, the unknown amplitude distortion $A(G_{MF}b_{1R}b_{2R})$ has no effect on the decision, except for a loss in SNR compared to that of the LPA case.

Concerning the unknown phase distortion in (2.26), let Δ_R be a short notation for $[\Phi(G_{MF}b_{1R}b_{2R}) + (\phi_{1R}+\phi_{2R})]$. The effect of a phase error is the rotation of the transmitted signal constellation while decision is still based on the original non-rotated constellation. With a solid state power amplifier, the AM-PM distortion $\exp(j\Phi(G_{MF}b_{1R}b_{2R}))$ is expected to be negligibly small [39, 40, 41]. Further, since ϕ_{iR}, $i \in \{1,2\}$, are the phases of $(|g_{iR}| + n_{iR})$, they will be relatively small at large SNR. In the case of BPSK modulation, if the Δ_R is in the interval $-\pi/2 < \Delta_R < \pi/2$, where $\pi/2$ is the angular distance, or phase margin, between a signal point to its nearest decision boundary, then $-10\log_{10}(\cos^2\Delta_R)$ dB more signal power is required to maintain the same BER as the case with no phase error. On the other hand, when the absolute value of the phase error is greater than $\pi/2$, then the BER will be greater than $1/2$, which is not a case of interest. In general, for M-ary PSK, as long as the phase error satisfies $-\pi/M < \Delta_R < \pi/M$, the SNR degradation is of the form $-10\log_{10}(f(\Delta_R))$, where $0 < f(\Delta_R) < 1$ is a function of the phase error. Given that in practice, it is unlikely a very dense MPSK is adopted, so π/M should be a sufficient margin for any phase error arising from channel estimation and amplitude-to-phase distortion caused by a non-linear amplitude. Another important point to note is that all the three schemes considered in the thesis, AF, PF, and MF, will be degraded by more or less the same amount in the presence of phase error. So their relative performance more or less remains unchanged. In short, the unknown phase noise,

$\exp(j\Phi(G_{MF}b_{1R}b_{2R}))\exp(j(\phi_{1R}+\phi_{2R}))$, which is expected to be small when compared to the phase margin π/M, M being the size of the PSK constellation, will only lead to a SNR degradation. The most important property of this MF protocol is that, unlike AF, it does not lead to any residual self-interference. Consequently, there will be no irreducible error floor, only a lateral shift in the BER curve.

2.3.3 BER Performance

When the amplifier is linear, a lowerbound on the BER of MF can be obtained by assuming the noise terms at the relay, n_{1R} and n_{2R}, are negligible. In this case, (2.23) simplifies to

$$\hat{y}_{R1} = G_{MF}g_{R1}g_{1R}g_{2R}s_2 + n_{R1}. \qquad \text{(MF-LPA)} \quad (2.28)$$

The combining rule that yields the largest SNR for this signal structure is

$$D_{Bound}^{LPA} = \frac{g_{21}^* y_{21}}{N_0} + \frac{G_{MF}g_{R1}^* g_{1R}^* g_{2R}^* \hat{y}_{R1}}{N_0}. \qquad \text{(MF-LPA)} \quad (2.29)$$

The corresponding SNR in this decision variable is

$$\gamma_{MF}^{LPA} = \frac{|g_{21}|^2}{N_0} + \frac{|G_{MF}g_{R1}g_{1R}g_{2R}|^2}{N_0}, \quad (2.30)$$

which will be larger than the SNR obtained from the actual combining rule (2.24) used at the receiver. As such, any BER derived from (2.30) will provide us a lower bound on the BER. In realizing that the first component in (2.30) is the square of a 3rd order cascade Rayleigh random variable, a lower bound on the average BER can be obtained from (2.30) using results from Appendix 2A. Specifically, (2A.12) with G_{AF} replaced by G_{MF}, $n = 3$ and $\lambda^2 = \sigma_{1R}^2\sigma_{2R}^2\sigma_{R1}^2$ gives the lower bound on the BER of MF with a linear power amplifier. Furthermore, the diversity order of MF protocol is shown to be 2 in Appendix 2B.

Figure 2.5 shows the BER of MF with BPSK modulation, SQRC pulse shaping with a roll-off factor of 0.5, and equally strong links. Also included in the figure are the BER curves of AF from the last section. Both lower bound and simulation results are provided for the case of a LPA at the relay. The analytical results are obtained from (2A.12) with $n = 3$, $\lambda^2 = \sigma_{1R}^2\sigma_{2R}^2\sigma_{R1}^2 = \sigma_g^6$, and 6 terms in the series ($k = 0$ to 5), where σ_g^2 is the variance of the fading processes in all the links. Like in the AF case, only simulation is used to study the BER of MF when the relay's amplifier is non-linear. The simulation model follows that

in Figure 2.2 (a). where 8 samples per symbol interval is used to model waveforms. The NLPA considered in the simulation has a saturation power level of 3.2 dB above the average power of the source BPSK signals. As mentioned earlier, this non-linear characteristic has practically no effect on the source signals. The receiver block in the simulator first filters the downlink signal using a matched filter, and then samples the matched filter's output at the symbol rate to obtain the sample y_{R1}. In the case of a LPA, the structure of y_{R1} follows that in (2.22). On the other hand for a NLPA, the structure of y_{R1} is approximately that shown in (2.27). In both cases, the combining rule is given by (2.23) and (2.24), and the decision rule is given by (2.12). No attempt is made to derive the "optimal" combining rule for the NLPA case because we assume the downlink receiver does not have prior knowledge of the amplifier characteristics at the relay.

It is observed from the figure that in the case of a LPA, the lower bound on the BER of MF agrees with simulation, and that MF is approximately 1.5 dB less power efficient than AF at the same BER. As predicted, the BER of MF is practically unaffected by amplifier non-linearity, which is a marked improvement from the irreducible error floors seen in AF with NLPA.

To further illustrate the effect of signal clipping on AF and MF, we show in Figure 2.6 the BER of the two protocols at a common link SNR of 30 dB and with the saturation power level of the NLPA as a variable. For the AF protocol, the BER improves with the NLPAs saturation level, up to $\rho = 9.5$ dB, the point where the CCDF of the instantaneous power of the forwarded signal becomes sufficiently small. In contrast, the BER of MF remains almost constant as the PA's saturation level varies. This implies that the MF protocol is resilient to power amplifier saturation. Although the MF protocol exhibits a slightly higher BER than AF when the amplifier is linear, this drawback is more than compensated by its robustness against non-linear power amplification. In the next section, we present a modification to the MF signaling structure such that the resultant system is not only immune to NLPA distortion, it also offers an improved BER when the amplifier is linear.

2.4 Phase Forward

In the last section, we demonstrated that MF is a technique that can be used to avoid the self-interference arising from the use of a NLPA at the relay. The only drawback is that

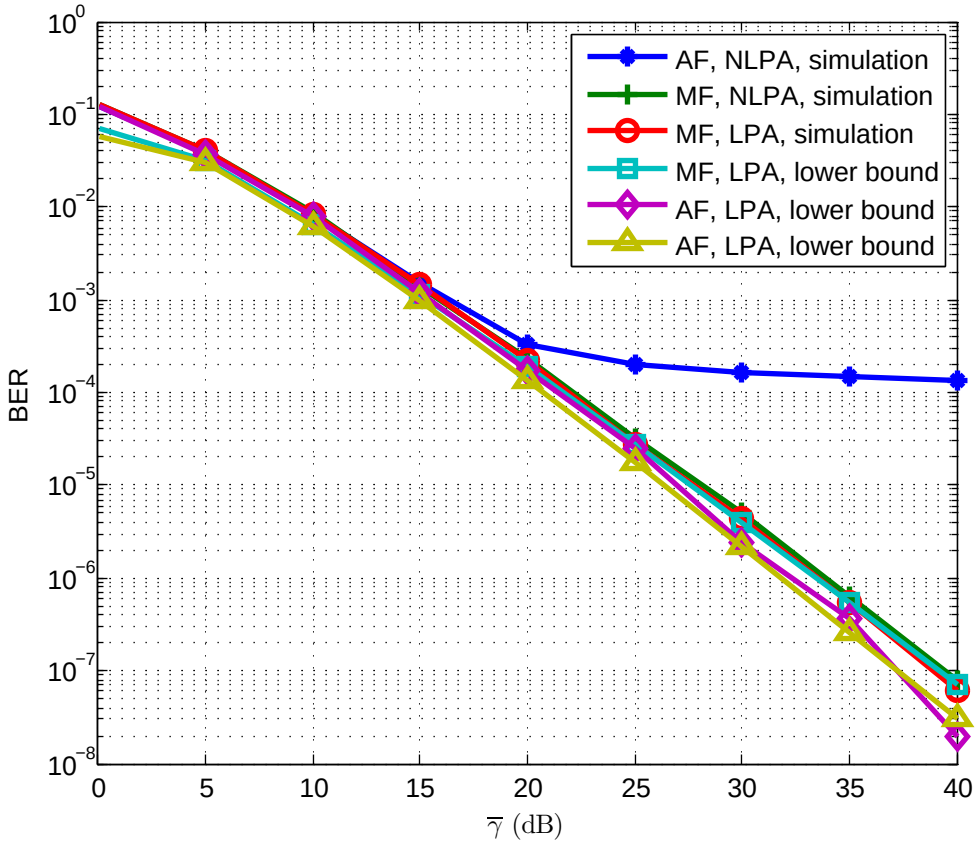

Figure 2.5: Comparison between MF and AF with LPA as well as NLPA. The modulation is BPSK and all the links in the system have the same average link-SNR $\bar{\gamma} = \bar{\gamma}_{1R} = \bar{\gamma}_{2R} = \bar{\gamma}_{R1} = \bar{\gamma}_{21}$.

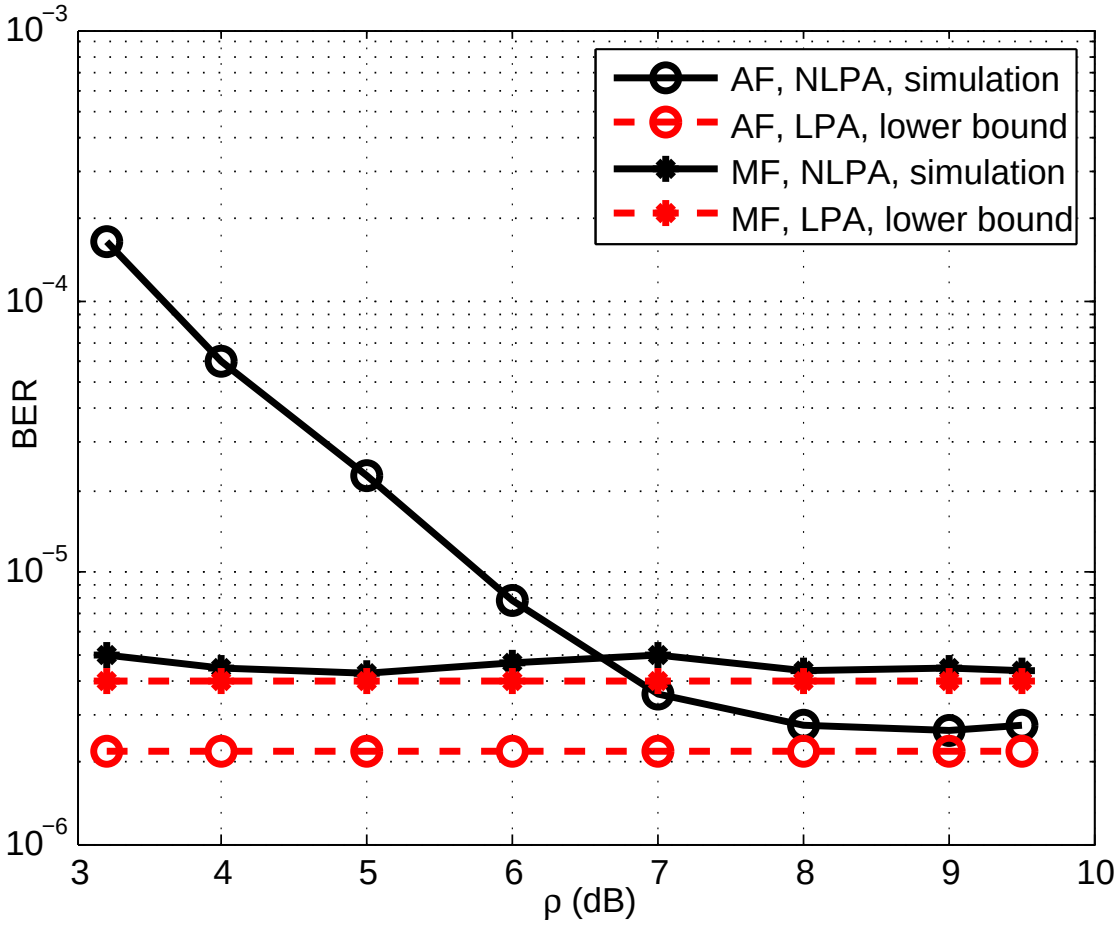

Figure 2.6: Comparison between MF and AF with different NLPA saturation power levels. The modulation is BPSK and all the links in the system have the same average link-SNR of 30 dB.

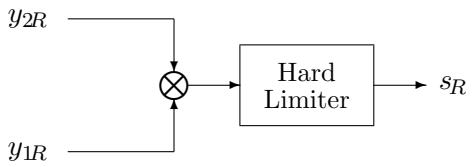

Figure 2.7: Hard limiter operation on the multiplied input symbols to generate the phase forward symbol s_R in (2.31).

with a LPA, MF is approximately 1.5 dB less power efficient than AF. Naturally, it is highly desirable to devise a scheme that is at least as power efficient as AF when the amplifier is linear while offers at the same time a robustness against NLPA distortion similar to that of MF. This brings us to the idea of PF, a technique first introduced in [31] to maintain constant envelope signaling at the relay when CPFSK modulation is employed in a one-way relaying system. A similar idea was also employed in [30] to address the high peak power issue in one-way relaying systems with star-QAM modulation. While the technique in [30] requires channel coding to function properly, the PF technique in [31] does not.

2.4.1 Signal Structure and Processing

For the two-way relaying system under investigation, we can have a PF relay by modifying the relay signal in MF as follows. Instead of using directly the product samples in (2.20) to generate a remodulated signal at the relay, the proposed two-way PF relay drops the term $G_{MF}b_{1R}b_{2R}$ in the equation and uses

$$s_R = e^{j\phi_{1R}}e^{j\phi_{2R}}e^{j\psi_{1R}}e^{j\psi_{1R}}s_1 s_2. \qquad \text{(PF)} \quad (2.31)$$

instead. The symbol s_R in (2.31) can be generated using a hard limiter (implemented in the digital domain) operating on (2.20); see Figure 2.7 for an illustration of the symbol processing at the relay. This leads to a forwarded signal comprising of symbols with unit-amplitude, just like the source PSK signals.

In essence, PF is MF with an automatic gain control (AGC) or intentional hard-limiting. As in the case of MF, the fading phases ψ_{1R} and ψ_{2R} can be compensated during coherent detection at the destination node. The only effective disturbances are the phase noises ϕ_{1R} and ϕ_{2R} of the processes $(|g_{1R}| + n_{1R})$ and $(|g_{2R}| + n_{2R})$, which are small at reasonably large SNR.

Given that the forwarded symbols in PF are of constant amplitude, the corresponding remodulated signal has a much lower PAPR than those of AF and MF. According to Figure 2.3, the CCDF of the instantaneous power in PF is almost identical to that of pulse shaped PSK. This means the same amplifier used at the source terminals to transmit PSK signals without non-linear distortion can be used at the relay to transmit the forwarded signal without distortion. In the absence of non-linear distortion, the downlink models in Figure 2.2 (a) and Figure 2.2 (b) are approximately equivalent. Consequently, the received sample at the matched filter output of S_1 is

$$y_{R1} = g_{R1} e^{j(\psi_{1R}+\psi_{2R})} e^{j(\phi_{1R}+\phi_{2R})} s_1 s_2 + n_{R1}. \qquad \text{(PF)} \quad (2.32)$$

After de-rotating this signal by $e^{-j(\psi_{1R}+\psi_{2R})} s_1^*$, we obtain the decision variable

$$\tilde{y}_{R1} = g_{R1} e^{j(\phi_{1R}+\phi_{2R})} s_2 + n_{R1}, \qquad \text{(PF)} \quad (2.33)$$

where we took the liberty to absorb the fading and data phases into the noise term. Finally, we need to combine $\tilde{y}_{R1}$ with the signal y_{21} to form the final decision variable. In order to determine the optimal combining weight for $\tilde{y}_{R1}$, we need to first analyze its signal and noise structures.

Consider the term $\exp(j\phi_{1R})$ in (2.33). It can be rewritten as $(|g_{1R}|+n_{1R})/\,||g_{1R}|+n_{1R}|$. For sufficiently large $|g_{1R}|$, we can ignore the noise term in the denominator and approximate $\exp(j\phi_{1R})$ as $(1+n_{1R}/|g_{1R}|)$. Similarly, $\exp(j\phi_{2R})$ is approximately $(1+n_{2R}/|g_{2R}|)$. Based on these approximations, we can rewrite (2.33) as

$$\begin{aligned}\tilde{y}_{R1} \approx & g_{R1}\left(1+\frac{n_{1R}}{|g_{1R}|}\right)\left(1+\frac{n_{2R}}{|g_{2R}|}\right)s_2 + n_{R1} \\ = & g_{R1}s_2 + g_{R1}\left(\frac{n_{1R}}{|g_{1R}|}+\frac{n_{2R}}{|g_{2R}|}+\frac{n_{1R}n_{2R}}{|g_{1R}||g_{2R}|}\right)s_2 + n_{R1}. \qquad \text{(PF)} \quad (2.34)\end{aligned}$$

Given that the signal component in the above approximation is $g_{R1}s_2$ while the composite noise term has a variance of

$$\sigma_N^2 = \left[|g_{R1}|^2\left(\frac{1}{|g_{1R}|^2}+\frac{1}{|g_{2R}|^2}+\frac{N_0}{|g_{1R}|^2|g_{2R}|^2}\right)+1\right]N_0, \quad (2.35)$$

the MRC rule for PF is thus

$$D = \frac{g_{21}^* y_{21}}{N_0} + \frac{g_{R1}^*}{\left[|g_{R1}|^2\left(\frac{1}{|g_{1R}|^2}+\frac{1}{|g_{2R}|^2}+\frac{N_0}{|g_{1R}|^2|g_{2R}|^2}\right)+1\right]N_0}\tilde{y}_{R1}. \qquad \text{(PF)} \quad (2.36)$$

2.4.2 BER Analysis for Both Linear and Non-Linear Amplifiers

The instantaneous SNR in the decision variable in (2.36) is

$$\gamma_{PF} = \frac{|g_{21}|^2}{N_0} + \left(\sum_{i \in \mathcal{L}} \frac{1}{|g_i|^2/N_0} + \frac{N_0}{|g_{1R}|^2 |g_{2R}|^2} \right)^{-1}, \tag{2.37}$$

where $\mathcal{L} = \{1R, 2R, R1\}$. Ignoring the product term in the denominator allows us to obtain the following upper bound on the SNR

$$\gamma_{PF} < \frac{|g_{21}|^2}{N_0} + \left(\sum_{i \in \mathcal{L}} \frac{1}{|g_i|^2/N_0} \right)^{-1}. \tag{2.38}$$

It should also be pointed out that the second SNR term $\gamma_R = \left(\sum_{i \in \mathcal{L}} \frac{1}{|g_i|^2/N_0} \right)^{-1}$ in (2.38) is identical to that achieved in an ideal 3-hop relaying chain [46, Eqns. (4)-(5)].

Before proceeding to the BER analysis of PF, let us compare it against the other two forwarding techniques based on the AoF [47] in the relay path. This parameter is a simple and yet effective measure of the severity of fading and can be used as a performance index when making comparisons of the three relay protocols. From the SNR analysis in Sections 2.2 and 2.3, we see that with a LPA, the relay paths in AF and MF are, in essence, cascaded Rayleigh channels at large SNR. Specifically for AF, its relay path is equivalent to a double Rayleigh channel (corresponding to the $n = 2$ case in Appendix 2A), while for MF, its relay path is equivalent to a triple Rayleigh channel ($n = 3$). According to [48], the AoF in these two cases can be determined from the general formula $(2^n - 1)$. This means an AoF of 3 for AF and an AoF of 7 for MF. As for the relay path in PF, it approximates an ideal 3-hop relaying chain under Rayleigh fading. The AoF in this case can be evaluated using (2C.5)-(2C.7). Specifically, with equal link SNR, the AoF of PF can be found to be (2C.8) in Appendix 2C, whose numerical value is 0.6969. This is the lowest amongst the three protocols. Based on these results, we can predict that PF should have the lowest BER when the amplifier is linear. Below is the detailed BER analysis for PF.

The average BER of PF with BPSK modulation can be determined using the moment generating function (MGF) approach [47], similar to that in the AF and MF cases shown earlier in Appendix 2A. One major difference though, in the case of AF and MF, the BER analysis is confined to that of a linear amplifier, whereas in the case of PF, the analysis presented below applies to both LPA and NLPA. Firstly, the MGF of the direct path SNR,

$\gamma_{21} = |g_{21}|^2/N_0$, is simply $\Phi_{\gamma_{21}}(s) = (1 - 2\bar{\gamma}_{21}s)^{-1}$ where $\bar{\gamma}_{21} = \sigma_{21}^2/N_0$ is the average SNR in the direct link. Secondly, the MGF of γ_R in (2.38) can be determined from [49, 50] as

$$\Phi_R(s) = \int_0^\infty -J_0(2\sqrt{-st}) \left[\frac{\partial}{\partial t}\Phi_{1/\gamma}(-t)\right] dt, \tag{2.39a}$$

$$= 1 - \sqrt{-s} \int_0^{\frac{\pi}{2}} \frac{\sec^2 \xi}{\sqrt{\tan \xi}} J_1(2\sqrt{-s \tan \xi})\Phi_{1/\gamma}(\tan \xi) d\xi, \tag{2.39b}$$

where

$$\Phi_{1/\gamma}(s) = \prod_{i \in \mathcal{L}} \sqrt{\frac{-2s}{\bar{\gamma}_i}} K_1\left(\sqrt{\frac{-2s}{\bar{\gamma}_i}}\right) \tag{2.40}$$

is the MGF of the reciprocal of γ_R, $J_\nu(\,\cdot\,)$ is the Bessel's function of the first kind of order ν, $K_1(\,\cdot\,)$ is the modified Bessel's function of the second kind of order 1, and $\bar{\gamma}_i$'s are the SNRs in the different links defined in Section 2.2. With the $\Phi_{21}(s)$ given above and $\Phi_{\gamma_R}(s)$ given by (2.39b) and (2.40), the average BER is $P_e = \frac{1}{\pi}\int_0^{\frac{\pi}{2}} \Phi_{\gamma_{21}}(-\frac{1}{2}\sin^{-2}\theta)\Phi_{\gamma_R}(-\frac{1}{2}\sin^{-2}\theta)d\theta$ which can be shown equal to

$$\begin{aligned} P_{e,PF} =& \frac{1}{2}\left(1 - \sqrt{\frac{\bar{\gamma}_{21}}{1+\bar{\gamma}_{21}}}\right) \\ & - \frac{1}{\pi}\int_0^{\frac{\pi}{2}}\int_0^{\frac{\pi}{2}} \frac{2\sin\theta\tan\xi\sec^2\xi J_1\left(\frac{\sqrt{2\tan\xi}}{\sin^2\theta}\right)}{(\sin^2\theta + \bar{\gamma}_{21})} \frac{\prod_{i\in\mathcal{L}} K_1\left(\sqrt{\frac{2\tan\xi}{\bar{\gamma}_i}}\right)}{\sqrt{\prod_{i\in\mathcal{L}}\bar{\gamma}_i}} d\xi\, d\theta. \end{aligned} \tag{2.41}$$

Although the above BER is not in closed-form, the double integral can be easily evaluated numerically. Furthermore, using the integral form of (2.39a), as shown in Appendix 2B, we can see a second order diversity in the PF protocol.

Figure 2.8 shows the BER of PF obtained through numerical integration of (2.41) and through simulation. The amplifiers used in the simulation have a power saturation level 3.2 dB higher than the average power of the source BPSK signals. It is observed that the numerical results and the simulation results agree with each other. This confirms that the non-linearity in the amplifier has no effect on PF and that it is appropriate to ignore the product noise term in (2.37). For comparison purpose, we also include in Figure 2.8 the AF and MF results for a linear power amplifier taken from previous figures. It is observed that PF is substantially better than AF and MF. The BER improvement can be attributed to the fact that amongst the three schemes, PF has the smallest AoF when the amplifier

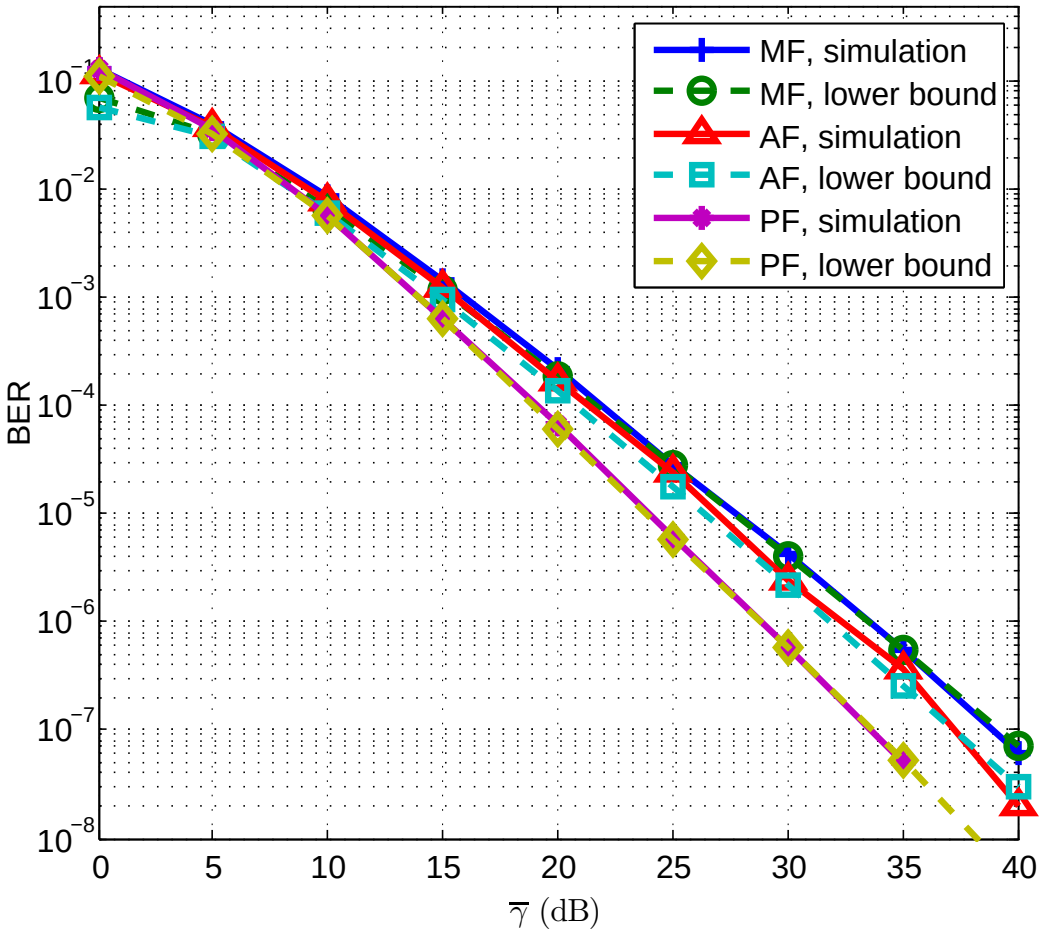

Figure 2.8: BER of PF compared to those of MF and AF. The modulation is BPSK and all the links in the system have the same average link-SNR $\bar{\gamma} = \bar{\gamma}_{1R} = \bar{\gamma}_{2R} = \bar{\gamma}_{R1} = \bar{\gamma}_{21}$. The AF and MF results assume a LPA while those of PF are valid for both linear and non-linear amplifiers.

is linear. Now, if we compare all three schemes based on the same NLPA, i.e, by inserting the BER curves of PF into Figure 2.5, we can see that PF is superior to AF and MF.

Next, we consider the scenario of asymmetric channels, i.e. the different links in the co-operative communication network do not have identical SNR. This can happen, for example, when the relay is midway between the two source nodes. Assuming a path-loss exponent of 4, this situation translates into a 12 dB higher SNR in the $S_1 \rightarrow R$ and $S_2 \rightarrow R$ links than in the direct link. Another situation that gives rise to asymmetric channels is when the relay is a mobile device while the two source nodes are fixed terminals. In this case, the relay is expected to have lower transmit power. Figure 2.9 shows the BER of PF, AF and MF when the $S_1 \rightarrow R$ and $S_2 \rightarrow R$ links are 10dB stronger than those in the direct path and in the downlink. This asymmetric channel condition allows us to study the impact of the uplink signal quality on the overall system performance. It is observed that the performance of AF and MF do not improve with an increase in the uplink signal quality. On the other hand, the BER of PF is lowered somewhat when the uplinks are 10 dB stronger than both the downlink and the direct path. Figure 2.10 further illustrates this behavioral difference. Here the downlink and direct path SNRs are fixed at 20 dB while the uplink SNR is varied from 20 to 32 dB. It is observed that the BER of PF can be reduced to 1/3 that of equally strong links when the uplink's SNR is 12 dB above that in the direct path.

2.4.3 Discussions

Higher Order Modulation with MF and PF Relays

The results in Figures 2.8-2.10 clearly demonstrate the advantages of PF over MF and AF from the BER perspective when the modulation is PSK and channel estimation is perfect. What would happen when other modulation formats and/or implementation complexity are also taken into consideration? Will PF still be able to maintain its advantages over the other two approaches? Another question is, how can channel estimation be achieved in the proposed MF and PF schemes? We first address the modulation issue.

From the discussion in Section 2.4.1, it should be clear that the proposed PF technique is only applicable to PSK modulations. On the other hand, it is well known that PSK is not as energy efficient when compared to QAM. So a natural question to ask is: how well the proposed PF scheme with PSK modulation actually performs when compared to schemes

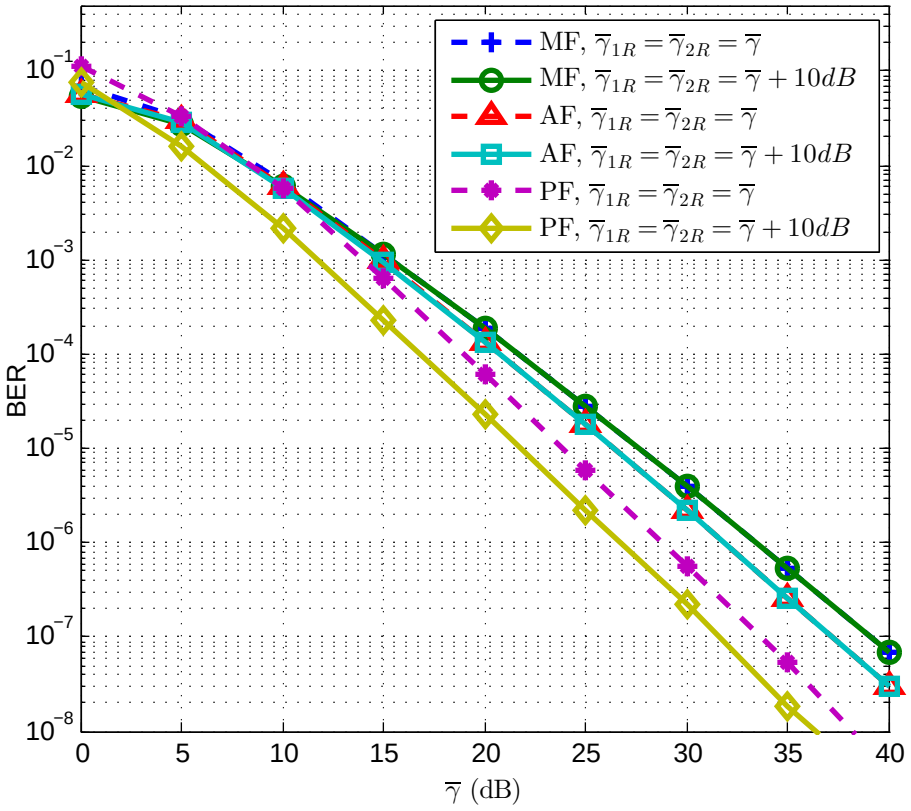

Figure 2.9: BER comparison of PF, MF, and AF as a function of the direct path and downlink's SNR, $\bar{\gamma} = \bar{\gamma}_{21} = \bar{\gamma}_{R1}$. The modulation is BPSK and the SNRs in the uplinks, $\bar{\gamma}_{1R}$ and $\bar{\gamma}_{2R}$, are 10dB stronger than those in the direct path and in the downlink.

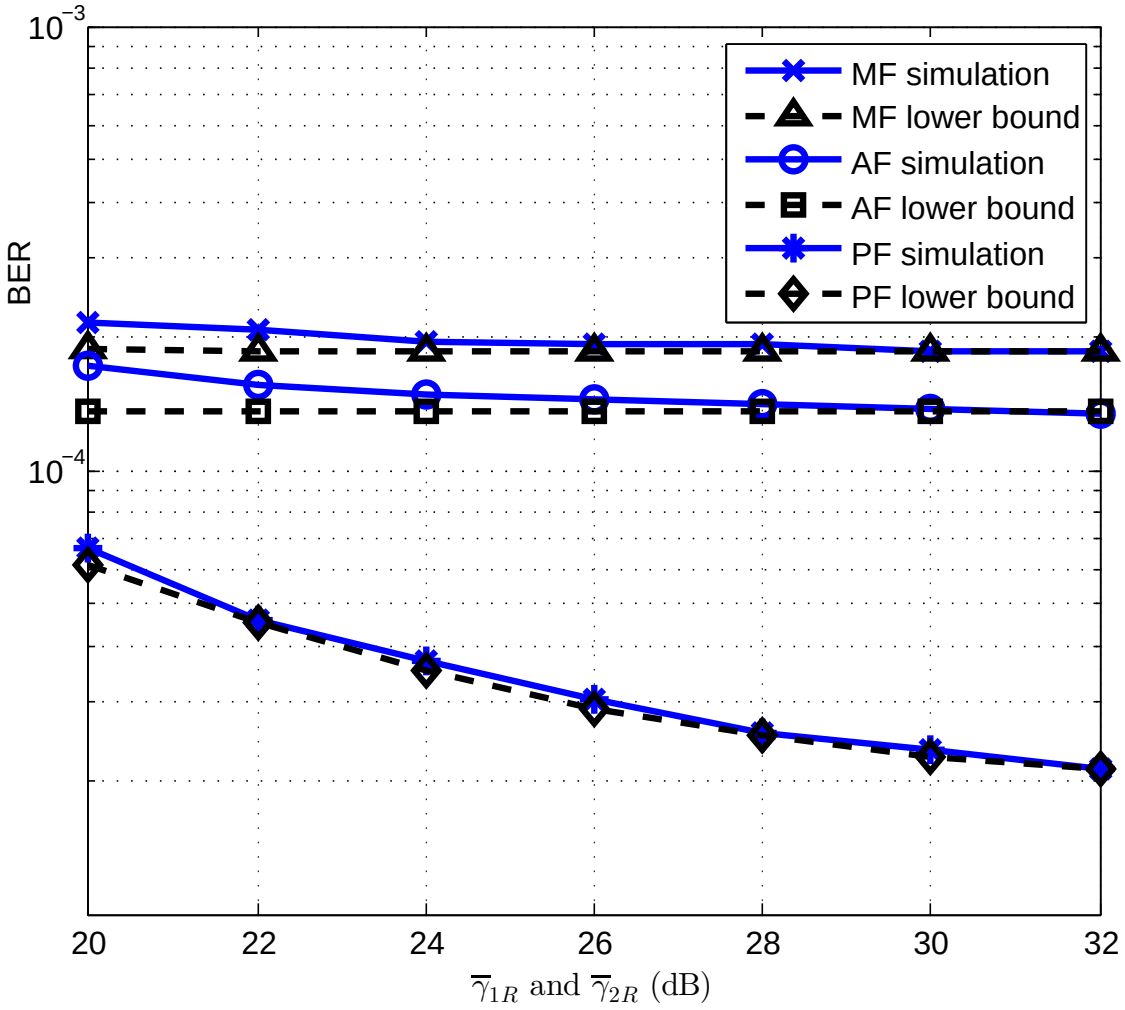

Figure 2.10: BER comparison of PF, MF, and AF at a direct path and downlink SNR of $\bar{\gamma} = \bar{\gamma}_{21} = \bar{\gamma}_{R1} = 20dB$ and varying uplink SNR $\bar{\gamma}_{1R}$, $\bar{\gamma}_{2R}$. The modulation is BPSK.

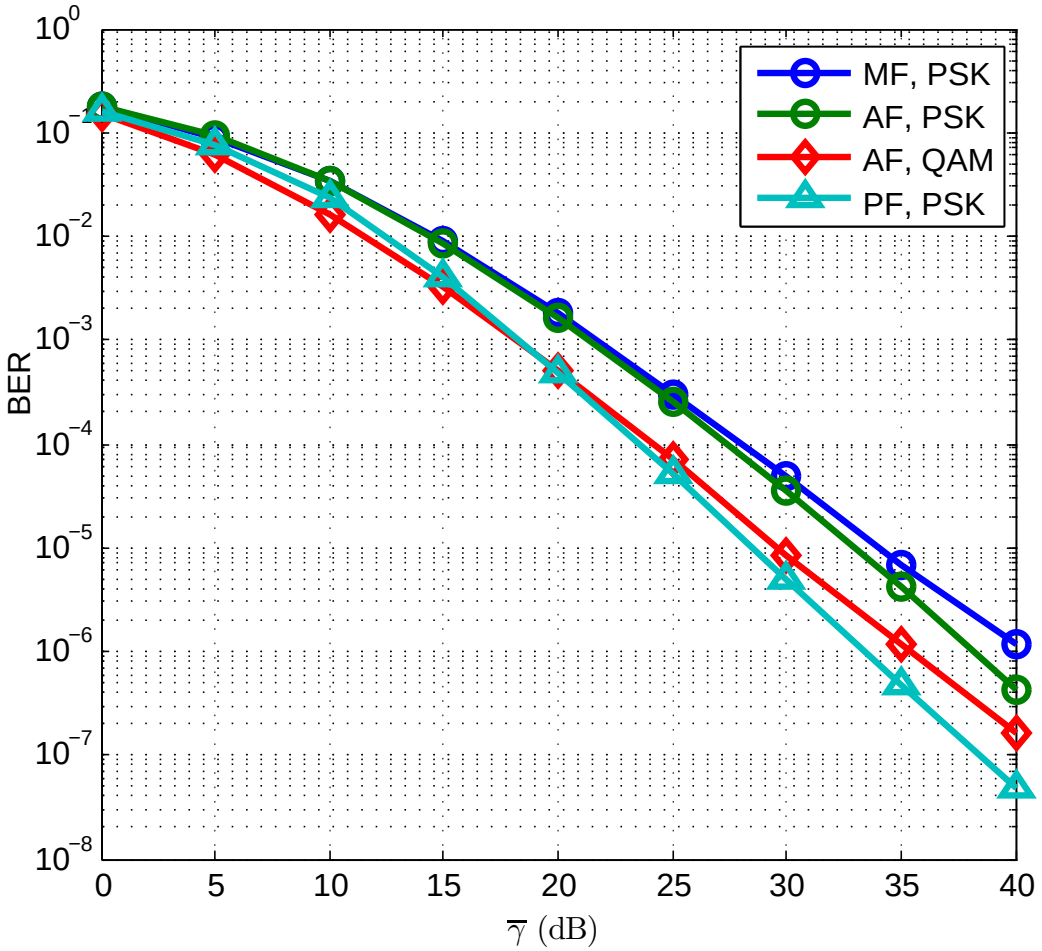

Figure 2.11: BER comparison of AF with (1) 16PSK/QAM, (2) MF with 16PSK, and (3) PF with 16PSK. The direct path and the downlink SNRs are the same, i.e. $\bar{\gamma} = \bar{\gamma}_{21} = \bar{\gamma}_{R1}$, while the uplink SNRs are 10 dB stronger, i.e. $\bar{\gamma}_{1R} = \bar{\gamma}_{2R} = \bar{\gamma} + 10dB$.

that can accommodate QAM, for example AF? The answer to this question is twofold. Firstly, in order to accommodate QAM in AF, the saturation power level of a practical amplifier must be increased dramatically, or, the input signal level in the uplink be backed off sufficiently. The former approach leads to more expensive hardware while the latter leads to a substantial drop in the BER performance. Secondly, we show in Figure 2.11 that the BER of AF with 16QAM using a LPA is actually higher than that of the proposed PF scheme with 16PSK modulation with a saturation level of 3.2 dB. Here an asymmetric channel condition identical to that in Figure 2.9 is considered. It is observed that PF with 16PSK outperforms AF with 16QAM in the high SNR region. This makes PF especially attractive as it has a less stringent requirement on amplifier linearity while at the same time more energy efficient.

Implementation Considerations

We further evaluate AF, MF, and PF from the implementation perspective and compare them against each other and against other alternatives such as DF and physical network coding, which is two-phase. Given all three schemes requires three transmission phases, they have very similar implementation complexity. In all three cases, the signals received in the first two phases must first be stored before they can be added/multiplied and broadcasted in the final phase. As described in Sections 2.2.1, 2.3.1, and 2.4.1, the requirement of signal storage implies the received uplink signals must first be filtered, sampled, and digitized to generate two discrete time signals. Sample-by-sample addition/multiplication of the two stored sequences is then performed to generate a product sample sequence for remodulation in the third phase. Control signaling is required for all these functions to operate properly. Hence, the main difference between a MF and AF relay is that the former employs a multiplier, while the later uses an adder that is simpler to implement. As for the PF relay, as shown in Figure 2.7, it has a hard limiter in additional to the multiplier used in MF relay. At the same time, as shown in the previous sections, MF and PF relays have more relaxed requirement on the linearity of the power amplifier compared to AF relay. The ability to operate under NLPA more than compensates the slight increase in the MF and PF implementation.

Moreover, channel estimation is not required at the MF or PF relay, since no intermediate decisions are made. In contrast, a DF relay needs to estimate the uplink channel gains before coherent demodulation can be performed. This could be an issue if the relay is a mobile unit where signal processing should be kept to a minimum. Note that a DF relay also needs to perform filtering, sampling, and redmodulation, just like the three schemes studied in this chapter. Even in physical network coding, which is two-phase, these operations are required, since most relays used in practice are half-duplex and the sum signal received in the first phase must first be stored before it can be processed and broadcasted in the second phase. In conclusion, there is not much difference amongst various signal forwarding strategies as far as implementation complexity is concerned.

An important application of the proposed relays is to improve network coverage by reducing blind spots in a cellular network. This overlaps with the function of a repeater [51] that has been frequently used to fill the coverage hole near a cell edge [52]. In the

following, we first examine the differences between a repeater and a AF relay since they are similar in processing the received signal. The discussion result is then extended to MF and PF relays.

The two user nodes of a two-way relay can represent a base station and a mobile terminal. Given that the relay is half duplex, at least two hops are needed to transmit a symbol from the base station to the mobile terminal. Specifically, for the three-phase two-way relay depicted in Figure 2.1, it takes 1.5 time slots to transmit a symbol. On the other hand, a repeater is essentially a "one-phase" one-way AF relay transparent to both the base station and mobile terminal, where the received signal is forwarded the same time it is received. This implies 1 time slot to transmit a symbol. Ideally, the repeater has higher throughput compared to the three-phase two-way relays. However, due to the amplification nature of AF relay, the repeater amplifies the noises in the received signals as well. This increases interference levels at both the mobile and base station when a direct path is present [53]. Furthermore, the overall delay profile is complicated by the repeater introduced signal processing delay and the indirect path delay [53]. Consequently, a repeater can cause system performance degradation in terms of increased BER as well inaccurate round trip delay measurement needed for handover. In contrast, while a AF relay amplifies the received noises as well, the noises can be mitigated through MRC at the receiver. Secondly, due to the orthogonal time slot used in transmitting relay signals, the aforementioned interference is avoided. Lastly, the relay path delays can be compensated as the relay is seen by the base station rather than being transparent compared to the repeater. This makes a AF relay more attractive over a repeater. Due to the non-regenerative processing of MF and PF relays, they both share much of the same interference and delay characteristics as the AF relay, except that they have better resistance to the NLPA than the AF relay. The improvement in system performance therefore provides incentives towards the adoption of the proposed relays instead of repeaters.

Channel Estimation Methods

Finally, we briefly discuss how channel estimation can be achieved in the proposed MF and PF systems and the impact of imperfect channel estimation has on system performance. Other references on channel estimation in relay/cooperative communication systems can be found in [32, 33]. As shown in (2.8),(2.11), (2.23), (2.24), (2.34),(2.36), knowledge of the

channel gains g_{1R}, g_{R1}, and g_{2R} are needed for signal detection and combining in AF and the proposed MF and PF protocols. This requires multiple pilot symbols to be inserted per frame of data. Furthermore, the pilot patterns employed in the different links should be orthogonal and mixing of these pilot patterns at the relay should be additive, even when the underlying protocol is MF or PF. One simple and obvious choice of the pilot patterns of users S_1, S_2, and the relay are $\mathbf{p}_1 = [1, 0, 0]$, $\mathbf{p}_2 = [0, 1, 0]$, and $\mathbf{p}_R = [0, 0, 1]$ respectively. Based on the signal models of the cooperative communication systems, the final received pilot symbols at user S_1's terminal is $\hat{\mathbf{p}} = [g_{1R}g_{R1}, g_{2R}g_{R1}, g_{R1}] + \mathbf{n}$, where $\mathbf{n}$ represents the noise terms in the received pilot symbols. The third term in $\hat{\mathbf{p}}$ provides directly an estimate of g_{R1} while dividing the first and second terms by the third term g_{R1} generates estimates of g_{1R} and g_{2R}. It can be shown that if equal gain combining is used instead of MRC, then only two pilot symbols per frame are required for signal detection in AF. For MF and PF, the number of pilot symbols per frame can be further reduced to 1 and mixing of the received uplink pilot symbols can be done multiplicatively.

From the inserted pilot symbols, the channel gains affecting the data symbols can be derived via interpolation. If the amplifier is linear, the channel estimation error arising from this interpolation process can be made quite small, especially with slow fading. When the amplifier is non-linear though, channel estimation in AF can be problematic because the channel estimates derived from the orthogonal pilot patterns $\mathbf{p}_1$ and $\mathbf{p}_2$ mentioned above can be substantially different from the actual gains affecting the data. This stems from the fact the sum of the faded uplink data symbols are not necessarily the same as the sum of the faded pilot symbols of the two users. As such, they will be amplified differently, leading to a mismatch. The result of this mismatch is imperfect self-interference cancellation in AF, and hence an irreducible error floor. While a similar mismatch also exists in the proposed MF protocol, it will only lead to a drop in SNR because of the multiplicative nature of interference cancellation, but not an irreducible error floor. Finally for the proposed PF scheme, amplifier non-linearity creates no problem during channel estimation because of the constant-modulus nature of the forwarded signal. The only source of degradation in this case is the channel noise.

2.5 Conclusion

Amplify-and-forward (AF) is a signal forwarding strategy commonly considered for cooperative communication. We demonstrate in this chapter that when this technique is used in a two-way cooperative network, the distortion introduced by a non-linear power amplifier at the relay can lead to an irreducible error floor. To circumvent this problem, we propose in this chapter two signal forwarding techniques for two-way cooperative communication that offer immunity against non-linear amplifier distortion. The first technique, termed multiply-and-forward (MF), scales the product of the two received signals at the relay before transmitting it over the downlinks to the destinations. The second technique, termed phase-forward (PF), has a similar product structure, except that the amplitude information in the product received signal is discarded (self-induced hard-limiting). Through analysis and simulation, we show in this chapter that both schemes do not exhibit an irreducible error floor even when the amplifier at the relay is non-linear. The PF scheme is particularly attractive as it not only offers immunity against non-linear power amplifier (NLPA) distortion, it can also substantially outperform AF even when a more costly linear power amplifier (LPA) is allowed in the latter system. An amount-of-fading (AoF) analysis is provided to explain this relative performance. In conclusion, MF and PF are suitable signal forwarding strategies for two-way cooperative communication when non-linearity in the amplifier is a concern.

Appendix 2A BER Lower Bound Derivation for the AF and MF Protocols

We derive in this Appendix BER lower bounds for the three-phase two-way AF and MF protocols with a LPA. For simplicity, we assume BPSK modulation at the sources, i.e. $s_1, s_2 \in \{\pm 1\}$. First, let g_i, $i = 1, 2, \ldots, n$, be independent zero mean complex Gaussian random variables with variances of σ_i^2. The random variable

$$X = \prod_{i=1}^{n} |g_i| \geq 0 \tag{2A.1}$$

is known as a cascaded Rayleigh random variable. As shown in [48], the pdf of X can be expressed as

$$p_X(x) = 2\left(2^n\lambda^2\right)^{-\frac{1}{2}} \mathrm{G}_{0,n}^{n,0}\left(\left(2^n\lambda^2\right)^{-1} x^2 \middle| \begin{matrix} - \\ \frac{1}{2},\ldots,\frac{1}{2} \end{matrix}\right), \tag{2A.2}$$

where $\lambda^2 = \prod_{i=1}^{n}\sigma_i^2$ and $\mathrm{G}_{p,q}^{m,n}\left(z \middle| \begin{matrix} a_1, a_2, \ldots, a_p \\ b_1, b_2, \ldots, b_q \end{matrix}\right)$ is the Meijer G function. Let $Y = \prod_{i=1}^{n}|g_i|^2$ be the square of X. It can be shown that the pdf of Y is

$$p_Y(y) = \frac{1}{\sqrt{y}}\left(2^n\lambda^2\right)^{-\frac{1}{2}} \mathrm{G}_{0,n}^{n,0}\left(\left(2^n\lambda^2\right)^{-1} y \middle| \begin{matrix} - \\ \frac{1}{2},\ldots,\frac{1}{2} \end{matrix}\right). \tag{2A.3}$$

Using the Laplace transform given in [54, 5.6.3-(1)], the MGF of Y, $\Phi_Y(s) = \mathbb{E}\left[e^{sY}\right]$, can be found equal to

$$\Phi_Y(-s) = \left(2^n\lambda^2 s\right)^{-\frac{1}{2}} \mathrm{G}_{1,n}^{n,1}\left(\left(2^n\lambda^2 s\right)^{-1} \middle| \begin{matrix} \frac{1}{2} \\ \frac{1}{2},\ldots,\frac{1}{2} \end{matrix}\right). \tag{2A.4}$$

Furthermore, using the identity $\mathrm{G}_{p,q}^{m,n}\left(z \middle| \begin{matrix} \mathbf{a}_p + c \\ \mathbf{b}_p + c \end{matrix}\right) = z^c \mathrm{G}_{p,q}^{m,n}\left(z \middle| \begin{matrix} \mathbf{a}_p \\ \mathbf{b}_p \end{matrix}\right)$ from [54, 5.4-(4)], we have

$$\mathrm{G}_{1,n}^{n,1}\left(\left(2^n\lambda^2 s\right)^{-1} \middle| \begin{matrix} \frac{1}{2} \\ \frac{1}{2},\ldots,\frac{1}{2} \end{matrix}\right) = \left(2^n\lambda^2 s\right)^{-\frac{1}{2}} \mathrm{G}_{1,n}^{n,1}\left(\left(2^n\lambda^2 s\right)^{-1} \middle| \begin{matrix} 0 \\ 0,\ldots,0 \end{matrix}\right). \tag{2A.5}$$

Consequently, $\Phi_Y(-s)$ can be further simplified to

$$\Phi_Y(-s) = \left(2^n\lambda^2 s\right)^{-1} \mathrm{G}_{1,n}^{n,1}\left(\left(2^n\lambda^2 s\right)^{-1} \middle| \begin{matrix} 0 \\ 0,\ldots,0 \end{matrix}\right). \tag{2A.6}$$

Next, we will show how to make use of the result in (2A.6) to determine the BER of AF and MF with a LPA. In both cases, the instantaneous SNR in the decision variable is of the form

$$\gamma = \frac{G^2}{N_0}Y + \frac{1}{N_0}Z, \tag{2A.7}$$

where $Y = \prod_{i=1}^{n}|g_i|^2$, with $n = 2$, $G = G_{AF}$, and $\lambda^2 = \sigma_{R1}^2\sigma_{2R}^2$ for AF, $n = 3$, $G = G_{MF}$, and $\lambda^2 = \sigma_{1R}^2\sigma_{2R}^2\sigma_{R1}^2$ for MF, and Z is an exponential random variable with a pdf of $f_Z(z) = (2\sigma_{21})^{-1}\exp(-z/\sigma_{21}^2)$, $z \geq 0$. The MGF of Z can be easily shown to be

$$\Phi_Z(s) = \frac{1}{1 - 2\sigma_{21}^2 s}. \tag{2A.8}$$

Using the MGF approach [47], this averaging of the conditional BER can be expressed in terms of a single integral as

$$P_e = \frac{1}{\pi}\int_0^{\frac{\pi}{2}} \Phi_Y\left(-\frac{G}{2N_0\sin^2\theta}\right)\Phi_Z\left(-\frac{1}{2N_0\sin^2\theta}\right)d\theta. \tag{2A.9}$$

After substituting (2A.6) and (2A.8) into (2A.9), the average BER becomes

$$P_e = \frac{1}{\pi}\int_0^{\frac{\pi}{2}} \frac{2\sin^2\theta}{2^n G^2\lambda^2/N_0}\mathrm{G}_{1,n}^{n,1}\left(\frac{2\sin^2\theta}{2^n G^2\lambda^2/N_0}\middle| \begin{matrix} 0 \\ 0,\ldots,0 \end{matrix}\right)\frac{\sin^2\theta}{\sin^2\theta+\bar{\gamma}_{21}}d\theta, \tag{2A.10}$$

where $\bar{\gamma}_{21} = \sigma_{21}^2/N_0$. Now, by expressing the term $\sin^2\theta/(\sin^2\theta+\bar{\gamma}_{21})$ as the infinite series

$$\frac{\sin^2\theta}{\sin^2\theta+\bar{\gamma}_{21}} = \sum_{k=0}^{\infty}\frac{(-1)^k(\sin^2\theta)^{k+1}}{\bar{\gamma}_{21}^{k+1}} \tag{2A.11}$$

and by making use of [54, 5.6.4-(19)] to solve the above integral, we can express the average BER in terms of an infinite sum of the Meijer G-functions and obtain

$$\begin{aligned} P_e =& \frac{1}{\sqrt{\pi}2^n G^2\lambda^2/N_0}\sum_{k=0}^{\infty}\frac{(-1)^k}{\bar{\gamma}_{21}^{k+1}}\mathrm{G}_{2,n+1}^{n,2}\left(\frac{N_0}{2^{n-1}G^2\lambda^2}\middle| \begin{matrix} -(k+\frac{3}{2}),0 \\ \underbrace{0,\ldots,0}_{n},-(k+2) \end{matrix}\right) \\ \approx& \frac{1}{\sqrt{\pi}2^n G^2\lambda^2/N_0}\sum_{k=0}^{K_T}\frac{(-1)^k}{\bar{\gamma}_{21}^{k+1}}\mathrm{G}_{2,n+1}^{n,2}\left(\frac{N_0}{2^{n-1}G^2\lambda^2}\middle| \begin{matrix} -(k+\frac{3}{2}),0 \\ \underbrace{0,\ldots,0}_{n},-(k+2) \end{matrix}\right). \end{aligned} \tag{2A.12}$$

Although there are infinite number of terms in the series, for all practical purpose, we can truncate it to a finite number of terms. Table 2.1 compares the numerical results obtained from numerical integration of (2A.10) and those obtained from (2A.12) at different SNRs. It is observed that using 6 terms in the series ($k = 0$ to $K_T = 5$ in (2A.12)) is sufficient to yield results that are almost identical to those obtained from numerical integration for SNR greater than 5dB.

Appendix 2B Diversity Order

The diversity order can be found by evaluating the following limit

$$\eta = -\lim_{\bar{\gamma}\to\infty}\frac{\log P_e(\bar{\gamma})}{\log\bar{\gamma}}, \tag{2B.1}$$

Table 2.1: Truncated series representation of the BER for (a) AF with a LPA ($n = 2$) and (b) MF with a LPA ($n = 3$)

SNR (dB)	Numerical integration $n = 2$ in (2A.10)	Truncated series $n = 2$ and $K_T = 5$ in (2A.12)	Numerical integration $n = 3$ in (2A.10)	Truncated series $n = 3$ and $K_T = 5$ in (2A.12)
0	1.0326e-01	6.5749e-02	1.0848e-01	7.0062e-02
5	3.0302e-02	3.1003e-02	3.1591e-02	3.2344e-02
10	6.0181e-03	6.0649e-03	6.5503e-03	6.6030e-03
15	9.6231e-04	9.6468e-04	1.1584e-03	1.1614e-03
20	1.3591e-04	1.3602e-04	1.8639e-04	1.8654e-04

where $P_e(\bar{\gamma})$ is the BER expression and $\bar{\gamma}$ is the average SNR. For the MF protocol, we can use the integral form of the BER in (2A.10) with $n = 3$, $G = G_{MF}$, and $\lambda^2 = \sigma_{1R}^2\sigma_{2R}^2\sigma_{R1}^2$. Further, in oder to show the diversity order in terms of $\bar{\gamma}$, we set $\sigma_{1R}^2 = \sigma_{2R}^2 = \sigma_{R1}^2 = \sigma^2$ and $\bar{\gamma} = \sigma^2/N_0$. Now, $P_e(\bar{\gamma})$ can be written as

$$P_e(\bar{\gamma}) = \frac{1}{\pi}\int_0^{\frac{\pi}{2}} \frac{\sin^4\theta(\bar{\gamma}+1)^2}{\bar{\gamma}^3(\sin^2\theta+\bar{\gamma})} \mathrm{G}_{1,3}^{3,1}\left(\frac{\sin^2\theta(\bar{\gamma}+1)^2}{\bar{\gamma}^3}\middle| \begin{matrix} 0 \\ 0,0,0 \end{matrix}\right) d\theta, \tag{2B.2}$$

Since the Meijer G-function is analytic [55], we can see that the integrand in (2B.2) is continuous over the range of integration. Consequently, the integral in $P_e(\bar{\gamma})$ can be eliminated based on mean value theorem

$$P_e(\bar{\gamma}) = \frac{\sin^4\theta_c(\bar{\gamma}+1)^2}{2\bar{\gamma}^3(\sin^2\theta_c+\bar{\gamma})} \mathrm{G}_{1,3}^{3,1}\left(\frac{\sin^2\theta_c(\bar{\gamma}+1)^2}{\bar{\gamma}^3}\middle| \begin{matrix} 0 \\ 0,0,0 \end{matrix}\right), \tag{2B.3}$$

where $\theta_c \in [0, \pi/2]$. At $\bar{\gamma}$ approaches infinity, the argument to the Meijer G function in the above equation approaches zero. Using Mathematica, we can have the following series representation of the above Meijer G function at $x = 0$,

$$F(x) = \mathrm{G}_{1,3}^{3,1}\left(x\middle| \begin{matrix} 0 \\ 0,0,0 \end{matrix}\right) = \frac{\ln^2(x)}{2} + 2\gamma_e\ln(x) + 2\gamma_e^2 + \frac{\pi^2}{3} + O(x), \tag{2B.4}$$

where γ_e is the Euler-Mascheroni constant. This means that as x approaches zero, the Meijer G function approaches infinity.

At high SNR, (2B.3) can be approximated by

$$P_e(\bar{\gamma}) = \frac{\sin^4\theta_c}{2\bar{\gamma}^2} \mathrm{G}_{1,3}^{3,1}\left(\frac{\sin^2\theta_c}{\bar{\gamma}}\middle| \begin{matrix} 0 \\ 0,0,0 \end{matrix}\right). \tag{2B.5}$$

To prepare the calculation of the diversity order, we consider the following series expansion of the $F'(x)/F(x)$ at $x = 0$ that is obtained from Mathematica.

$$\frac{\mathrm{G}_{1,3}^{3,1}\left(x\middle|\begin{matrix}0\\1,0,0\end{matrix}\right)}{\mathrm{G}_{1,3}^{3,1}\left(x\middle|\begin{matrix}0\\0,0,0\end{matrix}\right)} = -\frac{6\ln x + 2\gamma_e}{3\ln^2 x + 12\gamma_e \ln x + 12\gamma_e^2 + 2\pi^2} + O(x) \tag{2B.6}$$

Taking the limit of the above ratio at zero using L'Hopital's rule, we have

$$\lim_{x\to 0} \frac{\mathrm{G}_{1,3}^{3,1}\left(x\middle|\begin{matrix}0\\1,0,0\end{matrix}\right)}{\mathrm{G}_{1,3}^{3,1}\left(x\middle|\begin{matrix}0\\0,0,0\end{matrix}\right)} = -\lim_{\bar{\gamma}\to\infty} \frac{6}{6\ln x + 12\gamma_e} = 0 \tag{2B.7}$$

Substituting (2B.5) into (2B.1) and using (2B.7) when applying L'Hopital's rule, we have

$$\begin{aligned}\eta =& -\lim_{\bar{\gamma}\to\infty} \frac{\log\left(\frac{1}{2}\sin^4\theta_c\right)}{\log\bar{\gamma}} - \lim_{\bar{\gamma}\to\infty} \frac{\log\bar{\gamma}^{-2}}{\log\bar{\gamma}} - \lim_{\bar{\gamma}\to\infty} \frac{\mathrm{G}_{1,3}^{3,1}\left(\frac{\sin^2\theta_c}{\bar{\gamma}}\middle|\begin{matrix}0\\1,0,0\end{matrix}\right)}{\mathrm{G}_{1,3}^{3,1}\left(\frac{\sin^2\theta_c}{\bar{\gamma}}\middle|\begin{matrix}0\\0,0,0\end{matrix}\right)} \\ =& 2. \end{aligned} \tag{2B.8}$$

Thus, the diversity order of MF protocol is 2.

Similar to the MF protocol, by settting a common $\bar{\gamma}$, we can first express the BER of the PF protocol by substituting (2.40) into (2.39a) and using [55, 8.486-(10)],

$$\begin{aligned}P_e(\bar{\gamma}) =& \frac{1}{\pi}\int_0^{\frac{\pi}{2}}\int_0^{\frac{\pi}{2}} \frac{1}{1+\bar{\gamma}/\sin^2\theta} J_0\left(\sqrt{\frac{2\tan\xi}{\sin^2\theta}}\right) \\ &\times \frac{6\tan\xi\sec^2\xi}{\bar{\gamma}^2} K_1^2\left(\sqrt{\frac{2\tan\xi}{\bar{\gamma}}}\right) K_0\left(\sqrt{\frac{2\tan\xi}{\bar{\gamma}}}\right) d\xi d\theta \end{aligned} \tag{2B.9}$$

Using the mean value theorem, we can rewrite the BER expression in product terms

$$P_e(\bar{\gamma}) = \frac{A}{1+\bar{\gamma}/\sin^2\theta_c} \frac{1}{\bar{\gamma}^2} K_1^2\left(\sqrt{\frac{2\tan\xi_c}{\bar{\gamma}}}\right) K_0\left(\sqrt{\frac{2\tan\xi_c}{\bar{\gamma}}}\right), \tag{2B.10}$$

where A is a constant and $\xi_c, \theta_c \in [0, \pi/2]$. Substituting (2B.10) into (2B.1) and using L'Hopital's rule, we have the following result by noticing that $\lim_{x\to 0} xK_0(x) = 0$ and $\lim_{x\to 0} xK_1(x) = 1$,

$$\begin{aligned}\eta =& -\lim_{\bar{\gamma}\to\infty} \frac{\log\left(\frac{A}{1+\bar{\gamma}/\sin^2\theta_c}\right)}{\log\bar{\gamma}} - \lim_{\bar{\gamma}\to\infty} \frac{\log\bar{\gamma}^{-2}}{\log\bar{\gamma}} \\ & - \lim_{\bar{\gamma}\to\infty} \frac{\log K_1^2\left(\sqrt{\frac{2\tan\xi_c}{\bar{\gamma}}}\right)}{\log\bar{\gamma}} - \lim_{\bar{\gamma}\to\infty} \frac{\log K_0\left(\sqrt{\frac{2\tan\xi_c}{\bar{\gamma}}}\right)}{\log\bar{\gamma}} \\ =& 2. \end{aligned} \tag{2B.11}$$

This shows the diversity order of PF protocol is also 2.

Appendix 2C Amount of Fading

Consider the random variable (RV) γ whose reciprocal is the sum of the reciprocals of the independent RV's γ_i's

$$\frac{1}{\gamma} = \sum_{i=1}^{L} \frac{1}{\gamma_i}. \tag{2C.1}$$

By substituting (2.40) into (2.39b) and taking the first and second derivatives of $\Phi_\gamma(s)$, the first and second moments of γ can be obtained. From [50], we have

$$\frac{d\Phi_\gamma(s)}{ds} = \int_0^{\frac{\pi}{2}} \sec^2\xi J_0\left(2\sqrt{s\tan\xi}\right) \Phi_{1/\gamma}(\tan\xi)\, d\xi. \tag{2C.2}$$

To derive the second derivative of $\Phi_\gamma(s)$ from (2C.2), first we start with the following

$$\frac{d}{ds} J_0\left(2\sqrt{s\tan\xi}\right) = -J_1\left(2\sqrt{s\tan\xi}\right) s^{-\frac{1}{2}} \tan^{\frac{1}{2}}\xi. \tag{2C.3}$$

Using the series representation of $J_1(\,\cdot\,)$ [55, 8.441-(2)], we can rewrite the above equation as

$$\frac{d}{ds} J_0\left(2\sqrt{s\tan\xi}\right) = \sum_{k=0}^{\infty} \frac{(-1)^{k+1} s^k \tan^{k+1}\xi}{k!(k+1)!}.$$

Consequently, the second derivative is

$$\frac{d^2}{ds^2}\Phi_\gamma(s) = \int_0^{\frac{\pi}{2}} \sec^2\xi \left(\sum_{k=0}^{\infty} \frac{(-1)^{k+1} s^k \tan^{k+1}\xi}{k!(k+1)!}\right) \Phi_{1/\gamma}(\tan\xi)\, d\xi. \tag{2C.4}$$

Substituting $s = 0$ into (2C.2) and (2C.4) allows us to express the first and second moments as

$$m_1 = \left.\frac{d\Phi_\gamma(s)}{ds}\right|_{s=0} = \int_0^{\frac{\pi}{2}} \sec^2\xi \Phi_{1/\gamma}(\tan\xi) d\xi$$
$$= \int_0^{\infty} \Phi_{1/\gamma}(x) dx \tag{2C.5}$$

and

$$m_2 = \left.\frac{d^2\Phi_\gamma(s)}{ds^2}\right|_{s=0} = \int_0^{\frac{\pi}{2}} \sec^2\xi \tan\xi \Phi_{1/\gamma}(\tan\xi) d\xi$$
$$= \int_0^{\infty} x\Phi_{1/\gamma}(x) dx \tag{2C.6}$$

respectively.

The amount-of-fading [47] in a wireless channel can be determined from m_1 and m_2 according to

$$AoF = \frac{m_2 - m_1^2}{m_1^2}. \tag{2C.7}$$

For the special case when all the $\bar{\gamma}_i$'s are identical and equal to $\bar{\gamma}$, substituting $\Phi_{1/\gamma}(s)$ into (2C.5) and (2C.6) and evaluate the resultant equations using the Symbolic toolbox in Mathematica, we obtain the following analytical equation for the two moments:

$$m_1 = \frac{\sqrt{\pi}\bar{\gamma}}{8} \mathrm{G}_{3,3}^{3,2}\left(4 \left| \begin{matrix} \frac{1}{2}, \frac{3}{2}, 3 \\ \frac{3}{2}, \frac{5}{2}, \frac{7}{2} \end{matrix} \right.\right),$$

and

$$m_2 = \frac{\sqrt{\pi}\bar{\gamma}^2}{16} \mathrm{G}_{3,3}^{3,2}\left(4 \left| \begin{matrix} \frac{1}{2}, \frac{3}{2}, 4 \\ \frac{5}{2}, \frac{7}{2}, \frac{9}{2} \end{matrix} \right.\right).$$

Consequently, the AoF in (2C.7) is

$$AoF = \frac{4\mathrm{G}_{3,3}^{3,2}\left(4 \left| \begin{matrix} \frac{1}{2}, \frac{3}{2}, 4 \\ \frac{5}{2}, \frac{7}{2}, \frac{9}{2} \end{matrix} \right.\right)}{\sqrt{\pi}\mathrm{G}_{3,3}^{3,2}\left(4 \left| \begin{matrix} \frac{1}{2}, \frac{3}{2}, 3 \\ \frac{3}{2}, \frac{5}{2}, \frac{7}{2} \end{matrix} \right.\right)^2} - 1 \approx 0.6969, \tag{2C.8}$$

and is independent of $\bar{\gamma}$.

Chapter 3

Multiply-and-Forward and Phase-Forward with DPSK

Differential modulation, with differential detection, does not require explicit estimation of the CSI. Compared to coherent modulation, it therefore has simpler implementation as well as bandwidth saved from not sending pilot symbols. In relays with explicit self-interference cancellation, typically AF relays, CSI estimation needs to be performed based on the received signals prior to signal detection. Without pilots, current CSI esitmation methods are limited to quasi-static fading channels. Maximum likelihood (ML) detector based relays avoids the CSI estimation by making joint detection of both symbols. Such relays are often associated with relatively high computation complexity. In particular, when the ML is employed at the relay, the decode and re-encode processes associated with high computational complexity undermines the simplicity of the differential modulation. The MF/PF two way relay protocol introduced in the previous chapter has inherent multiplicative self-interference cancellation capability. It has the same form of operation as fading channel de-rotation used in differetial detection. The idea of combining these two operations together can greatly simplify the signal detection in a two way relay system. We explore in this chapter multiplicative two way relays with differential modulation.

3.1 Introduction

As discussed in Chapter 2, two way relay systems are often used with coherent modulation. Coherent modulation requires accurate estimation of the CSI at the user terminals S_1 and S_2 for detection. It is often assumed perfect CSI of all of the channels is available at these nodes. In practice, the knowledge of the CSI is acquired via the transmission of pilot symbols. The overhead created by the pilots reduces the bandwidth efficiency of the cooperative communication system. Secondly, the design of pilot symbols for the two-way relay is challenging when compared to contentional point-to-point communication systems. This motivates the adoption of differential modulation in two way cooperative communications.

Similar to their coherent modulation two way relay counterparts, there are regenerative [56, 57, 58, 59] and non-regeneratvie [59, 60, 61] relays with differential modulation. Without CSI, two approaches are used in signal detection. The first approach is maximum likelihood (ML) based. In [59], a ML based detector is derived to detect the signal directly at the user terminal in the last phase. Though the ML based detector was derived for both AF and DF relays, it has relatively high computaton complexity and is based on the assumption of quasi-static fading and reciprocal channels. In [56], an approximation of the ML detector using a multiuser detector is proposed to denoise-and-forward (DNF) the received signals at the relay. Quasi-static channel is also assumed for the ML detector. When multiple relays are available in the DNF two way relay system, post combining is possible via hard decision on each relay path, while soft decision doesn't seem viable. Differential distributed space-time coding (DDSTC) has been considered in [57, 58]. In [57], the three-phase relaying scheme requires double transmission of information symbols, which is drawn from an expanded source constellation, in order to allow the relay to extract data from each source node. In [58], the 2P protocol first selects two relays that are making correct joint dectection on the two user terminal symbols and then encodes the DDSTC symbols for broadcasting in the second phase.

The second aproach to detect DPSK signals in a two way relay is to perform self-interference cancellation before signal detection. When AF relays are used, common practice is to exploit orthogonality among signal expectations and estimate the CSI via time averages [60, 61] over a data frame. In [60], two time averages are made to remove self-interference. In

[61], a single time average is made to perform self-interference cancellation. In both cases, the time average based self-interference cancellation methods are limited by two factors. First, the methods are intended to work at quasi-static fading environment or at very slow fading environment, e.g. with fade rate up to 2×10^{-4} in [61]. Secondly, due to the time average processing during CSI estimation, a frame delay is inevitable at the receiving user terminal.

In this chapter, we extend the MF relay protocol from the last chapter to MDPSK modulation. Compared to the self-interference cancellation using time averages, our proposed MF relay, as will be shown later, has simple forwarding operation at the relay as well as simple self-interference cancellation at the user terminals. Consequently, this procedure can be performed without frame delay before sigal combining. Moreover, as opposed to the quasic-static channel assumption made in the existing methods, the MF relay works in a fast fading environment, just as conventional "two symbol" differential detection. The structure of the MF two way relay is the same as a multi-diversity point-to-point DPSK system. The only difference is that the relay path signal is a noisy copy of the source transmitted signal and is multiplied by a noisy copy of the self-interference.

The chapter is organized as follows. We first introduce in Section 3.2 the signal and system model for the MF three-phase two-way relay system with differential modulation. Further, the concept of PF relay is also considered with DPSK modulation. In Section 3.3, the BER performace of the DPSK MF and PF relays are analyzed under the static and time varying fading assumptions. An analysis of the diversity order of the MF relay is also provided. Without the CSI estimation overhead that is needed in the coherent MF relay system, the DPSK MF relay has better scalability. Section 3.4 generalizes the DPSK MF relay to multiple relays with a theoretical analysis on the BER and diveristy order. Section 3.5 presents simulation results for the DPSK MF and PF relay systems under various channel conditions, including time-selective fading. The effect of NLPA is also examined to ensure that the DPSK MF relay protocol is resistant to NLPA. Finally, Section 3.6 summarizes this chapter and provides future work direction.

3.2 System Model

The three-phase two-way relay cooperative system using DPSK modulation share the same structure as the one in Section 2.2, except that the self-information cancellation and detection are modfied for MDPSK modulation. The signal structures are identical to those in Chapter 2 except that we now have to introduce a time-index k for differential encoding and decoding. Specifically, we have

$$y_{ij}[k] = g_{ij}[k]s_i[k] + n_{ij}[k], \tag{3.1}$$

where $s_i[k]$ is a differentially encoded symbol and i, j are from $\{1, 2, R\}$, $i \neq j$. The transmitted symbol $s_i[k]$'s, $i \in \{1, 2\}$, are differentially modulated according to

$$s_i[k] = s_i[k-1]d_i[k], \tag{3.2}$$

where the data symbol $d_i[k]$ is drawn from the PSK symbol set $X = \{e^{j\frac{2\pi(k-1)}{M}}\}_{k=1}^{M}$ with equal probability. Further the average power of $s_i[k]$ is $P_s = \frac{1}{2}\mathbb{E}\big[|s_i[k]|^2\big] = \frac{1}{2}$, and the $g_{ij}[k]$'s and $n_{ij}[k]$'s follow the same naming conventions in Section 2.2.

At user S_1, the received direct path signal is a conventional point-to-point DPSK modulated signal, which has a decision variable of

$$D_{21} = y_{21}^*[k-1]y_{21}[k]. \tag{3.3}$$

At the relay, the two received signals $y_{1R}[k]$ and $y_{2R}[k]$ are multiplied and scaled for broadcasting in the third phase similarly to the MPSK modulation in (2.20).

$$s_R[k] = G_{MF}\, y_{1R}[k]y_{2R}[k], \qquad \text{(DPSK MF)} \tag{3.4}$$

where G_{MF} is a scalar used to regulate the average transmit power at the relay. Specifically, it is given by (2.21) since the transmitted DPSK signals have the same power as the PSK signals.

In the last phase, assuming a LPA at the relay, the received signal at S_1 can be expanded by substituting (3.1) and (3.4) into $y_{R1}[k]$,

$$\begin{aligned} y_{R1}[k] =& g_{R1}[k]\, s_R[k] + n_{R1}[k] \\ =& G_{MF}\, g_{R1}[k](g_{1R}[k] + n_{1R}[k])(g_{2R}[k] + n_{2R}[k])s_1[k]\, s_2[k] + n_{R1}[k], \end{aligned} \tag{3.5}$$

where once again, we extract $s_1[k]$ and $s_2[k]$ from the received uplink samples $g_{1R}[k]s_1[k] + n_{1R}[k]$ and $g_{2R}[k]s_2[k] + n_{2R}[k]$, just like we did earlier in Section 2.3. It is obvious that the differentially encoded symbols $s_1[k]$ and $s_2[k]$ are simply multiplied. This structure of the signal makes self-interference differential detection simple.

To understand how self-interference cancellation can be performed in the proposed DPSK MF relay system, lets first rewrite (3.5) as

$$y_{R1}[k] = g_\alpha[k]\, s_1[k]\, s_2[k] + n_{R1}[k], \tag{3.6}$$

where

$$g_\alpha[k] = G_{MF}\, g_{R1}[k](g_{1R}[k] + n_{1R}[k])(g_{2R}[k] + n_{2R}[k]) \tag{3.7}$$

is the effective channel gain in the downlink whose phase is unknown to the users detector. To remove the effect of this unknown phase and to perform self-interference cancellation, user S_1's detector multiplies $y_{R1}[k]$ by $(y_{R1}[k-1]\, d_1[k])^*$ to obtain the decision statistics

$$\begin{aligned} D_{R1}[k] =&\ (y_{R1}[k-1]\, d_1[k])^* y_{R1}[k] \\ =&\ g_\alpha^*[k-1]g_\alpha[k]d_2[k] + g_\alpha^*[k-1]n_{R1}[k] + g_\alpha[k]n_{R1}^*[k-1] + n_{R1}^*[k-1]n_{R1}[k], \end{aligned} \tag{3.8}$$

where the differential encoding rule in (3.2) is used to arrive at the second line of the equation. In the ideal case of large SNR and relatively static fading, $g_\alpha[k] = g_\alpha[k-1]$ and hence $g_\alpha[k]g_\alpha^*[k-1] \approx |G_{MF}\, g_{R1}[k]\, g_{1R}[k]\, g_{2R}[k]|^2$, which has zero phase. This allows the detection of user S_2's data symbol in (3.8).

In coherent two-way relay, we assume perfect CSI is avialable for all links. However, with differential modulation, such information is not available, and we use equal gain combining (EGC) [47] to combine the relay path decision variable (3.8) with the direct path decision variable (3.3) to form the final decision variable $D[k]$,

$$D[k] = D_{21}[k] + D_{R1}[k], \tag{3.9}$$

where $D_{21}[k]$ and D_{R1} are given by (3.3) and (3.8), respectively. The decision is then made according to (2.12).

3.2.1 DPSK PF Relay

In the previous chapter, though the coherent modulated MF relay has shown good resistance to NLPA, it performs worse than AF relay by 1.5 dB in terms of BER when LPA is available. The PF relay was consequently developed to achieve better BER performance than MF protocol under both LPA and NLPA. Due to the multiplicative nature of its signal combining at the relay, the PF relay is expected to work with differential modulation in a similar fashion as the MF relay. In this section, we explore the idea of combining PF protocol with DPSK modulation.

The DPSK modulated PF relay shares much of the same operations as the DPSK MF relay, except the signal combining function at the relay for transmission in the last phase. Specifically, in the first two phases of the DPSK PF relay, each of the user terminals S_1 and S_2 transmits in turn following the same procedure as the DPSK MF relay. In the third phase, the DPSK PF relay performs the additional hard limiting operation on the transmitted signal of the MF relay in (3.4) to obtain

$$s_R[k] = e^{j\psi_{1R}[k]} e^{j\psi_{1R}[k]} s_1[k]\, s_2[k], \qquad \text{(DPSK PF)} \quad (3.10)$$

where $\psi_{iR}[k]$ is the phase of the received signal in the first two phases

$$\psi_{iR}[k] = \arg[g_{iR} + n_{iR}], i \in \{1, 2\}, \quad (3.11)$$

and $s_i[k]$ is the differentially encoded transmitted symbols given by (3.2). Considering a LPA relay, the received signal y_{R1} at S_1 can be expressed as

$$\begin{aligned} y_{R1}[k] =& g_{R1}[k] e^{j\psi_{1R}[k]} e^{j\psi_{1R}[k]} s_1[k]\, s_2[k] + n_{R1}[k] \\ =& g_\beta[k]\, s_1[k]\, s_2[k] + n_{R1}[k], \end{aligned} \quad (3.12)$$

where $g_\beta[k]$

$$g_\beta[k] = g_{R1}[k] e^{j\psi_{1R}[k]} e^{j\psi_{1R}[k]} \quad (3.13)$$

is the overall channel gain on the relay path. Similar to the MF relay, the unknown channel gain in $g_\beta[k]$ and self-interference are removed by multiplying $y_{R1}[k]$ by $(y_{R1}[k-1]\, d_1[k])^*$ to

obtain

$$\begin{aligned} D_{R1}[k] =& \ (y_{R1}[k-1]\, d_1[k])^* y_{R1}[k] \\ =& \ g_\beta^*[k-1] g_\beta[k] d_2[k] + g_\beta^*[k-1] n_{R1}[k] + g_\beta[k] n_{R1}^*[k-1] + n_{R1}^*[k-1] n_{R1}[k], \end{aligned} \tag{3.14}$$

where the symbols $d_1[k]$, $s_1[k]$ and $s_2[k]$ are absorbed in the noise terms. For large uplink $\bar{\gamma}_{1R}$ and $\bar{\gamma}_{2R}$, the relay can be approximated as noise free and consequently $\phi_{1R}[k]$ and $\phi_{2R}[k]$ vanishes in (3.13). Further, with static fading, $g_\beta[k]$ is equvalent to $g_{R1}[k]$ since $\psi_{1R}[k]$ and $\psi_{2R}[k]$ are constant phase offsets and don't affect the decision. This implies that the relay path signal of the PF protocol is equivalent to a conventional fading channel under the assumption of static fading and large uplink SNRs. Combined with direct path signal, the BER performance of DPSK PF relay can potentially approach that of a conventional point-to-point two branch DPSK system.

Without out exact channel information, we combine the direct path decision variable D_{21} given by (3.3) and the relay path decision variable D_{R1} in (3.14) through addition

$$D[k] = D_{21}[k] + D_{R1}[k], \tag{3.15}$$

The decision is then made according to (2.12).

3.3 BER Performance

In this section, we study the BER performance of the proposed DPSK modulated MF and PF two way relays. First, we provide a BER lower bound for the the MF protocol under the assumption of a LPA at the relay using the results developed in Appendix 2A. Next, an exact BER analysis of the DPSK PF two way relay is given using the characteristic function (CF) approach. The analytic results are duely verified by simulation in section 3.5 with discussions.

3.3.1 DPSK MF relay

We consider an ideal noiseless relay to obtain a lower bound on the BER. Further, static fading is assumed in all the links. Since this scenario corresponds to a second order

diversity BDPSK system with independent fading gains $g_{21}[k]$ and $g_{\alpha}[k]$, the corresponding conditional BER can be found in [62, 47] and is reproduced below as

$$P_e\left(\gamma_{21},\gamma_{MF}\right)=\frac{1}{2}e^{-(\gamma_{21}+\gamma_{MF})}+\frac{1}{8}(\gamma_{21}+\gamma_{MF})e^{-(\gamma_{21}+\gamma_{MF})}, \tag{3.16}$$

where γ_{21} is the direct path instantaneous SNR and γ_{MF} is the effective SNR in the relay path. Specifically,

$$\begin{aligned}\gamma_{21}&=\frac{|g_{21}|^2}{N_0}\\ \gamma_{MF}&=\frac{G_{MF}^2}{N_0}|g_{1R}|^2|g_{2R}|^2|g_{R1}|^2\end{aligned} \tag{3.17}$$

Averaging the conditional SNR in (3.16) over the pdfs of γ_{21} and γ_{MF} gives the BER lower bound of the relay system. In [47], the average BER of DPSK with diversity reception is derived from the product form representation of the conditional BER using the MGF method. This approach leads to a single finite integral when the diversity order is high. For smaller diversity orders, such as the case of a single two way relay system at hand involving only one relay, we can use the summation form of $P_e\left(\gamma_{21},\gamma_{MF}\right)$ in (3.16) directly. Adopting the later approach leads to an exact expression with just a few terms, avoiding integration in the result.

First, the average BER P_e is obtained by averaging $P_e\left(\gamma_{21},\gamma_{MF}\right)$ over the joint pdf of $p(\gamma_{21},\gamma_{MF})$, which is $p(\gamma_{21})p(\gamma_{MF})$ based on the channel independence assumption,

$$\begin{aligned}P_e=&\mathbb{E}[P_e\left(\gamma_{21},\gamma_{MF}\right)]\\ =&\int_0^{+\infty}\int_0^{+\infty}P_e\left(\gamma_{21},\gamma_{MF}\right)p(\gamma_{21})p(\gamma_{MF})d\gamma_{21}d\gamma_{MF}\\ =&\frac{1}{2}\int_0^{+\infty}e^{-\gamma_{21}}p(\gamma_{21})d\gamma_{21}\int_0^{+\infty}e^{-\gamma_{MF}}p(\gamma_{MF})d\gamma_{MF}\\ &+\frac{1}{8}\int_0^{+\infty}\gamma_{21}e^{-\gamma_{21}}p(\gamma_{21})d\gamma_{21}\int_0^{+\infty}e^{-\gamma_{MF}}p(\gamma_{MF})d\gamma_{MF}\\ &+\frac{1}{8}\int_0^{+\infty}e^{-\gamma_{21}}p(\gamma_{21})d\gamma_{21}\int_0^{+\infty}\gamma_{MF}e^{-\gamma_{MF}}p(\gamma_{MF})d\gamma_{MF}\end{aligned} \tag{3.18}$$

By recognizing that each of the integral in the above equation can be expressed as either a MGF or a first derivative of the MGF [63], we can rewrite P_e in (3.18) in terms of the

MGFs evaluated at $s = -1$, i.e.

$$P_e = \frac{1}{2}\Phi_{\gamma_{21}}(-1)\Phi_{\gamma_{MF}}(-1) + \frac{1}{8}\Phi'_{\gamma_{21}}(-1)\Phi_{\gamma_{MF}}(-1) + \frac{1}{8}\Phi_{\gamma_{21}}(-1)\Phi'_{\gamma_{MF}}(-1) \tag{3.19}$$

The MGF and its first order derivative of the direct path's SNR γ_{21} are readily available,

$$\begin{aligned} \Phi_{\gamma_{21}}(s) =& \frac{1}{1-\bar{\gamma}_{21}s} \\ \Phi'_{\gamma_{21}}(s) =& \frac{\bar{\gamma}_{21}}{(1-\bar{\gamma}_{21}s)^2} \end{aligned} \tag{3.20}$$

As for the relay path's SNR γ_{MF} in (3.17), it is the magnitude square of the a cascaded Rayleigh fading term, scaled by $\frac{G_{MF}^2}{2N_0}$. Using (2A.6) from Appendix 2A and [54, (5.5-14)], the MGF and its first order derivative of γ_{MF} are found to be

$$\begin{aligned} \Phi_{\gamma_{MF}}(s) =& (-\zeta s)^{-1}\, \mathrm{G}_{1,3}^{3,1}\left((-\zeta s)^{-1}\middle| \begin{matrix} 0 \\ 0,0,0 \end{matrix}\right) \\ \Phi'_{\gamma_{MF}}(s) =& \frac{(-\zeta s)^{-1}}{-s}\mathrm{G}_{1,3}^{3,1}\left((-\zeta s)^{-1}\middle| \begin{matrix} -1 \\ 0,0,0 \end{matrix}\right), \end{aligned} \tag{3.21}$$

where $\zeta = 2^3\lambda^2\frac{G_{MF}^2}{2N_0}$ and $\lambda^2 = \sigma_{1R}^2\sigma_{1R}^2\sigma_{R1}^2$. By subsituting λ^2 and G_{MF} in (2.21) into the definition of ζ, we have

$$\zeta = \frac{\bar{\gamma}_{1R}\bar{\gamma}_{2R}\bar{\gamma}_{R1}}{(\bar{\gamma}_{1R}+1)\,(\bar{\gamma}_{2R}+1)}. \tag{3.22}$$

Finally, substituting (3.20), (3.21) and (3.22) into (3.19), we arrive at the average BER lower bound of the DPSK modulated MF two way relay

$$P_e = \frac{\mathrm{G}_{1,3}^{3,1}\left(\frac{1}{\zeta}\middle| \begin{matrix} 0 \\ 0,0,0 \end{matrix}\right)}{2\,(1+\bar{\gamma}_{21})\,\zeta}\left[1 + \frac{\bar{\gamma}_{21}}{4\,(1+\bar{\gamma}_{21})} + \frac{1}{4}\mathrm{G}_{1,3}^{3,1}\left(\frac{1}{\zeta}\middle| \begin{matrix} -1 \\ 0,0,0 \end{matrix}\right)\Big/\mathrm{G}_{1,3}^{3,1}\left(\frac{1}{\zeta}\middle| \begin{matrix} 0 \\ 0,0,0 \end{matrix}\right)\right]. \tag{3.23}$$

The BER bound obtained is exact and does not involve any integration. The Meijer G function in the expression can be calculated using software packages such as Matlab or Mathematica.

3.3.2 Diversity Order of DPSK MF Relay

With the average BER obtained from the last section, we can further study the diversity order of the DPSK modulated two way relay system. In particular, if we set $\bar{\gamma}_{1R} = \bar{\gamma}_{2R} =$

$\bar{\gamma}_{R1} = \bar{\gamma}$ in (3.23), then

$$P_e(\bar{\gamma}) = \frac{\frac{1}{\bar{\gamma}} \mathrm{G}_{1,3}^{3,1}\left(\frac{1}{\bar{\gamma}} \middle| \begin{matrix} 0 \\ 0,0,0 \end{matrix}\right)}{2\left(1+\bar{\gamma}\right)} \left[1 + \frac{\bar{\gamma}}{4\left(1+\bar{\gamma}\right)} + \frac{1}{4}\mathrm{G}_{1,3}^{3,1}\left(\frac{1}{\bar{\gamma}} \middle| \begin{matrix} -1 \\ 0,0,0 \end{matrix}\right) \Big/ \mathrm{G}_{1,3}^{3,1}\left(\frac{1}{\bar{\gamma}} \middle| \begin{matrix} 0 \\ 0,0,0 \end{matrix}\right)\right], \quad (3.24)$$

where ζ is replaced by $\bar{\gamma}$ as a large SNR approximation. Now subsitute the above equation into (2B.1) and we have the following,

$$\begin{aligned} \eta = &- \lim_{\bar{\gamma}\to\infty} \frac{\log\left(\frac{1}{2\bar{\gamma}(\bar{\gamma}+1)}\right)}{\log\bar{\gamma}} - \lim_{\bar{\gamma}\to\infty} \frac{\log \mathrm{G}_{1,3}^{3,1}\left(\frac{1}{\bar{\gamma}} \middle| \begin{matrix} 0 \\ 0,0,0 \end{matrix}\right)}{\log\bar{\gamma}} \\ &- \lim_{\bar{\gamma}\to\infty} \frac{\log\left[1 + \frac{\bar{\gamma}}{4(1+\bar{\gamma})} + \frac{1}{4}\mathrm{G}_{1,3}^{3,1}\left(\frac{1}{\bar{\gamma}} \middle| \begin{matrix} -1 \\ 0,0,0 \end{matrix}\right) \Big/ \mathrm{G}_{1,3}^{3,1}\left(\frac{1}{\bar{\gamma}} \middle| \begin{matrix} 0 \\ 0,0,0 \end{matrix}\right)\right]}{\log\bar{\gamma}} \end{aligned} \quad (3.25)$$

The first limit term in the above equation can be easily found to be 2. The second term, based on the previous results in Appendix 2B, is zero. For the last term, we first notice that $1 + \frac{\bar{\gamma}}{4(1+\bar{\gamma})}$ approaches a constant when $\bar{\gamma}$ approaches infinity. For the Meijer G function ratio, using [54, 5.4-(8)], we have

$$\frac{\mathrm{G}_{1,3}^{3,1}\left(x \middle| \begin{matrix} -1 \\ 0,0,0 \end{matrix}\right)}{\mathrm{G}_{1,3}^{3,1}\left(x \middle| \begin{matrix} 0 \\ 0,0,0 \end{matrix}\right)} = \frac{\mathrm{G}_{1,3}^{3,1}\left(x \middle| \begin{matrix} 0 \\ 0,0,0 \end{matrix}\right) - \mathrm{G}_{1,3}^{3,1}\left(x \middle| \begin{matrix} 0 \\ 1,0,0 \end{matrix}\right)}{\mathrm{G}_{1,3}^{3,1}\left(x \middle| \begin{matrix} 0 \\ 0,0,0 \end{matrix}\right)} \quad (3.26)$$

Based on the previous results in Appendix 2B, the above ratio approaches 1 as x approaches zero. Consequently,

$$\lim_{\bar{\gamma}\to\infty} \frac{\log\left[1 + \frac{\bar{\gamma}}{4(1+\bar{\gamma})} + \frac{1}{4}\mathrm{G}_{1,3}^{3,1}\left(\frac{1}{\bar{\gamma}} \middle| \begin{matrix} -1 \\ 0,0,0 \end{matrix}\right) \Big/ \mathrm{G}_{1,3}^{3,1}\left(\frac{1}{\bar{\gamma}} \middle| \begin{matrix} 0 \\ 0,0,0 \end{matrix}\right)\right]}{\log\bar{\gamma}} = \frac{\lim_{\bar{\gamma}\to\infty} \log 1\frac{1}{2}}{\lim_{\bar{\gamma}\to\infty} \log\bar{\gamma}} = 0 \quad (3.27)$$

By now, each of the limits in (3.25) are known. We can therefore arrived at the conclusion that the diversity order of the DPSK modulated two way MF relay system is 2. This means that the DPSK MF relay can fully exploit the diversity available, the same as the AF relay in [60]. Compared to the denoise-and-forward two way relay [56], whose diversity is about half the number of relays, the MF two way relay can fully utilize the diversity available.

Furthermore, compared to DDSTC modulated two-way relay in [58], which also achieves full diversity, the MF relay does not need a relay selection process that requires both CRC decoding and centralized selection.

3.3.3 BER of DPSK PF Relay

In this section we analyze the BER performance of the binary DPSK PF relay protocol using the CF approach. Without loss of generality, assume $d_2[k]$ is $+1$. We begin with the well known result on the direct path decision variable D_{21}, which can be rewritten in matrix format as

$$\begin{aligned} D_{21} &= 2\,\mathfrak{Re}\{y_{21}^*[k-1]y_{21}[k]\} \\ &= \mathbf{y}_{21}^H\,\mathbf{F}\,\mathbf{y}_{21}, \end{aligned} \tag{3.28}$$

where $\mathbf{y}_{21} = [\,y_{21}[k-1]\;\; y_{21}[k]\,]^T$, $\mathbf{F} = \begin{bmatrix} 0 & 1 \\ 1 & 0 \end{bmatrix}$ and $\mathfrak{Re}\{\cdot\}$ is the real operator. Acording to [62], the CF of D_{21} is

$$\Phi_{21}(s) = \frac{1}{\|\mathbf{I} + 2s\mathbf{\Phi}_{21}\mathbf{F}\|}, \tag{3.29}$$

where $\|\cdot\|$ denotes the determinant of a matrix and $\mathbf{\Phi}_{21}$ is the covariance matrix

$$\mathbf{\Phi}_{21} = \frac{1}{2}\mathbb{E}\big[\mathbf{y}_{21}\mathbf{y}_{21}^H\big] = \begin{bmatrix} \sigma_{21}^2 + N_0 & \sigma_{21}^2 J_0 \\ \sigma_{21}^2 J_0 & \sigma_{21}^2 + N_0 \end{bmatrix}, \tag{3.30}$$

where $J_0 = J_0(2\pi f_d T)$. The poles of $\Phi_{21}(s)$ are

$$p_1 = \frac{-1}{2\left(\bar{\gamma}_{21}^2[1 + J_0] + 1\right)N_0} < 0, \tag{3.31}$$

$$p_2 = \frac{1}{2\left(\bar{\gamma}_{21}^2[1 - J_0] + 1\right)N_0} > 0. \tag{3.32}$$

For the relay path, we can similary define $\mathbf{y}_{R1} = [\,y_{R1}[k-1]\,d_1[k]\;\; y_{R1}[k]\,]^T$ and rewrite D_{R1} as

$$\begin{aligned} D_{R1} &= 2\,\mathfrak{Re}\{(y_{R1}[k-1]\,d_1[k])^* y_{21}[k]\} \\ &= \mathbf{y}_{R1}^H\,\mathbf{F}\,\mathbf{y}_{R1}, \end{aligned} \tag{3.33}$$

The corresponding CF is

$$\Phi_{R1}(s) = \frac{1}{\|\mathbf{I} + 2s\mathbf{\Phi}_{R1}\mathbf{F}\|}, \tag{3.34}$$

where

$$\mathbf{\Phi}_{R1} = \frac{1}{2}\mathbb{E}\left[\mathbf{y}_{R1}\mathbf{y}_{R1}^H\right] = \begin{bmatrix} \sigma_{R1}^2 + N_0 & \sigma_{R1}^2 e^{-j(\Delta_{1R}+\Delta_{2R})} J_0 \\ \sigma_{R1}^2 e^{j(\Delta_{1R}+\Delta_{2R})} J_0 & \sigma_{R1}^2 + N_0 \end{bmatrix}, \tag{3.35}$$

where $\Delta_{iR} = \psi_{iR}[k] - \psi_{iR}[k-1]$ for $i \in \{1, 2\}$. Consequently, the correponding poles of $\phi_{R1}(s)$ can be found as

$$Q_1 = \frac{\bar{\gamma}_{R1}^2 J_0 \cos(\Delta_{1R} + \Delta_{2R}) - \sqrt{\left(\bar{\gamma}_{R1}^2 + N_0\right)^2 - \left(\bar{\gamma}_{R1}^2 J_0 \sin(\Delta_{1R} + \Delta_{2R}\right)^2}}{2\left((\bar{\gamma}_{R1}^2 + N_0)^2 - (\bar{\gamma}_{R1}^2 J_0)^2\right) N_0} < 0, \tag{3.36}$$

$$Q_2 = \frac{\bar{\gamma}_{R1}^2 J_0 \cos(\Delta_{1R} + \Delta_{2R}) + \sqrt{\left(\bar{\gamma}_{R1}^2 + N_0\right)^2 - \left(\bar{\gamma}_{R1}^2 J_0 \sin(\Delta_{2R} + \Delta_{2R}\right)^2}}{2\left((\bar{\gamma}_{R1}^2 + N_0)^2 - (\bar{\gamma}_{R1}^2 J_0)^2\right) N_0} > 0. \tag{3.37}$$

As the decision variable in (3.15) is the sum of two independ variables D_{21} from direct path and D_{R1} from relay path, the CF is the product of the two corresponding CFs. Thus the CF of D can be written as

$$\begin{aligned} \Phi_D(s) &= \Phi_{21}(s)\, \Phi_{R1}(s) \\ &= \frac{p_1 p_2 Q_1 Q_2}{(s-p_1)(s-p_2)(s-Q_1)(s-Q_2)}, \end{aligned} \tag{3.38}$$

where the poles are given by (3.31), (3.32), (3.36) and (3.37). Conditioned on Δ_{1R} and Δ_{2R}, the conditional BER of the binary DPSK PF relay is

$$\begin{aligned} Pr\left[D < 0 | \Delta_{1R}, \Delta_{2R}\right] &= -\sum_{p_2, Q_2} Residues\left\{\frac{\Phi_D(s)}{s}\right\} \\ &= \frac{-p_1 Q_1 Q_2}{(p_2-p_1)(p_2-Q_1)(p_2-Q_2)} + \frac{-Q_1 p_1 p_2}{(Q_2-Q_1)(Q_2-p_1)(Q_2-p_2)}. \end{aligned} \tag{3.39}$$

Finally, the average BER can be obtained by averaging (3.39) over Δ_{1R} and Δ_{2R},

$$P_e = \int_{-\pi}^{\pi}\int_{-\pi}^{\pi} Pr\left[D < 0 | \Delta_{1R}, \Delta_{2R}\right] p\left(\Delta_{1R}\right) p\left(\Delta_{2R}\right)\, d\Delta_{1R}\, d\Delta_{2R}, \tag{3.40}$$

where the pdf of Δ_{1R} and Δ_{2R} are specified by (3A.9) with $\rho_z = \frac{\sigma_{1R}^2 J_0}{\sigma_{1R}^2 + N_0}$ in $p(\Delta_{1R})$ and $\rho_z = \frac{\sigma_{2R}^2 J_0}{\sigma_{2R}^2 + N_0}$ in $p(\Delta_{2R})$, respectively. The above finite double integral can then be evaluated numerially on computer.

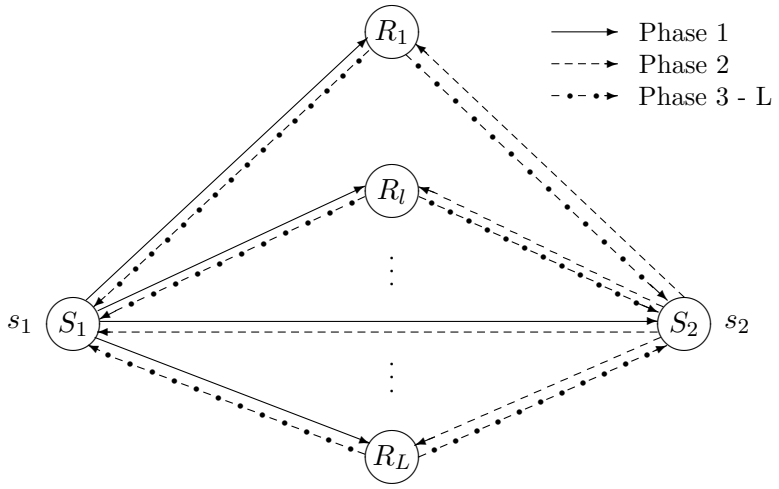

Figure 3.1: Multiple Relay Implemementation of the DPSK modulated MF System.

3.4 MF with Multiple Two Way Relays

The differentially modulated MF two way relay requires no channel estimation and it thus saves the overhead on the pilots that is needed in a coherent modulation based relay system. This feature of the DPSK MF relay is especially suitable for easy scalability because there is no added computation complexity associated with the CSI estimation at the receivers. A multiple two relay system is dipicted by Figure 3.1. It can be viewed as a generalization of the three-phase two-way relay discussed in the previous sections. Instead of one relay, there are L relays assisting the two terminals S_1 and S_2 to exchange information. Further, like the three-phase two-way relay system, a direct path is available between the two terminals. The operation of the generalized relay system is similar to the three-phase two-way MF relay except that in the broadcast phase, each of the relays broadcasts its own transmitted signal on a channel that is orthogonal to the rest of the relays. The orthogonal channels can be implemented by additional frequency band or time slots.

Following the same notation convention used in the previous sections, the received signal at terminal S_1 can be written as

$$\begin{aligned} y_{R_l1}[k] =& g_{R_l1}[k]\, s_{R_l}[k] + n_{R_l1}[k] \\ =& G_l\, g_{R_l1}[k](g_{1R_l}[k] + n_{1R_l}[k])(g_{2R_l}[k] + n_{2R_l}[k])s_1[k]\, s_2[k] + n_{R_l1}[k], \end{aligned} \tag{3.41}$$

The decision variable contributed from each received relay path is then obtained after CSI compensation and self information cancellation,

$$D_{R_l 1} = (y_{R_l 1}[k-1]\, d_1[k])^* y_{R_l 1}[k]. \tag{3.42}$$

The final decision variable $D[k]$ is obtained summing all the decision variables using EGC rule

$$D[k] = D_{21}[k] + \sum_{l=1}^{L} D_{R_l 1}[k]. \tag{3.43}$$

The BER analysis of the generalized DPSK MF relay involves a single direct path that is Rayleigh faded and L cascaded Rayleigh fadings arise from the relay paths. The analysis for the fast fading scenario seems to be forbidable so we turn our attention to the case of quasi-static fading, in which the channels remain the same for two consecutive transmission blocks. Under the quasi-static channel assumption, we are able to find the BER lower bound corresponding to the scenario when there are no noises at the relays. First we start with the $L+1$ channel BDPSK BER from [47],

$$P_e(\gamma_t) = \frac{1}{2^{2L+1}} e^{-\gamma_t} \sum_{l=0}^{L} c_l \gamma_t^l, \tag{3.44}$$

where

$$c_l = \frac{1}{l!} \sum_{k=0}^{L-l} \binom{2L+1}{k} \tag{3.45}$$

and

$$\gamma_t = \sum_{l=0}^{L} \gamma_l. \tag{3.46}$$

For notation simplicity, we have re-indexed the SNR's as $\gamma_0 = \gamma_{21}$, $\gamma_1 = \gamma_{MF_1}$, $\gamma_2 = \gamma_{MF_2}$, ..., and $\gamma_L = \gamma_{MF_L}$. Averaging over all the instantaneous SNRs in the above equatoin, we

have the average BER expressed in terms of the MGF functions evaluated at $s = -1$.

$$\begin{aligned}
P_e &= \mathbb{E}[P_e(\gamma_t)] \\
&= \mathbb{E}\left[\frac{1}{2^{2L+1}} e^{-(\gamma_0+\gamma_1+\ldots+\gamma_L)} \sum_{l=0}^{L} c_l (\gamma_0+\gamma_1+\ldots+\gamma_L)^l\right] \\
&= \mathbb{E}\left[\frac{1}{2^{2L+1}} \sum_{l=0}^{L} c_l \left(\sum_{\sum_{u=0}^{L} k_u = l} \binom{l}{k_0, k_1, \ldots, k_L} \prod_{u=0}^{L} \gamma_u^{k_u} e^{-\gamma_u}\right)\right] \\
&= \frac{1}{2^{2L+1}} \sum_{l=0}^{L} c_l \left(\sum_{\sum_{u=0}^{L} k_u = l} \binom{l}{k_0, k_1, \ldots, k_L} \prod_{u=0}^{L} \Phi_{\gamma_u}^{(k_u)}(s=-1)\right),
\end{aligned} \tag{3.47}$$

where the multinomial coefficient is calculated as

$$\binom{l}{k_0, k_1, \ldots, k_L} = \frac{l!}{k_0!\, k_1!\, \ldots\, k_L!}. \tag{3.48}$$

In the above derivation, the mutlinomial theorem is used to expand the l-th power of the sum of the instantaneous SNR's. Further, $\Phi_{\gamma_u}^{(k_u)}(s)$ is the k_u-th derivative of the MGF of γ_u. This result shows that if we know the MGF of all the received instantaneous SNR's and their derivatives up to L-th order, we are able to find the lower bound of the differentially modulated MF two way relay system.

The MGF and derivatives of the direct path SNR $\gamma_0 = \gamma_{21}$ can be summarized as one equation

$$\Phi_{\gamma_0}^{(k)}(s) = \frac{d^k}{ds^k} \Phi\gamma_0(s) = \frac{k!\, \bar{\gamma}_0^k}{(1-\bar{\gamma}_0 s)^{k+1}}. \tag{3.49}$$

For $k = 0$, the above equation is the MGF of γ_0.

The caclulation of the derivatives of the MGF of the relay path instantaneous SNR is more involved and it is easier to deal with the Meijer G function only. First we rewrite the MGF of the instantaneous SNR of the l-th ($1 \le l \le L$) relay path as the following composite function

$$\begin{aligned}
\Phi_{\gamma_l}(s) &= (-\zeta_l s)^{-1}\, \mathrm{G}_{1,3}^{3,1}\left((-\zeta_l s)^{-1} \middle| \begin{matrix} 0 \\ 0,0,0 \end{matrix}\right) \\
&= \mathrm{G}_{1,3}^{3,1}\left((-\zeta_l s)^{-1} \middle| \begin{matrix} 1 \\ 1,1,1 \end{matrix}\right) \\
&= G(u(s)),
\end{aligned} \tag{3.50}$$

where $G(u) = \mathrm{G}_{1,3}^{3,1}\left(u^{-1}\middle|\begin{matrix}1\\1,1,1\end{matrix}\right)$, $u(s) = -\zeta_l s$ and $\zeta_l = 2^3\lambda_l^2\frac{G_{MF_l}^2}{2N_0}$. The k-th derivative of $G(u)$ can be found as

$$\begin{aligned}G^{(k)}(u) = \frac{d^k}{du^k}G(u) =& u^{-k}\mathrm{G}_{2,4}^{4,1}\left(u^{-1}\middle|\begin{matrix}1,1-k\\1,1,1,1\end{matrix}\right)\\ =&(-1)^k u^{-k}\mathrm{G}_{1,3}^{3,1}\left(u^{-1}\middle|\begin{matrix}1-k\\1,1,1\end{matrix}\right)\\ =&(-1)^k u^{-(k+1)}\mathrm{G}_{1,3}^{3,1}\left(u^{-1}\middle|\begin{matrix}-k\\0,0,0\end{matrix}\right)\end{aligned} \tag{3.51}$$

With the derivatives of $G(u)$ and $u(s)$ known, the k-th derivative of the composite function $\Phi_{\gamma_l}(s)$ in (3.50) can be calculated using Faa di Bruno's formula [64], which is the generalization of the derivative chain rule to higher orders. In general, the k-th derivative of a composite function involves all the derivatives of both the functions, which form the composite function, up to order k. For the linear function $u(s)$, however, the higher order derivatives of $\Phi_{\gamma_l}(s)$ can be simplified to involve only the k-th order of $G(u)$ and the first order derivative of $u(s)$. Specifically,

$$\begin{aligned}\Phi_{\gamma_l}^{(k)}(s) =&\frac{d^k}{ds^k}\Phi_{\gamma_l}(s)\\ =&\frac{d^k\,G(u)}{du^k}\left(\frac{d\,u(s)}{ds}\right)^k\\ =&(-1)^k\left(-\zeta_l s\right)^{-(k+1)}\mathrm{G}_{1,3}^{3,1}\left((-\zeta_l s)^{-1}\middle|\begin{matrix}-k\\0,0,0\end{matrix}\right)(-\zeta_l)^k\\ =&\frac{1}{\zeta_l}(-s)^{-(k+1)}\mathrm{G}_{1,3}^{3,1}\left((-\zeta_l s)^{-1}\middle|\begin{matrix}-k\\0,0,0\end{matrix}\right),\end{aligned} \tag{3.52}$$

where

$$\zeta_l = \frac{\bar{\gamma}_{1R_l}\bar{\gamma}_{2R_l}\bar{\gamma}_{R_l1}}{\left(\bar{\gamma}_{1R_l}+1\right)\left(\bar{\gamma}_{2R_l}+1\right)}, \tag{3.53}$$

for $0 \le l \le L$. Using (3.45), (3.49), (3.52) and (3.53) in (3.47), the lower bound of the DPSK MF relay system can be written as

$$P_e = \frac{1}{2^{2L+1}}\sum_{l=0}^{L}c_l\left(\sum_{\sum_{u=0}^{L}k_u=l}\binom{l}{k_0,k_1,\ldots,k_L}\frac{k_0!\,\bar{\gamma}_0^{k_0}}{(1+\bar{\gamma}_0)^{k_0+1}}\prod_{u=1}^{L}\frac{1}{\zeta_l}\mathrm{G}_{1,3}^{3,1}\left(\frac{1}{\zeta_l}\middle|\begin{matrix}-k_u\\0,0,0\end{matrix}\right)\right). \tag{3.54}$$

The above BER bound is quite complex and don't seem to provide insights on the BER performance. To see the high SNR BER behavior, we set the SNR's in all the links to $\bar{\gamma}$ and let $\bar{\gamma} \to \infty$. Further, using the following relationship found by Mathematica

$$\lim_{\bar{\gamma}\to\infty} \mathrm{G}_{1,3}^{3,1}\left(\frac{1}{\bar{\gamma}}\middle| \begin{matrix} -k_u \\ 0,0,0 \end{matrix}\right) = k!\, \mathrm{G}_{1,3}^{3,1}\left(\frac{1}{\bar{\gamma}}\middle| \begin{matrix} 0 \\ 0,0,0 \end{matrix}\right)$$

P_e at high SNR can be approximated as

$$P_e(\bar{\gamma}) = \frac{\alpha(L)}{\bar{\gamma}^{L+1}} \left[\mathrm{G}_{1,3}^{3,1}\left(\frac{1}{\bar{\gamma}}\middle| \begin{matrix} 0 \\ 0,0,0 \end{matrix}\right)\right]^L, \tag{3.55}$$

where

$$\alpha(L) = 2^{-(2L+1)} \sum_{l=0}^{L} c_l \left(\sum_{\sum_{u=0}^{L} k_u = l} \binom{l}{k_0, k_1, \ldots, k_L} \prod_{u=1}^{L} k_u! \right) \tag{3.56}$$

is a positive coefficient determined by L. Finally, with the help of (2B.7), we can find the diversity order of the multiple relay system as

$$\begin{aligned} \eta =& -\lim_{\bar{\gamma}\to\infty} \frac{\log \alpha(L)}{\log \bar{\gamma}} - \lim_{\bar{\gamma}\to\infty} \frac{\log \bar{\gamma}^{-(L+1)}}{\log \bar{\gamma}} - \lim_{\bar{\gamma}\to\infty} \frac{\log \left[\mathrm{G}_{1,3}^{3,1}\left(\frac{1}{\bar{\gamma}}\middle| \begin{matrix} 0 \\ 0,0,0 \end{matrix}\right)\right]^L}{\log \bar{\gamma}} \\ =& L+1. \end{aligned} \tag{3.57}$$

This shows that the DPSK MF two way relay achieves the full diversity available. It is worthwhile to note that in the event the direct path is not available, full diversity can still be achieved.

3.5 Numerical Results and Discussion

In this section, the DPSK modulated MF relay is simulated under different channel conditions. The simulation results are verified against the theoretical BER performance bound wherever applicable. Further, unless otherwise stated, all the power amplifiers in the system are assumed to be linear.

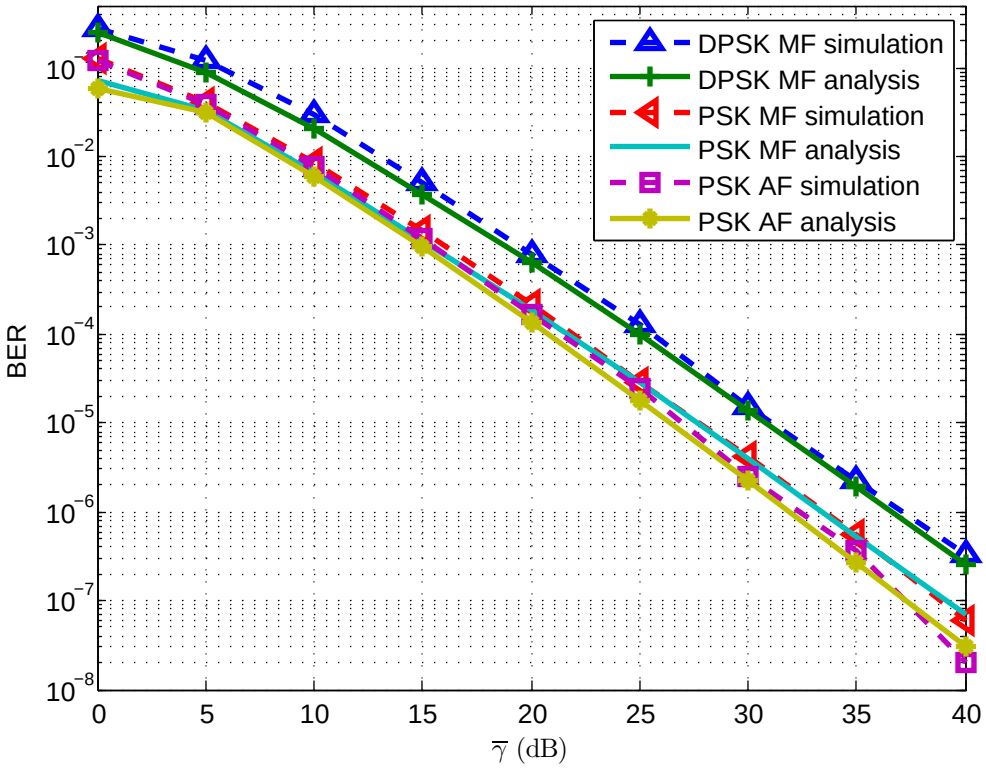

Figure 3.2: BER of DPSK MF relay compared with coherent relays in static fading. The modulation is BPSK and all the links in the system have the same average link-SNR $\bar{\gamma} = \bar{\gamma}_{1R} = \bar{\gamma}_{2R} = \bar{\gamma}_{R1} = \bar{\gamma}_{21}$.

First a static fading enviornment is considered. In Figure 3.2, the BER curve of the proposed DPSK MF two-way relay is plotted against the coherent AF and MF two-way relays studied in Chapter 2. In the figure, binary modulation is used and all the links in the relay systems have equal SNR's. Compared to the coherent detection schemes, it is observed that the differentially modulated PSK MF scheme is 3 dB and 4.5 dB worse than the coherent PSK MF and coherent PSK AF protocols, respectively. Obviously, the lack of precise CSI and the subsequent use of EGC lead to this performance loss. However, the use of DPSK, as opposed to coherent PSK, leads to a higher spectral efficiency, as there is no need to transmit any pilot for channel estimation purpose. It is observed from the figure that in the low SNR region of 0 dB to 15 dB, there is a gap between the BER lower bound given by (3.23) and the actual BER obtained by simulation. This gap is caused by the omission of the relay noises in the BER analysis. Nonetheless, as the uplink SNR's improve in the high SNR region, from 20 dB and onwards, the BER becomes limited by fading and the gap between the two is negligible.

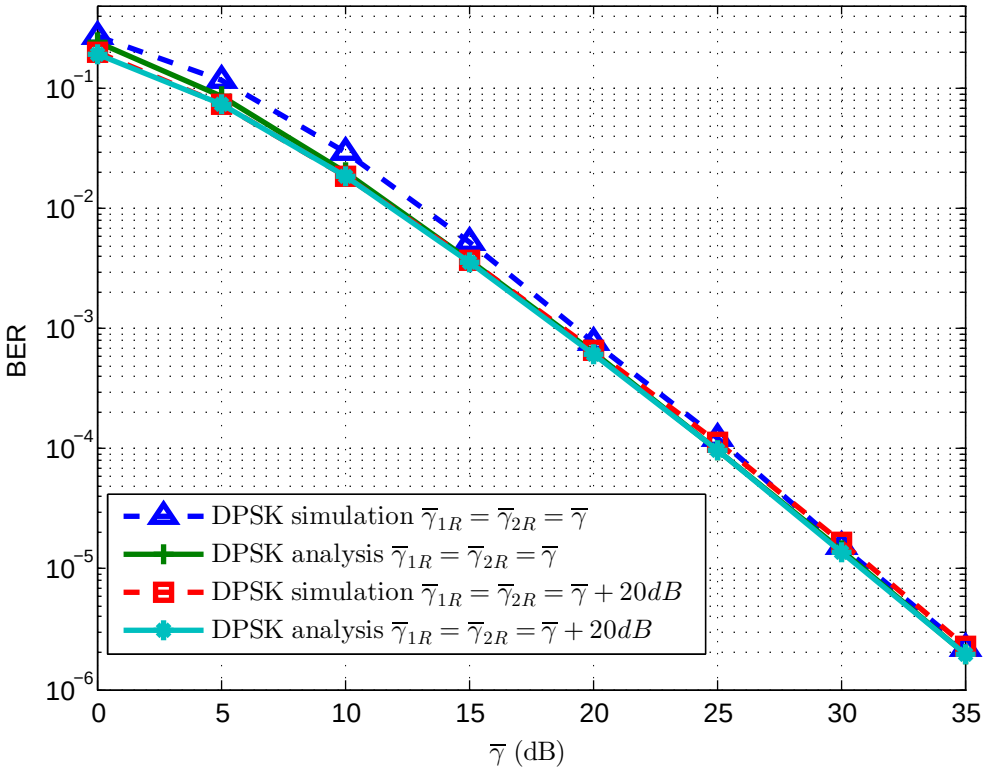

Figure 3.3: BER of DPSK MF relay with stronger uplinks. The modulation is BPSK and all the links in the system have the same average link-SNR except $\bar{\gamma} = \bar{\gamma}_{1R} = \bar{\gamma}_{2R} = \bar{\gamma}_{21} + 20dB$.

Next, impact of asymmetrical channels on the BER performance is considered. Specifically, we evaluate the case where the uplinks have better signal quality. This scenario corresponds to the typical case that the relay is located in the middle of the two terminals. Figure 3.3 shows the BER of DPSK MF when the $S_1 \to R$ and $S_2 \to R$ links are 20 dB stronger than those in the direct path and in the downlink. It is seen that increasing the uplink SNR's $\bar{\gamma}_{1R}$ and $\bar{\gamma}_{2R}$ improves the BER by 1 dB in the low SNR region from 0 dB to 15 dB. Beyond 20 dB, the marginal return by increasing $\bar{\gamma}_{1R}$ and $\bar{\gamma}_{2R}$ becomes negligible. This behavior is slightly different from the coherent AF or MF relay, which exhibits virtually no BER improvement for the same SNR increase as shown in Figure 2.9.

One of the challenges in the implementation of the differential modulated two-way relay systems is the realization of self-interference cancellation in AF based relays. For AF relays, it is often assumed that the channel remains static during a transmission block [60, 61] so that the relay can take a time average of the received signals for CSI estimation. For example, the generalized differential modulation AF relay [61] can achieve good performance

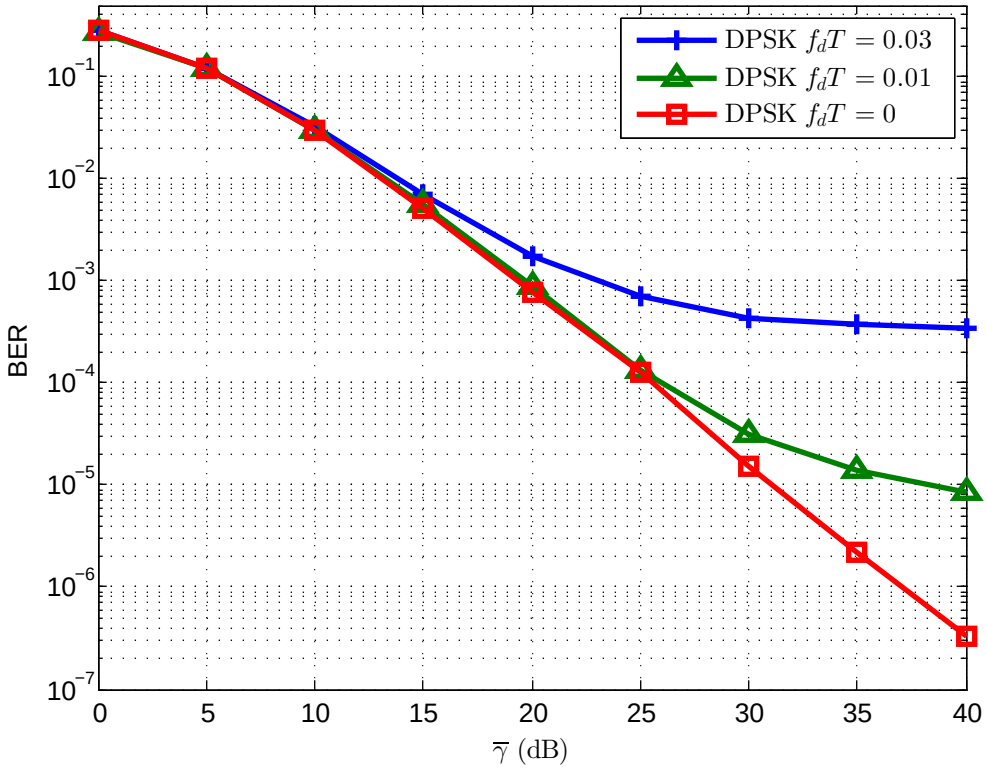

Figure 3.4: Simulation BER of DPSK MF relay with time varying fading. The modulation is BPSK and all the links in the system have the same average link-SNR.

in a static fading channel with long block length. However, the BER quickly grows to 0.1 at an SNR of 30 dB when the normalized Doppler frequency becomes 2×10^{-4}. The same assumption of a static fading channel is also adopted in the regenerative relays such as the ML relay in [59] and denoise-and-forward (DNF) relay in [56]. The MF relay, on the otherhand, is not limited by the static fading. In Figure 3.4, simulated BER results of the DPSK MF relay are plotted for both static and time selective fading. The time selective fading process in each of the links follows Jake's model [65], in which the Doppler spreads normalized to symbol duration, f_dT, are 0.01 and 0.03, respectively. The plot shows that the MF relay indeed works in a time varying fading environment. However, similar to the point-to-point DPSK transmission, there exists an increasing error floor when f_dT becomes higher. This is because in differential detection, the previously received signal is used as an estimate of the fading channel; see (3.3) and (3.8). For time varying fading, such an estimate is not fast enough to track the changes in the fading channel, e.g. phase reversal caused during a deep fade [66]. As a result, when fading dominates in the high SNR region, an irreduceable error floor occurs. The correlation between two adjacent fading gains $g_{ij}[k-1]$

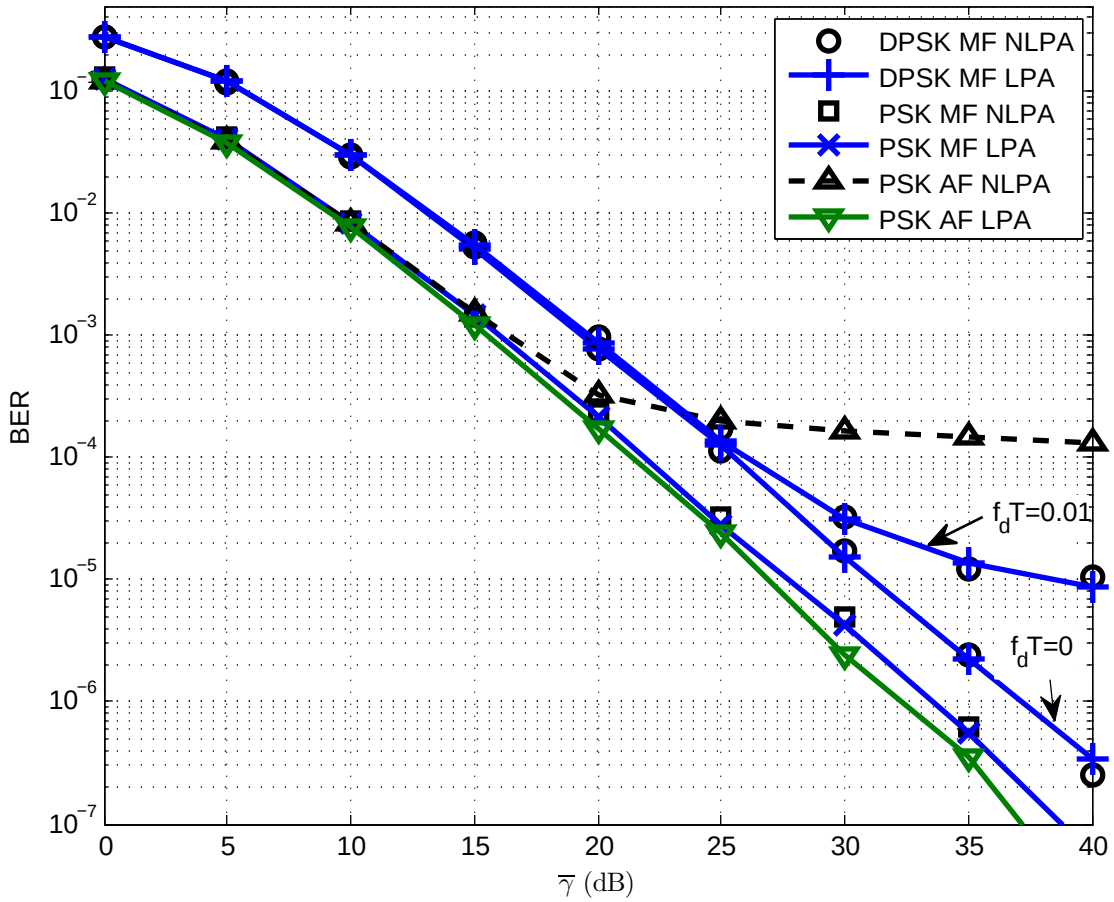

Figure 3.5: Simulation BER of DPSK MF relay with NLPA. The modulation is BPSK for AF relay and BDPSK for MF relay. All the links have the same average link-SNR. The NLPA has a saturation power of 3.2 dB.

and $g_{ij}[k]$ is $\sigma_{ij}^2 J_0(2\pi f_d T)$. Higher f_dT leads to smaller correlation, which in turn results in larger channel estimation error in the differential detection. Consequently, higher f_dT results in higher error floor in the DPSK MF two-way relay.

In Chapter 2 we found that the MF relay with coherent MPSK modulation is resistant to the power amplifier nonlinearity. Does this property still hold for the differentially modulated MF relay? To answer this question, we first notice that the DPSK MF relay transmitted symbol s_R in (2.20) has exactly the same form as PSK MF relay transmitted symbol in (3.4). As such, they experience the same fading and noise disturbances. Further, since the transmitted DPSK symbols are drawn from the same signal constellation as PSK, the DPSK MF relay is expected to exhibit the same resilient to NLPA distortion as the PSK MF relay This is verified via simulation under both static fading and slow fading, and the

results are demonstrated in Figure 3.5. For comparison, coherent PSK MF and AF relay results are also included in the plot. In the plot, BPSK is used for the coherent modulated AF/MF relay and BDPSK is used for the MF relay. All of the relays are using a NLPA with a saturation power of 3.2 dB, which corresponds to the highest instantaneous power of a BPSK sigal shown in Figure 2.3. We see that while PSK AF relay system experiences a high error floor of 1×10^{-4}, the DPSK MF relay shows no obersable BER degradation, just as the coherent PSK MF relay.

Figure 3.6 and 3.7 plot the BER results of DPSK modulated MF and PF relays under symmetrical channel configuration with all links having the same SNR, and asymetrical channels with the uplink SNR $\bar{\gamma}_{1R}$ and $\bar{\gamma}_{2R}$ 20 dB stronger. Further, Figure 3.6 considers static fading, while Figure 3.7 corresponds to time varying fading with $f_d T = 0.01$. For comparison purpose, point-to-point DPSK results with first and second order diversity are also included in the plots.

From the figures, it can be seen that DPSK MF relay is less sensitive than DPSK PF relay to the channel coditions considered. For DPSK MF relay, increasing the uplink SNRs results in BER improvement mainly in the low SNR region. Further, the MF relay shows second order diversity DPSK modulation. The BER of DPSK PF relay, on the other hand, significantly depends on the uplink SNRs. For the case of symmetrical channels, though the PF relay shows an improvement of 2 dB over point-to-point DPSK, diversity effect is not realized. When the uplink SNR $\bar{\gamma}_{1R}$ and $\bar{\gamma}_{2R}$ are 20 dB stronger, we can see that DPSK PF relay improves significantly, becoming better than DPSK MF relay by 5 dB, and become close to the second order point-to-point DSPK. When time varying fading is present, as shown by Figure 3.7, the DPSK PF protocol has higher error floor than MF protocol.

Obviously, unlike coherent PSK PF relay studied in the previous chapter, DPSK PF relay does not outperform DPSK MF relay all the time. The differentially modulated PF protocol only performs better than the MF protocol under better channel conditions. This can be explained in part by the signal combining rule at the receiver. With precise knowledge of CSI, the coherent detector can perform MRC in (2.36). However, for DPSK PF, the relay path signal is simply added to that of the direct path, thus redenering the system less efficient. As a result, the DPSK PF protocol should be only used in good channel conditions.

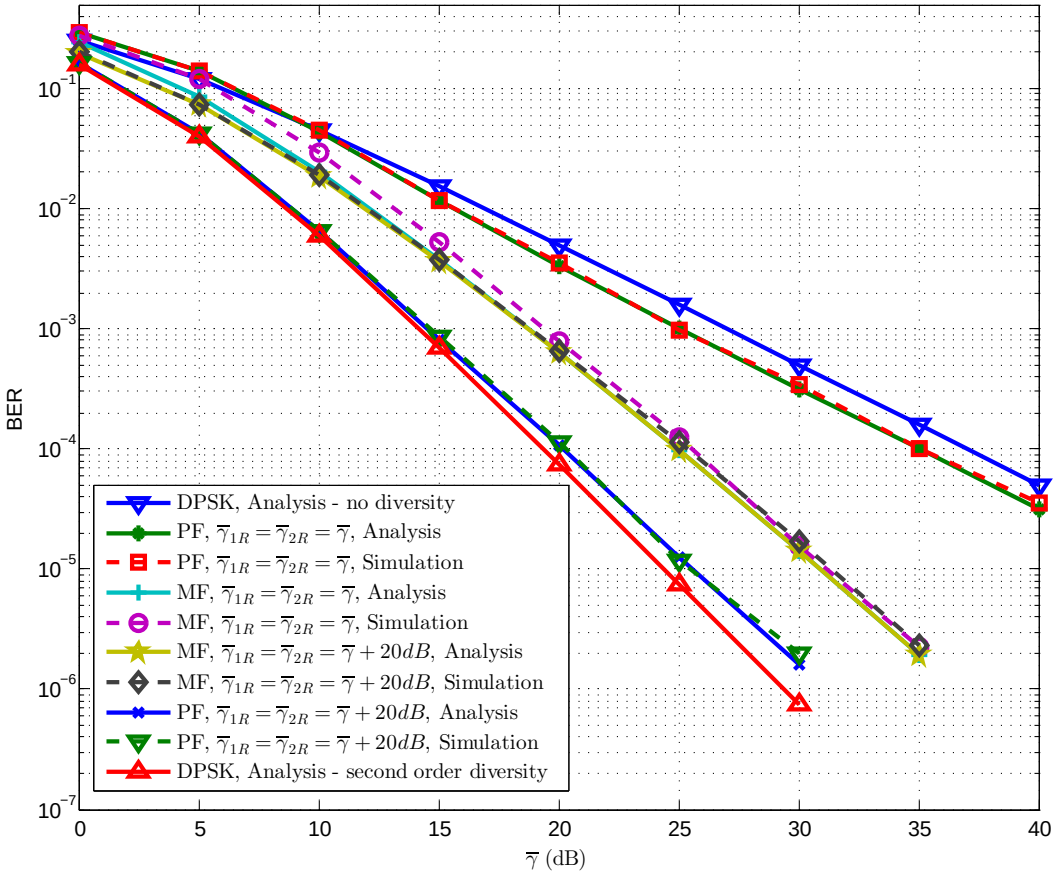

Figure 3.6: Simulation BER of BDPSK PF relay compared with MF relay under static fading.

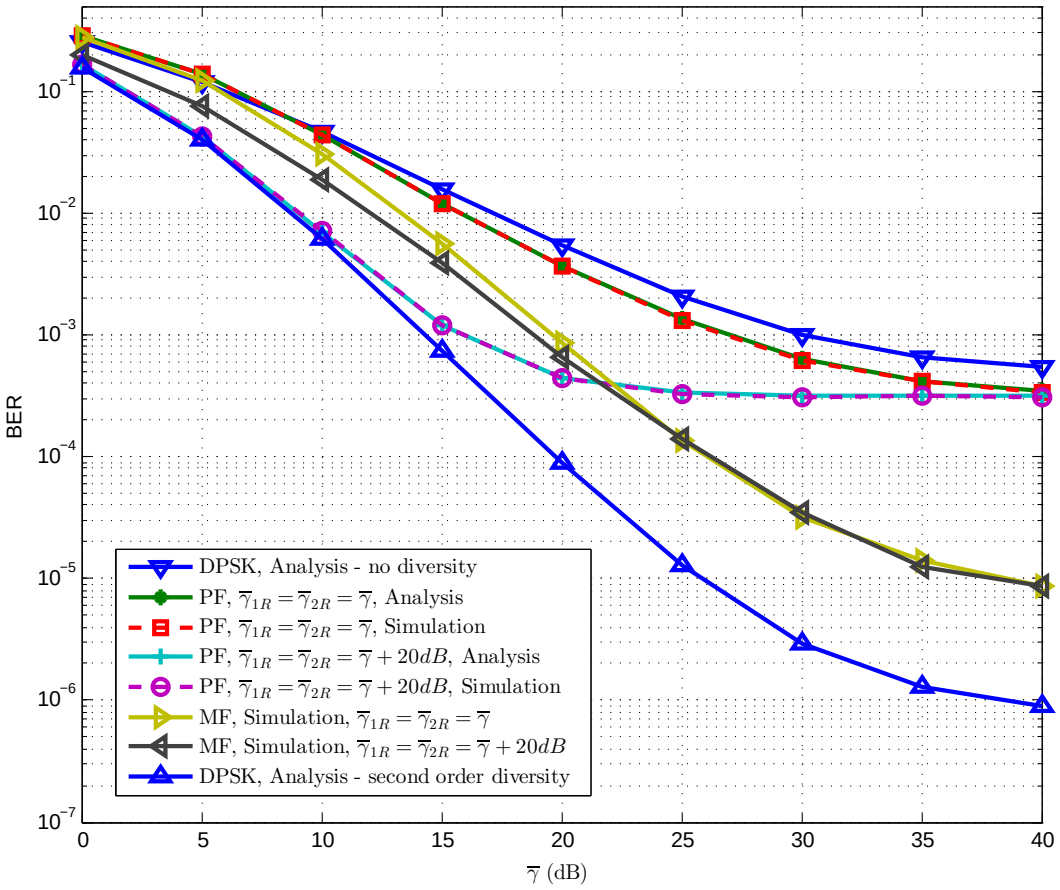

Figure 3.7: Simulation BER of BDPSK PF relay compared with MF relay under time varying fading, $f_d T = 0.01$.

3.6 Conclusion

In this chapter, the MF and PF relays proposed in Chapter 2 are further extended to work with DPSK modulation. The immediate benefit is that pilot symbols are no longer needed as in the case of coherent two way relay. The multiplicative self-interference cancellation of the DPSK MF relay is simple and yet effective, which leads to a similar implementation complexity as conventional differential detection. In particular, compared to the subtractive self-interference methods in [61], the DPSK MF and PF relays can bypass the CSI estimation that is necessary for self-interference cancellation in AF based protocols. A closed form BER lower bound for the binary DPSK MF relay is derived and verified via simulation. Based on the lower bound, we further derived the diversity order of the DPSK MF relay system. The proposed relay system achieves the full diversity order that is available.

For differentially modulated two way relays in the literature, the assumption of static fading is a common basis for the relay systems to perform CSI estimation for self-interference cancellation. However, the DPSK MF relay considered in this chapter is not built on such an assumption and it works in fast fading environment. This is a marked improvement over the existing two-way relays that employ DPSK modulation.

Similar to the PSK MF relay, the DPSK MF relay is resistant to power amplifier non-linearity. Simulation results indicate that even when the MF relay is equipped with the same power amplifier as the two terminals, which is insufficient to amplify the relay transmitted signal linearly, the MF relay system shows no noticeable BER degradation. Combined with differential modulation, MF two-way relay has the potential to deliver robust performance at low complexity, low cost and high power efficiency.

In the previous chapter, PF two-way relay was developed for coherent PSK modulation to achieve both good resistance to power amplifier non-linearity and good BER performance (over both AF and MF relay). This idea is tested with DPSK modulation in this chapter. Compared to MF relay, the PF relay offers similar implementation complexity at the relay and also have low requirement on the linear region of the power amplifier. The BER of PF relay, however, doesn't out perform the MF relay in all situations. It is actually worse than MF relay when the link SNRs are equally strong. But when uplink SNRs are stronger and

static fading is present, it is found that the DPSK PF two-way relay performs better than the DPSK MF relay. This suggests the use of PF relay when the relay is located in between the two user terminals.

Last but not least, the DPSK MF relay protocol is generalized to multiple relays in view of the scalability of the DPSK MF relay. Its BER under static fading is derived, which further allows us to provide an analysis of diversity order on the generalized system.

Appendix 3A PDF of the Phase Difference in (3.40)

Consider a circular complex Gaussian random process $z(t)$, whose power spectrum is symmetrical about y-axis. We are interested in finding the pdf of the phase difference between $z(t)$ and $z(t+\tau)$. In [67], A discussion of the more general Gaussian perturbed signal model is presented. However the results are given in integral form, which cannot be used directly in our analysis. In the following, we provide the analytical result for the signals under consideration.

First, let's write $z(t)$ and $z(t+\tau)$ in terms of cartesian forms as

$$z(t) = x_1 + jy_1 \tag{3A.1}$$

$$z(t+\tau) = x_2 + jy_2 \tag{3A.2}$$

Due to circular symmetry, the real and imaginary part of $z(t)$ are independent and identically distributed with zero mean. Further, the symmetrical power spectrum of $z(t)$ implies that the cross correlation between the real and imaginary parts are zero. Let $\mathbf{z} = [x_1 \ y_1 \ x_2 \ y_2]^T$, then the pdf of $\mathbf{z}$ can be written as

$$p(\mathbf{z}) = \frac{1}{(2\pi)^2\sigma_z^4(1-\rho^2)} \exp\left\{-\frac{x_1^2 - 2\rho_z x_1 x_2 + x_2^2 + y_1^2 - 2\rho_z y_1 y_2 + y_2^2}{2\sigma_z^2(1-\rho^2)}\right\}, \tag{3A.3}$$

where $\sigma_z^2 = \frac{1}{2}\mathbb{E}\big[|z(t)|^2\big]$ and $\rho_z = \frac{1}{2}\mathbb{E}[z(t+\tau)z^*(t)]$.

To find the pdf of the phase difference between $z(t)$ and $z(t+\tau)$, we next express them in their polar form as following,

$$z(t) = r_1 e^{j\theta_1} \tag{3A.4}$$

$$z(t+\tau) = r_2 e^{j\theta_2} \tag{3A.5}$$

Now let $\mathbf{w} = [r_1 \ \theta_1 \ r_2 \ \theta_2]^T$, the joint pdf of $\mathbf{w}$ can be calculated from $p(\mathbf{z})$ based on the transformation functions $x_i = r_i \cos\theta_i$ and $y_i = r_i \sin\theta_i$, $i \in \{1, 2\}$, with a Jacobian of $r_1 r_2$. Specifically, the pdf $p(\mathbf{w})$ is

$$p(\mathbf{w}) = \frac{r_1 r_2}{(2\pi)^2 \sigma_z^4 (1-\rho^2)} \exp\left\{-\frac{r_1^2 + r_2^2 - 2r_1 r_2 \cos(\theta_1 - \theta_2)}{2\sigma_z^2(1-\rho^2)}\right\}, \tag{3A.6}$$

Integrating (3A.6) over r_1 and r_2 would give us the joint pdf of θ_1 and θ_2,

$$p(\theta_1, \theta_2) = q(\theta_1 - \theta_2), \tag{3A.7}$$

where

$$q(\xi) = \left(\frac{1-\rho_z^2}{4\pi^2}\right) \frac{\left|\rho_z^2 \cos^2\xi\right| \arctan\left(\sqrt{\frac{\rho_z^2 \cos^2\xi}{1-\rho_z^2\cos^2\xi}}\right) + \sqrt{1-\rho_z^2\cos^2\xi} + \frac{\pi}{2}\rho_z \cos\xi}{[1-\rho_z^2\cos^2\xi]^{\frac{3}{2}}}. \tag{3A.8}$$

Notice that the joint pdf only depends on the phase difference $\Delta = \theta_1 - \theta_2$. As a result, the pdf of Δ can be expressed in terms of $q(\Delta)$ as

$$p(\Delta) = \left(\frac{1-\rho_z^2}{2\pi}\right) \frac{\left|\rho_z^2 \cos^2\Delta\right| \arctan\left(\sqrt{\frac{\rho_z^2 \cos^2\Delta}{1-\rho_z^2\cos^2\Delta}}\right) + \sqrt{1-\rho_z^2\cos^2\Delta} + \frac{\pi}{2}\rho_z \cos\Delta}{[1-\rho_z^2\cos^2\Delta]^{\frac{3}{2}}}. \tag{3A.9}$$

Chapter 4

Phase-Forward with CPFSK Modulation

In Chapter 2, we studied coherent PSK MF and PSK PF two way relays that are resistant towards power amplifier non-linearity. Multiplying the received signals at the relay preserved the phase information in the event of non-linear distortion at the power amplifier. However, there is still signal waveform variation due to pulse shaping. This is true even for the PF relay transmitted signals, whose symbols have constant amplitude. In Chapter 3, differential encoding is employed in the MF two way relay to avoid the transmission of pilot symbols. It is desirable to further reduce the amplitude variations at the relay while eliminating the pilot symbols. In this chapter we propose the idea of PF relaying for three-phase two-way relay cooperative network employing constant envelope modulation with discriminator detection in a Rayleigh fading environment. It was found that, compared to one-way relaying, two-way PF relaying suffers only a moderate loss in energy efficiency (of 1.25 dB). On the other hand, PF improves the transmission efficiency by 33%. Furthermore, we believe that the loss in energy efficiency can be reduced if power is allocated to the different nodes in this cooperative network in an optimal fashion. In this chapter we explore both the PF relay as well as the DF based relay for the CPFSK modulation. It was found that the latter has a similar BER performance as PF while requiring additional processing at the relay. It can thus be reached that the proposed PF technique is indeed the preferred way to maintain constant envelope signaling throughout the signaling chain in a three-phase two-way relaying system.

4.1 Introduction

In the last two chapters, we considered PF in three-phase two-way cooperative relay systems that use PSK modulation at the user terminals and PSK-like modulation at the relay. While PSK symbols at different symbol intervals all have the same magnitude, the transmitted PSK signal does not have a constant signal envelope because of pulse shaping. In this chapter, we consider the use of continuous phase frequency shift keying (CPFSK) in three-phase two-way cooperative communication systems with a PF relay. Similar to a PSK PF two-way relay, the CPFSK PF two-way relay performs self induced hard limiting after multiplying two recieved signals at the relay. However, unlike PSK PF, a CPFSK PF signal has constant signal envelope at all times. Note that CPFSK modulations are widely used in public safety (police, ambulane) and private mobile communication systems (taxi, dispatch, courier fleets) even though are are, in general, not as bandwidth efficient as linear modulations. The use of constant envelope modulations in cooperative communications had been considered in [68, 69, 31]. Specifically in [31], CPFSK and PF was proposed for 2-node MRC-type cooperative communication system with time-selective Rayleigh fading and discriminator detection. The authors reported that PF has a lower BER than DF. It also delivers the same performance as AF when dual-antenna selection is available at the relay. They concluded that PF is a cost-effective alternative to AF and DF, since it does not need signal regeneration at the relay nor does it need expensive linear amplifiers.

To further confirm the usefullness of the proposed CPFSK PF scheme, we compare it against a phase combining PF technique that is based on DF and multi-level CPFSK re-modulation at the relay. Specifically we consider the so-called decode-superposition-forward (DSF) and deocde-XOR-forward (DXF) protocols for three-phase two-way relaying.

This chapter is organized as follows. We first describe in Section 4.2 the signal and system model for the proposed CPFSK PF relaying scheme and competing DF schemes based on multi-level CPFSK re-modulation at the relay. The detection and combining strategies are presented in Section 4.3, followed by a discussion on the implementation concerns of the proposed relaying protocols. The BER analysis of the three protocols is provided in Section 4.5. Numerical results are provided in Section 4.6 and conclusions of this investigation are given in Section 4.7.

4.2 System Model

The basic three-phase two-way cooperative communication network considered in this chapter is identical to that in Figure 2.1 except that the modulation at the user terminals are now replaced by CPFSK modulations and the relay signal is replaced by a phase-superimposed constant envelope signal. The general equation for signals at different nodes of the cooperative network is:

$$y_{ij}(t) = g_{ij}(t)s_i(t) + n_{ij}(t), \tag{4.1}$$

where $i \in \{1, 2\}$, $j \in \{1, 2, R\}$ and $i \neq j$, $g_{ij}(t)$ is the i.i.d. circular complex Gaussian process that represent Rayleigh fading in the $i \to j$ link, and $n_{ij}(t)$ is the AWGN process at the receiver on the $i \to j$ link. Specifically, $s_1(t)$ and $s_2(t)$ are CPFSK signals of the form

$$s_i(t) = e^{j\theta_i(t)}, \qquad i \in \{1, 2\}, \tag{4.2}$$

where

$$\theta_i(t) = \pi h \left(\sum_{n=0}^{k-1} d_{i,n} \right) + \pi h d_{i,k} \frac{(t - kT)}{T}, \qquad kT < t \leq (k+1)T, \tag{4.3}$$

is the information carrying phase, with $d_{i,k} \in \{\pm 1\}$ being the data bit in the k-th symbol interval for User i, $i \in \{1, 2\}$, h being the modulation index, and T being the bit-duration. Note that the derivative of the information bearing phase is

$$\dot{\theta}_i(t) = \pi h d_{i,k}/T, \qquad kT < t \leq (k+1)T, \tag{4.4}$$

which is proportional to the data bit $d_{i,k}$. This property is crucial in understanding the decision rule made by the discriminator detector presented in the next section. Another property of CPFSK that is important to the understanding of the results is the bandwidth of the signal. It is well known [70] that CPFSK signals, are in general, not band-limited. As such, a common practice is to adopt the frequency range that contains 99% of the total signal power as the bandwidth of the signal. This is referred to as the 99% bandwidth [70]. As an example, consider the so-called Minimum Shift Keying (MSK) scheme, i.e. CPFSK with $h = 1/2$. Using the results from [62], the 99% bandwidth of MSK is found to be $1.1818/T$.

Due to the constant envelope nature of the transmitted signal in (4.2), a highly power efficient, though non-linear, power amplifier can be employed at the two user terminals.

Naturally, it is desirable to maintain the same constant envelop characteristic at the relay. In the following sections, we first apply the phase forward concept to the CPFSK two way relay to achieve this goal. Next, we consider two DF based forwarding techniques that are suitable to be used for combining with the direct path received signal. When DF forwarding strategies are implemented at a two-way relay, the two symbols from the two users are combined to form a new symbol by network coding, such as the popular XOR coding. However, this may post an issue when the user attempts to combine the relay path sigal with the direct path signal because the the former signal is a mixure of both user signal and the later contains information of a single user. Therefore, self-interference cancellation must be performed prior to signal combing at the user terminal in the third phase. Based on the fact the the information are beared in the phase, we devise the phase superpostition based DF methods that allow self-interference cancellation prior to the signal combining.

4.2.1 Phase-Forward of CPFSK

In the proposed PF scheme, the signal transmitted by the relay is

$$s_R(t) = \exp\left\{j(\arg[y_{1R}(t)] + \arg[y_{2R}](t)\right\}), \tag{4.5}$$

where $\arg[y_{1R}(t)]$ and $\arg[y_{2R}(t)]$ are the phases of the signals $y_{1R}(t)$ and $y_{2R}(t)$ respectively. Note that $s_R(t)$ is both constant envelope and continuous-phase, just like the data signals $s_1(t)$ and $s_2(t)$. As observed from (4.5), the forwarded signal has constant envelope. Moreover, the phase of $s_R(t)$ is the sum of the phases of the two uplink signals $y_{1R}(t)$ and $y_{2R}(t)$. Since this phase superposition is equivalent to a multiplication of (the hard-limited versions of) the signals $y_{1R}(t)$ and $y_{2R}(t)$ in the time domain, refer to Figure 2.7, the corresponding frequency domain convolution will lead to a spectrum expansion if the relay is destined to transmit without any bandwidth limitation.

One nice feature of the CPFSK PF relaying technique is that constant envelope signaling is maintained at the relay without requiring it to perform any demodulation and re-modulation. A natural question to ask is, how does PF compare to DF strategies that employ constant envelope signaling at the relay? To be able to answer this question, we introduce next the 3-Level Decode-and-Phase-Forward (3-DPF) scheme and the Alternate 4-Level Decode-and-Phase-Forward (A4-DPF) scheme as possible alternatives to PF. For

both schemes, the relay first make decisions on user S_1 and user S_2's data based on the its received signals $y_{1R}(t)$ and $y_{2R}(t)$. It then applies the decisions, $\hat{d}_{1,n}$ and $\hat{d}_{2,n}$, to (4.2) and (4.3) to re-generate user S_1 and user S_2's signals according to $\hat{s}_1(t) = \exp\{j\hat{\theta}_1(t)\}$ and $\hat{s}_2(t) = \exp\{j\hat{\theta}_2(t)\}$.

4.2.2 3-Level Decode and Phase Forward (3-DPF)

With this detection and forward strategy, the relay adds the detected phases in $\hat{s}_1(t)$ and $\hat{s}_2(t)$ synchronously to form the relay signal

$$s_R(t) = \exp\left\{j\left(\hat{\theta}_1(t) + \hat{\theta}_2(t)\right)\right\} = \hat{s}_1(t)\hat{s}_2(t). \tag{4.6}$$

This signal is both constant envelope and continuous-phase, just like the data signals $s_1(t)$ and $s_2(t)$. Furthermore, because of synchronous mixing, we can view $s_R(t)$ as a 3-level CPFSK signal with modulation index h and symbol values $+2, 0, -2$ that occur with priori probabilities $\frac{1}{4}, \frac{1}{2}, \frac{1}{4}$. The 3 signal levels and the corresponding priori probabilities are due to the fact that the detected bits $\hat{d}_{1,n}$ and $\hat{d}_{2,n}$ at the relay are $\{\pm 1\}$ binary random variables. Another consequence of synchronous phase mixing is that the bandwidth of $s_R(t)$ is less than the sum bandwidth of $\hat{s}_1(t)$ and $\hat{s}_2(t)$, even though $s_R(t) = \hat{s}_1(t)\hat{s}_2(t)$. Considering MSK modulation, the sum bandwidth is two times $1.1818/T$ or $2.3636/T$. The 99% bandwidth of the corresponding $s_R(t)$, on the other hand, is only $1.832/T$ based on numerical calculation of the convolution of two MSK power density spectrums [62].

4.2.3 Alternate 4-level Decode and Phase Forward (A4-DPF)

In general, we can construct a constant-envelope relay signal based on the superposition of the detected phases as follows

$$s_R(t) = \exp\left\{j\left(w_1\hat{\theta}_1(t) + w_2\hat{\theta}_2(t)\right)\right\} \tag{4.7}$$

where w_1 and w_2 are weighting coefficients [9,10,12]. In the case where $w_1 = 2$ and $w_2 = 1$, $s_R(t)$ becomes a conventional 4-level CPFSK scheme with modulation h and symbol values $+3, +1, -1, -3$ all occurring with equal probability. This signal will have a wider bandwidth than the 3-level relay signal in the previous section but it will also provide a better BER performance (typical power-bandwidth tradeoff). One thing though, the unequal weightings

on the two detected phases will translate into an asymmetric error performance at S_1 and S_2. This problem can be alleviated by alternating the weighting rules between even and odd time slots as follows:

$$\begin{aligned} w_1 = 2, w_2 = 1; &\qquad \text{even time slot,} \\ w_1 = 1, w_2 = 2; &\qquad \text{odd time slot.} \end{aligned} \tag{4.8}$$

We call this strategy Alternate 4-level detect and phase forward or A4-DPF.

4.3 Discriminator Detection of the Relay Signals

As shown in (4.1), the transmitted signals at S_1, S_2 and R, will in general, experience time-selective fading. This makes the implementation of coherent detection rather complicated. As such we consider the much simpler discriminator detector. This non-coherent detector does not need channel state information when making data decisions and it thus spares the receiver from performing complicated channel tracking and sequence detection tasks. Without loss of generality, we demonstrate in the following sections how User S_1 detects the data intended for it from User S_2, i.e. the $d_{2,k}$'s, using a discriminator detector. The detection of User S_1's data at Node S_2 follows exactly the same procedure. It is further assumed that ideal low-pass filters (LPF) are used to limit the amount of noise admitted into the detector, with the bandwidth of each receive LPF set to the 99% bandwidth of its incoming signal. As such, the noise processes in (4.1) are all band-limited white Gaussian noises.

4.3.1 Detection of CPFSK PF Signals

To see how discriminator detector works in the proposed CPFSK PF system, we first rewrite the two received signals at the relay as

$$y_{1R}(t) = g_{1R}(t)e^{j\theta_1(t)} + n_{1R}(t) = a_{1R}(t)e^{j\psi_{1R}(t)} \tag{4.9}$$

and

$$y_{2R}(t) = g_{2R}(t)e^{j\theta_2(t)} + n_{2R}(t) = a_{2R}(t)e^{j\psi_{2R}(t)} \tag{4.10}$$

where $a_{1R}(t) = |y_{1R}(t)|$, $a_{2R}(t) = |y_{2R}(t)|$, $\psi_{1R}(t) = \arg[y_{1R}(t)]$ and $\psi_{2R}(t) = \arg[y_{2R}(t)]$. As stated in (4.5), the relay broadcasts

$$\begin{aligned} s_R(t) &= \exp\{j\theta_R(t)\}, \\ \theta_R(t) &= \psi_{1R}(t) + \psi_{2R}(t), \end{aligned} \tag{4.11}$$

to S_1 and S_2 in the last phase. Substituting (4.11) into (4.1) with $i = R$ and $j = 1$, the received signal at S_1 during the third phase can now be written as

$$y_{R1}(t) = g_{R1}(t)e^{j\theta_R(t)} + n_{R1}(t) = a_{R1}(t)e^{j\psi_{R1}(t)}, \tag{4.12}$$

where $a_{R1}(t)$ and $\psi_{R1}(t)$ are respectively the amplitude and phase. In order to detect the signal from S_2, User S_1 first removes its own phase $\theta_1(t)$ from $\psi_{R1}(t)$. The resultant complex signal is

$$\begin{aligned} \tilde{y}_{R1}(t) &= a_{R1}(t)e^{j\tilde{\psi}_{R1}(t)}, \\ \tilde{\psi}_{R1}(t) &= \psi_{R1}(t) - \theta_1(t). \end{aligned} \tag{4.13}$$

It then combines $\tilde{y}_{R1}(t)$, non coherently, with the signal

$$y_{21}(t) = g_{21}(t)e^{j\theta_2(t)} + n_{21}(t) = a_{21}(t)e^{j\psi_{21}(t)} \tag{4.14}$$

from (4.1) with $i = 2$ and $j = 1$, where $a_{21}(t)$ and $\psi_{21}(t)$ are respectively the received signal amplitude and phase from the direct path. Specifically at the decision making instant, which is taken to be the mid-symbol position in each bit interval, the non-coherent detector adds the phase derivatives $\dot{\psi}_{21}(t)$ and $\dot{\tilde{\psi}}_{R1}(t)$ according to the maximal ratio combining principle [31]

$$D = D_{21} + D_{R1} \tag{4.15}$$

where

$$\begin{aligned} D_{21} &= 2a_{21}^2\dot{\psi}_{21} = \begin{bmatrix} y_{21}^* & \dot{y}_{21}^* \end{bmatrix} \begin{bmatrix} 0 & -j \\ j & 0 \end{bmatrix} \begin{bmatrix} y_{21} \\ \dot{y}_{21} \end{bmatrix}, \\ D_{R1} &= 2a_{R1}^2\dot{\tilde{\psi}}_{R1} = \begin{bmatrix} \tilde{y}_{R1}^* & \dot{\tilde{y}}_{R1}^* \end{bmatrix} \begin{bmatrix} 0 & -j \\ j & 0 \end{bmatrix} \begin{bmatrix} \tilde{y}_{R1} \\ \dot{\tilde{y}}_{R1} \end{bmatrix}, \end{aligned} \tag{4.16}$$

and then makes a decision on the data bit in question, d_2, according to

$$\hat{d}_{2,k} = \text{sgn}(D). \tag{4.17}$$

An intuitive understanding of the above decision rule can be gained by considering the ideal situation where there are no fading and noise in *all* the links. In this case, the received phase derivatives at the relay and at node S_1 during the first and second phases of transmission are $\dot{\psi}_{1R}(t) = \pi h d_{1,k}/T$, $\dot{\psi}_{2R}(t) = \pi h d_{2,k}/T$, and $\dot{\psi}_{21}(t) = \pi h d_{2,k}/T$; see (4.4). Furthermore, the received phase derivative at user S_1 during the third phase is simply $\dot{\psi}_{R1}(t) = \pi h(d_{1,k} + d_{2,k})/T$. As a result, $\dot{\tilde{\psi}}_{R1}(t) = \dot{\psi}_{R1}(t) - \dot{\theta}_1(t) = \pi h d_{2,k}/T$. This means the sign of the decision variable D in (4.15) equals the sign of the data bit $d_{2,k}$. Naturally, in the presence of fading and noise, these phase derivatives are subjected to distortions. However, as long as the channels average SNR is at a decent level, the decision rule in (4.17) will still enable us to recover the data reliably. Further discussion on the optimality of (4.15) can be found in [31].

4.3.2 Detection of the 3-DPF and A4-DPF Signals

From the discussion in Sections 4.2.2 and 4.2.3, we can see that 3-DPF is a specific case of A4-DPF. For both schemes, the relay broadcasts a signal of the form $s_R(t) = \exp\{j\theta_R(t)\}$ in the final phase of cooperation, where $\theta_R(t) = \left(w_1\hat{\theta}_1(t) + w_2\hat{\theta}_2(t)\right)$ is the phase of the relayed signal, $\hat{\theta}_1(t)$ and $\hat{\theta}_2(t)$ are the detected phases at the relay, $(w_1, w_2) = (1, 1)$ for 3-DPF, and (w_1, w_2) alternates between $(3, 1)$ and $(1, 3)$ for A4-DPF. Using (4.12) as the definition of the received signal at S_1 during the third phase, we first remove S_1's own phase from $\psi_{R1}(t)$ according to

$$\begin{aligned} \tilde{y}_{R1} &= a_{R1}(t)e^{j\tilde{\psi}_{R1}(t)}, \\ \tilde{\psi}_{R1}(t) &= \left(\psi_{R1}(t) - w_1\theta_1(t)\right)/w_2. \end{aligned} \tag{4.18}$$

and then combine the derivative of $\tilde{\psi}_{R1}(t)$ non coherently with $\dot{\psi}_{21}(t)$, the received phase derivative at S_1 in Phase 2, according to (4.15) and (4.16). As in the case of PF, the decision rule is given by (4.17).

One nice feature about DF-based strategies is that the modulation index used at the relay, h_R, needs not to be identical to h, the modulation index used by S_1 and S_2. This flexibility is especially important if we want to impose stringent bandwidth requirement on the signal transmitted by the relay. If the relay does use a different modulation index, the effective form of the forwarded phase is $\theta_R(t) = \rho\left(w_1\hat{\theta}_1(t) + w_2\hat{\theta}_2(t)\right)$, where $\rho = h_R/h$ is

the ratio of modulation indices. In this case, (4.18) should be modified to

$$\begin{aligned} \tilde{y}_{R1} &= a_{R1}(t)\, e^{j\tilde{\psi}_{R1}(t)}, \\ \tilde{\psi}_{R1}(t) &= \left(\psi_{R1}(t) - \rho\, w_1\, \theta_1(t)\right)/(\rho\, w_2). \end{aligned} \tag{4.19}$$

before combining with $\dot{\psi}_{21}(t)$ according to (4.15) and (4.16).

4.4 Implementation Issues

We provide in this section some implementation guidelines for the proposed PF strategy. Comparison with the considered DF schemes, in terms of implementation complexity, will also be made.

According to (4.5), a PF relay needs to first convert the signals $y_{1R}(t)$ and $y_{2R}(t)$ in (4.1) into the constant envelope signals $\hat{y}_{1R} = \exp\{j \arg[y_{1R}(t)]\}$ and $\hat{y}_{2R} = \exp\{j \arg[y_{2R}(t)]\}$ before transmitting the product signal $s_R(t) = \hat{y}_{1R}(t)\hat{y}_{2R}(t)$ in the final phase of relaying. Given that the relay is half-duplex and cannot transmit and receive at the same time, it must first detect and store (the sufficient statistics of) the data packets it receives from S_1 and S_2 in their entireties before generating and forwarding the product constant envelope signal in the final phase. The procedure requires frame synchronization at the relay to ensure proper time-alignment of $\hat{y}_{1R}(t)$ and $\hat{y}_{2R}(t)$. This can be done by inserting a special sync pattern into each data packet and correlating the received signals with this pattern at the relay. As for storage of the entire frames of $\hat{y}_{1R}(t)$ and $\hat{y}_{2R}(t)$, this will be done in the digital domain via sampling and quantization. The minimum sampling frequency will be twice the bandwidth of $s_R(t)$, rather than twice the bandwidth of individual $\hat{y}_{1R}(t)$ and $\hat{y}_{2R}(t)$. This stems from the fact that signal mixing (multiplication) is a bandwidth-expanding process. We found that when the two source signals in (4.1) (namely $s_1(t)$ and $s_2(t)$) are MSK, then the product signal $s_R(t)$ has a bandwidth of $1.832/T$, where $1/T$ is the bit rate. So in this case, a sampling frequency of $4/T$ would be sufficient to create signal samples that capture all the information about the product signal. As for quantization, it is relatively straight forward because, unlike the original received signals $y_{1R}(t)$ and $y_{2R}(t)$, the real and imaginary components of $\hat{y}_{1R}(t)$ and $\hat{y}_{2R}(t)$ all have finite dynamic range. Specifically, the values of these components are confined to the interval $[-1, +1]$. Given the limited dynamic range, we can use a simple $(b+1)$ bits uniform quantizer, where b is chosen such that the

signal-to-quantization noise ratio (SQNR) is much higher than the channel SNR seen at the destination receiver. Since the SQNR of a uniform quantizer (assuming that the real and imaginary components of $\hat{y}_{1R}(t)$ and $\hat{y}_{2R}(t)$ are uniformly distributed in $[-1, +1]$) varies according to $2^{2(b+1)}$ [71], an 8-bit ($b = 7$) quantizer can already yield a SQNR of 48 dB, which is much higher than the anticipated channel SNR.

From the above discussion, it becomes clear that the proposed PF scheme requires a total of

$$N_{PF} = 4(b+1)KN \tag{4.20}$$

bits to store the signals $\hat{y}_{1R}(t)$ and $\hat{y}_{2R}(t)$ at the relay, where $f_s = K/T$ is the sampling frequency, $(b+1)$ is the number of bits used in quantization, N is the number of bits in each data packet, and the factor of 4 is the total number of real and imaginary components in $\hat{y}_{1R}(t)$ and $\hat{y}_{2R}(t)$. In contrast, the 3-level Decode-and-Phase-Forward (3-DPF) and Alternate 4-level Decode-and-Phase-Forward (A4-DPF) schemes described in Sections 4.2.2 and 4.2.3 require only

$$N_{DPF} = 2N \tag{4.21}$$

bits to store the decoded bit streams $\{\hat{d}_{1,n}\}_{n=1}^{N}$ and $\{\hat{d}_{2,n}\}_{n=1}^{N}$. However, this reduction in storage requirement comes at the expense of additional computations required for demodulation and re-modulation at the relay. According to (4.16), the discriminator detector used for demodulation needs to compute the phase derivatives in the original received signal $y_{1R}(t)$ and $y_{2R}(t)$ at the decision making instants. These derivatives can be expressed in terms of the constant envelope signals $\hat{y}_{1R}(t)$ and $\hat{y}_{2R}(t)$ as $-j\,\hat{y}_{1R}^{*}(t)\dot{\hat{y}}_{1R}(t)$ and $-j\,\hat{y}_{2R}^{*}(t)\dot{\hat{y}}_{2R}(t)$, where $\hat{y}^{*}$ and $\dot{\hat{y}}$ represent respectively signal conjugation and derivative. Let us assume the two signal derivatives $\dot{\hat{y}}_{1R}(t)$ and $\dot{\hat{y}}_{2R}(t)$ are computed in the digital domain with $\hat{y}_{1R}(t)$ and $\hat{y}_{2R}(t)$ represented by samples spaced T/K seconds apart, where K is an integer that is large enough to ensure that the sampling frequency $f_s = K/T$ is higher than twice the bandwidth of the product signal $s_R(t) = \hat{y}_{1R}(t)\hat{y}_{2R}(t)$. Then the corresponding discrete-time differentiator is simply a K-tap digital finite impulse response filter [1] with a computational

[1] Note that in theory, we can use a higher ($> K$) order differentiator to improve the accuracy of the derivative estimate. However, it is unclear if this is actually beneficial in practice, given that such a differentiator inevitably involves using samples that span multiple bits and the bit transitions may actually degrade the accuracy of the derivative estimate at the decision making instants.

complexity of K complex multiply-and-add (CMAD) for each decoded bit $\hat{d}_{1,n}$ or $\hat{d}_{2,n}$. As a result, the total demodulation complexity is

$$C_{DEMOD} = 2KN \qquad \text{(CMAD)} \tag{4.22}$$

As for the re-modulation complexity in DPF, if we assume a table look-up based modulator, then the basic operations are waveform fetching and concatenation. These operations can be assumed insignificant when compared to the multiply-and-add operations mentioned above. Although a table-look-up re-modulator requires storage of all possible modulation waveforms, this should not be counted towards the storage requirement of the two DPF schemes, since the modulator is always required to transmit a nodes own data, irrespective of whether it uses PF or DPF while in the relay mode. Another implementation structure that is common to PF and DPF is the analog-to-digital converter front end.

In summary, from the computational complexity point of view, PF is simpler because it avoids the CMAD operations required for demodulation at the relay. Although it requires substantially more storage, the tradeoff still favors PF because memory is inexpensive while additional computational load can, in general, lead to quicker battery drain and even the need of a more powerful processor. We note further that the complexity of PF can be further reduced if we adopt direct bandpass processing. This is achieved by first passing $\tilde{y}_{1R}(t)$ and $\tilde{y}_{2R}(t)$, the bandpass versions of $y_{1R}(t)$ and $y_{2R}(t)$, through a bandpass filter, followed by bandpass limiting [72], then bandpass sampling [73] and quantization. As shown in [73], the sampling frequency of the bandpass signals is roughly the same as that of their complex baseband versions. So no high speed analog to digital converter (ADC) is required. By direct bandpass processing, we can bypass up and down conversions in PF altogether, which in turn reduces the number of multiplication and addition required to perform these steps in a digital modulator/demodulator. It should be emphasized that with decode-and-phase-forward, down and up conversion are unavoidable.

4.5 Performance Analysis

4.5.1 The BER of PF

The BER performance of the PF scheme with discriminator detection is evaluated using the CF approach; see [31]. In the analysis, the variances of the fading processes $g_{ij}(t)$ in (4.1), where $i, j \in \{1, 2, R\}$ and $i \neq j$, are denoted as σ_{ij}^2, with $\sigma_{1R}^2 = \sigma_{R1}^2$, $\sigma_{2R}^2 = \sigma_{R2}^2$, and $\sigma_{12}^2 = \sigma_{21}^2$. On the other hand, the variances of the noise processes $n_{ij}(t)$ in these equations are denoted as $\sigma_{n_{ij}}^2$, with $\sigma_{n_{12}}^2 = \sigma_{n_{21}}^2 = \sigma_{n_{1R}}^2 = \sigma_{n_{2R}}^2 = N_0 B_{12}$ and $\sigma_{n_{R1}}^2 = \sigma_{n_{R2}}^2 = N_0 B_3$, where N_0 is the noise power spectral density (PSD), B_{12} the bandwidth of the receive LPFs in Phases 1 and 2, and B_3 the bandwidth of the receive LPF in Phase 3. In this investigation, B_{12} is always set to the 99% bandwidth of $s_1(t)$ and $s_2(t)$, while B_3 is either the same as B_{12}, or set to the 99% bandwidth of the relay signal $s_R(t)$. Given the nature of the symbol-by-symbol detectors described in the previous section, we take the liberty to drop the symbol index k in $d_{1,k}$ and $d_{2,k}$ in the performance analysis.

First, it is observed that the terms D_{21} in (4.16) is a quadratic forms of complex Gaussian variables $(y_{21}, \dot{y}_{21})$ when conditioned on $\dot{\theta}_2$; refer to Appendix 4A of this chapter for the statistical relationships between different parameters in the general channel model

$$y(t) = g(t)e^{j\theta(t)} + n(t) = a(t)e^{j\psi(t)}, \tag{4.23}$$

where $g(t)$ and $n(t)$ are, respectively, $\mathcal{CN}(0, \sigma_g^2)$ and $\mathcal{CN}(0, N_0)$, $\theta(t)$ is the signal phase, and $a(t)$ and $\psi(t)$ are the amplitude and phase of $y(t)$, respectively. Without loss of generality, we assume $d_{2,k} = +1$ and hence $\dot{\theta}_2(t) = \pi h/T$. By substituting $\theta = \dot{\theta}_2$ into (4A.5) and (4A.8), and with $\mathbf{F}$ in (4A.10) set to the $\begin{bmatrix} 0 & -j \\ j & 0 \end{bmatrix}$ matrix in (4.16), we can find the two poles of the CF of D_{21} as following:

$$p_1 = -\frac{1}{2\alpha_{21}\beta_{21}(1+\rho_{21})} < 0, \qquad p_2 = +\frac{1}{2\alpha_{21}\beta_{21}(1-\rho_{21})} > 0, \tag{4.24}$$

where α_{21}, β_{21}, ρ_{21} are determined from (4A.10) under the conditions $\dot{\theta} = \pi h/T$, $\sigma_g^2 = \sigma_{g_{21}}^2$ and $\sigma_n^2 = N_0 B_{12}$; B_{12} the bandwidth of the receive filter in Phases 1 and 2.

How about the term D_{R1} in (4.16)? This term can be rewritten as $D_{R1} = 2a_{R1}^2\dot{\Psi}_{R1} = 2\left(a_{R1}^2\dot{\psi}_{R1} - a_{R1}^2\dot{\theta}_1\right)$, or in the quadratic form as

$$D_{R1} = \begin{bmatrix} y_{R1}^* & \dot{y}_{R1}^* \end{bmatrix} \begin{bmatrix} -2\dot{\theta}_1 & -j \\ j & 0 \end{bmatrix} \begin{bmatrix} y_{R1} \\ \dot{y}_{R1} \end{bmatrix}, \tag{4.25}$$

which is once again a quadratic form of complex Gaussian variables. This quadratic form, however, depends on a number of parameters. First is the data phase derivation $\dot{\theta}_1$. Second, it depends on the forwarded phase derivative $\dot{\theta}_R = \dot{\psi}_{1R} + \dot{\psi}_{2R}$, which in turns depends on both $\dot{\psi}_{1R}$ and $\dot{\psi}_{2R}$; refer to (4.11). Of course, $\dot{\psi}_{1R}$ depends on $\dot{\theta}_1$, while $\dot{\psi}_{2R}$ depends on $\dot{\theta}_2$, refer to (4.9) and (4.10). Note that D_{21} and D_{R1} are statistically independent. Conditioned on $\dot{\psi}_{1R}$, $\dot{\psi}_{2R}$, $\dot{\theta}_1$, $\dot{\theta}_2 = \pi h/T$, and $\mathbf{F} = \begin{bmatrix} -2\dot{\theta}_1 & -j \\ j & 0 \end{bmatrix}$, we can determine from (4A.10) the poles of the CF of D_{R1} as

$$\begin{aligned} Q_1 &= \frac{\left(\chi_{R1}^2 - \dot{\theta}_1\alpha_{R1}^2\right) - \sqrt{\alpha_{R1}^2\left(\dot{\theta}_1^2\alpha_{R1}^2 - 2\theta_1^2\chi_{R1}^2 + \beta_{R1}^2\right)}}{2\left(1-\rho_{R1}^2\right)} < 0, \\ Q_2 &= \frac{\left(\chi_{R1}^2 - \dot{\theta}_1\alpha_{R1}^2\right) + \sqrt{\alpha_{R1}^2\left(\dot{\theta}_1^2\alpha_{R1}^2 - 2\theta_1^2\chi_{R1}^2 + \beta_{R1}^2\right)}}{2\left(1-\rho_{R1}^2\right)} > 0. \end{aligned} \tag{4.26}$$

where α_{R1}, β_{R1}, ρ_{R1}, χ_{R1}^2 are determined from (4A.10) under the conditions $\dot{\theta} = \dot{\psi}_{1R} + \dot{\psi}_{2R}$, $\sigma_g^2 = \sigma_{gR1}^2$, and $\sigma_n^2 = N_0B_3$; B_3 the bandwidth of the receive filter in Phase 3.

Recall that we assume $d_2 = \pm 1$ and hence $\dot{\theta}_2(t) = \pi h/T$. In this case, the detector makes a wrong decision when $D < 0$. Since the CF of D is

$$\Phi_D(s) = \frac{(p_1p_2)(Q_1Q_2)}{(s-p_1)(s-p_2)(s-Q_1)(s-Q_2)},$$

the probability that $D < 0$ is the sum of residues of $-\Phi_D(s)/s$ at the right plane poles p_2 and Q_2, yielding

$$\begin{aligned} Pr\left[D < 0 \middle| \dot{\theta}_1, \dot{\theta}_2 = \pi h/T, \dot{\psi}_{1R}, \dot{\psi}_{2R}\right] = \\ \frac{-p_1}{p_2 - p_1}\frac{Q_1Q_2}{(p_2-Q_1)(p_2-Q_2)} + \frac{-Q_1}{Q_2-Q_1}\frac{p_1p_2}{(Q_2-p_1)(Q_2-p_2)}. \end{aligned} \tag{4.27}$$

Finally, since $\dot{\psi}_{1R}$ and $\dot{\psi}_{2R}$ are random variables given $\dot{\theta}_1$ and $\dot{\theta}_2$, respectively, the unconditional error probability can be expressed in semi-analytical form as

$$\begin{aligned} P_b = \frac{1}{2} \sum_{d_1=-1}^{+1} \int_{-\infty}^{\infty} \int_{-\infty}^{\infty} Pr\left[D < 0 | \dot{\theta}_1 = \pi h d_1/T, \dot{\theta}_2 = \pi h d_2/T, \dot{\psi}_{1R}, \dot{\psi}_{2R}\right] \\ \times p\left(\dot{\psi}_{1R} \middle| \dot{\theta}_1 = \frac{\pi h d_1}{T}\right) p\left(\dot{\psi}_{2R} \middle| \dot{\theta}_2 = \frac{\pi h d_2}{T}\right) d\dot{\psi}_{1R} d\dot{\psi}_{2R} \end{aligned} \tag{4.28}$$

where the marginal probability density functions and can be determined from (4A.5)-(4A.6) in Appendix 4A.

4.5.2 BER of 3-DPF and A4-DPF Signals

The two multi-level DPF signals broadcasted by the relay in (4.6) and (4.7) are constructed from decisions made by the relay about user nodes S_1 and S_2's data. Although different from (4.5), the exact BER analysis of these signals can still be determined via the CF approach. This stems from the fact that the decision variable D of these DPF schemes are again quadratic forms of complex Gaussian variables when conditioned on the data phase derivatives $\dot{\theta}_1$ and $\dot{\theta}_2$, as well as their decoded versions $\dot{\hat{\theta}}_1$ and $\dot{\hat{\theta}}_2$ at the relay. Specifically, the poles of the CF of D_{21} are identical to those in the PF case, and can be found in (4.24). As for the poles of the CF of D_{R1}, we should first replace the term $\dot{\theta}$ in the Appendix by $\dot{\theta}_R = w_1\dot{\hat{\theta}}_1 + w_2\dot{\hat{\theta}}_2$ and then modify the $\mathbf{F}$ matrix in (4A.10) to

$$\mathbf{F} = \begin{bmatrix} -2\frac{w_1}{w_2}\dot{\theta}_1 & \frac{-j}{w_2} \\ \frac{j}{w_2} & 0 \end{bmatrix} \tag{4.29}$$

The resultant poles are found to be

$$\begin{aligned} Z_1 &= \frac{\left(\chi_{R1}^2 - w_1\dot{\theta}_1\alpha_{R1}^2\right) - \sqrt{\alpha_{R1}^2\left[\left(w_1\dot{\theta}_1\right)^2\alpha_{R1}^2 - 2w_1\dot{\theta}_1\chi_{R1}^2 + \beta_{R1}^2\right]}}{2\left(1-\rho_{R1}^2\right)\alpha_{R1}^2\beta_{R1}^2} w_2 < 0, \\ Z_2 &= \frac{\left(\chi_{R1}^2 + w_1\dot{\theta}_1\alpha_{R1}^2\right) - \sqrt{\alpha_{R1}^2\left[\left(w_1\dot{\theta}_1\right)^2\alpha_{R1}^2 - 2w_1\dot{\theta}_1\chi_{R1}^2 + \beta_{R1}^2\right]}}{2\left(1-\rho_{R1}^2\right)\alpha_{R1}^2\beta_{R1}^2} w_2 > 0, \end{aligned} \tag{4.30}$$

where α_{R1}, β_{R1}, ρ_{R1} and χ_{R1}^2 are determined from (4A.10) under the conditions $\dot{\theta} = w_1\dot{\hat{\theta}}_1 + w_2\dot{\hat{\theta}}_2$, $\sigma_g^2 = \sigma_{g_{R1}}^2$, and $\sigma_n^2 = N_0 B_{12}$; B_{12} the bandwidth of the receive filter in Phase 3. As

in the case of PF, the conditional BER is expressed in the form

$$Pr\left[D<0\,\middle|\dot{\theta}_1,\dot{\theta}_2=\pi h/T,\dot{\psi}_{1R},\dot{\psi}_{2R}\right]= \frac{-p_1}{p_2-p_1}\frac{Z_1Z_2}{(p_2-Z_1)(p_2-Z_2)}+\frac{-Z_1}{Z_2-Z_1}\frac{p_1p_2}{(Z_2-p_1)(Z_2-p_2)}. \tag{4.31}$$

The only difference between (4.31) and (4.27) is that the former is conditioned on the hard decisions $\dot{\hat{\theta}}_1$ and $\dot{\hat{\theta}}_2$ made at the relay, while the latter is based on the soft decisions $\dot{\psi}_{1R}$ and $\dot{\psi}_{2R}$. If we let $P_{e,1}$ and $P_{e,2}$ be the probabilities that the relay makes a wrong decision about S_1 and S_2's data respectively, then the unconditional BER is

$$\begin{aligned}P_b=\frac{1}{2N_w}\sum_{d_1=-1}^{+1}\sum_{w_1,w_2}\Bigg\{&(1-P_{e,1})(1-P_{e,2})Pr\left[D<0\,\middle|\dot{\theta}_1=\frac{\pi hd_1}{T},\dot{\theta}_2=\frac{\pi h}{T},\dot{\hat{\theta}}_1=\dot{\theta}_1,\dot{\hat{\theta}}_2=\dot{\theta}_2\right]\\ &+(1-P_{e,1})P_{e,2}Pr\left[D<0\,\middle|\dot{\theta}_1=\frac{\pi hd_1}{T},\dot{\theta}_2=\frac{\pi h}{T},\dot{\hat{\theta}}_1=\dot{\theta}_1,\dot{\hat{\theta}}_2=-\dot{\theta}_2\right]\\ &+P_{e,1}(1-P_{e,2})Pr\left[D<0\,\middle|\dot{\theta}_1=\frac{\pi hd_1}{T},\dot{\theta}_2=\frac{\pi h}{T},\dot{\hat{\theta}}_1=-\dot{\theta}_1,\dot{\hat{\theta}}_2=\dot{\theta}_2\right]\\ &+P_{e,1}P_{e,2}Pr\left[D<0\,\middle|\dot{\theta}_1=\frac{\pi hd_1}{T},\dot{\theta}_2=\frac{\pi h}{T},\dot{\hat{\theta}}_1=-\dot{\theta}_1,\dot{\hat{\theta}}_2=-\dot{\theta}_2\right]\Bigg\}\end{aligned} \tag{4.32}$$

where $N_w=1$ for 3-DPF and $N_w=2$ for A4-DPF, and the inner summation is over the two different permutations of w_1 and w_2 in (4.8). It should be pointed out the error probabilities $P_{e,1}$ and $P_{e,2}$ can be determined by integrating the marginal pdf in (4A.6) from $-\infty$ to 0 when the data bit is a $+1$, or from 0 to $+\infty$ when the data bit is a -1. The end result is of the form [31, 74]

$$P_{e,i}=\frac{1}{2}\left(1-|\rho_i|\right);\qquad\qquad i\in\{1,2\}, \tag{4.33}$$

where $|\rho_1|$ and $|\rho_2|$ are $|\rho|$ in (4A.5) obtained under the conditions $\sigma_g^2=\sigma_{1R}^2$, $\sigma_n^2=N_0B_{1R}$ and $\sigma_g^2=\sigma_{2R}^2$, $\sigma_n^2=N_0B_{2R}$ respectively.

4.6 Numerical Results

We present next some numerical results for the proposed three-phase two-way PF and DPF relaying schemes. For simplicity, we only consider the case of MSK, i.e. $h=1/2$, and plot the BER of the resultant cooperative communication system as a function of the SNR in the direct link between S_1 and S_2. In general, the SNR of a link is defined as the fading

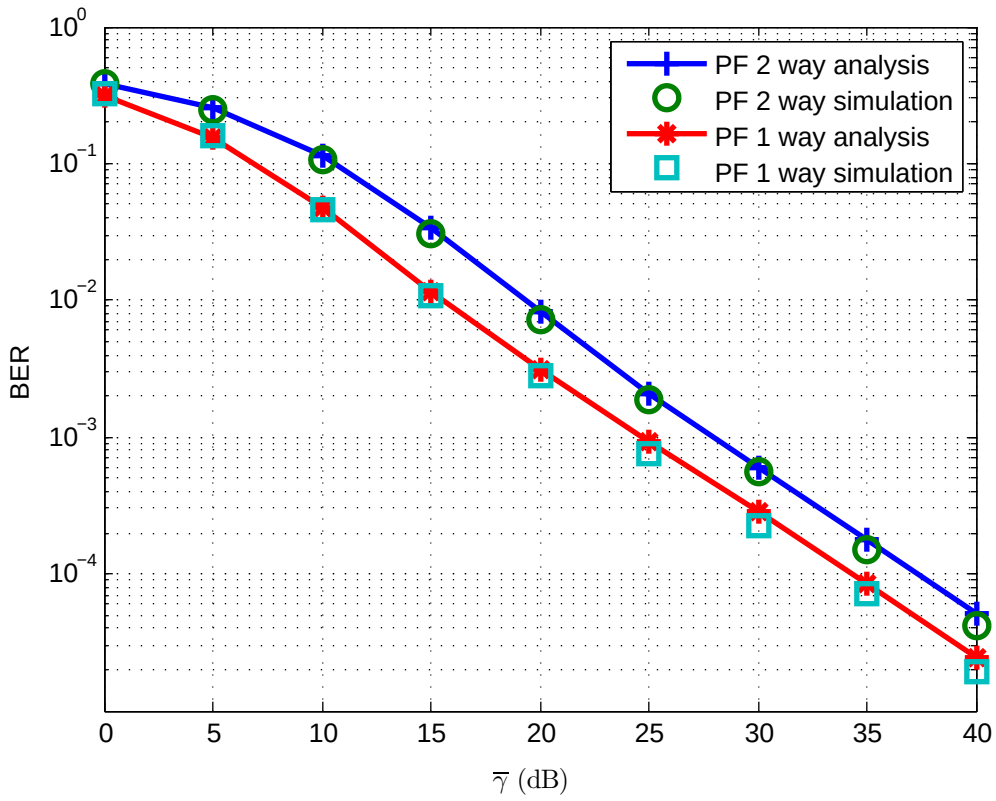

Figure 4.1: BER of three-phase two-way PF cooperative transmission in a static Rayleigh fading channel; $B_{12} = 1.1818/T$ and $B_3 = 1.832/T$.

variance σ_g^2 to noise variance σ_n^2 ratio in that link. Since the energy per transmitted bit is $E_b = \sigma_{12}^2 T$ and the noise variance is $\sigma_n^2 = N_0 B_{12} = N_0 \times 1.1818/T$ in the direct link, where N_0 is the noise power spectral density and $1.1818/T$ is the 99% bandwidth of MSK, the SNR is equivalent to $0.85E_b/N_0$. Unless otherwise stated, all the links are assumed to have the same SNR and the same fade rate $f_d T$.

Figure 4.1 considers the case of static fading whereas Figure 4.2 considers the case of time-selective fading with a normalized Doppler frequency of $f_d T = 0.03$ in all the links. To put the two-way relaying results into perspective, we compare them against the one-way relaying results from [31] for MSK source signal and phase-forward relay signal. The BER curves shown in these figures were obtained from the semi-analytical expression in (4.17) and as well as from simulation. The two sets of results are in good agreement.

In the static fading case, it is observed from Figure 4.1 that two-way relaying is consistently 3 dB less power efficient than one-way relaying over a wide range of BER. In the fast fading case, two-way relaying has an irreducible error floor around 10^{-3} while that of

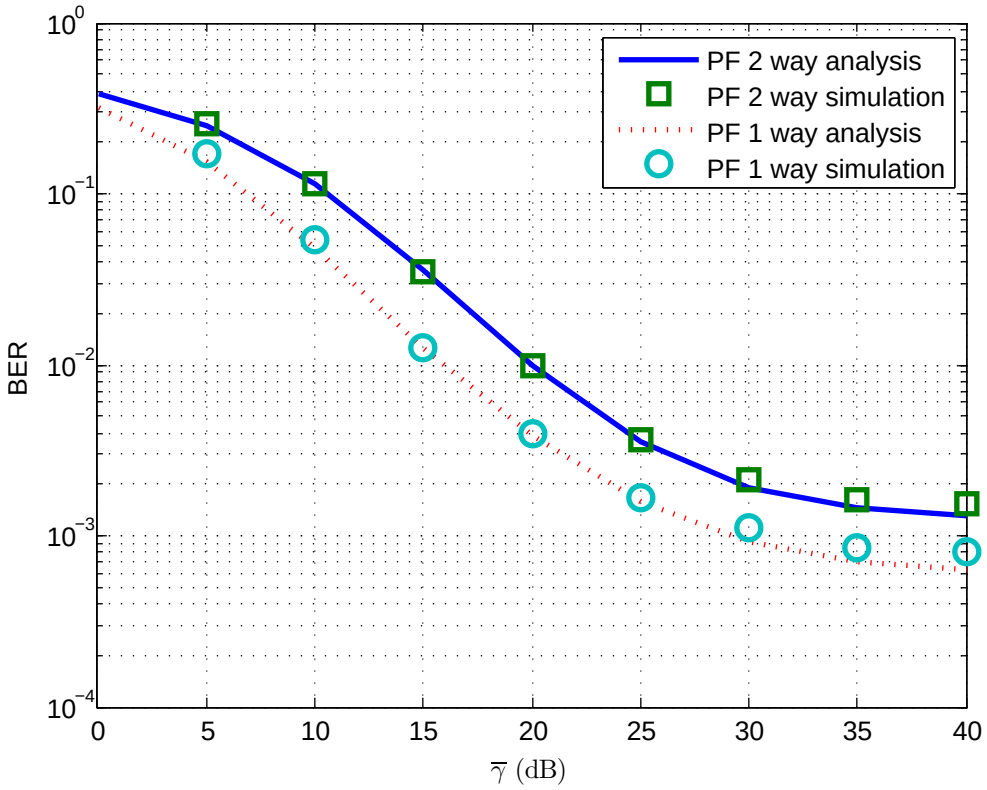

Figure 4.2: BER of three-phase two-way PF cooperative transmission in a time-selective Rayleigh fading channel; $f_d T = 0.03$; $B_{12} = 1.1818/T$ and $B_3 = 1.832/T$.

one-way relaying sits at 6×10^{-4}. Above the irreducible error floors and at a BER of 10^{-2}, the difference between one and two-way relaying is about 5 dB.

One source for the degraded performance stated above is simply energy normalization. In both figures, we assume all the nodes transmit with a bit-energy of E_b. This means one-way relaying needs a total of $4E_b$ transmit two bits while two-way relaying needs only $3E_b$ to transmit the same amount of information. So if we normalize the energy, the difference between the two schemes in the static fading case actually reduces to only 1.5 dB. We regard this loss as acceptable, given that two-way relaying improves the transmission efficiency by 33%.

The results obtained above were based on using a receive low pass filter (LPF) in the $R \rightarrow S_1$ path whose bandwidth, B_3, equals the 99% bandwidth of the relay signal. As mentioned earlier, because of the spectral convolution effect, the bandwidth of the relay signal is larger than that of the original MSK signal and is found to be $1.832/T$. A natural question is, how would PF perform if the signal in the $R \rightarrow S_1$ path is band-limited to that of the MSK signal? Specifically, what is the tradeoff between a reduced noise figure but an increased signal distortion because of tighter filtering? Figure 4.3 shows the effect of using the same LPF in the relay path and the direct path, i.e. $B_3 = B_{12} = 1.1818/T$. The simulation results show that with a narrower filter in the relay path, the proposed PF scheme actually achieves a better performance. We attribute this to the fact that non-coherent detection is not match filtering, and the reduction in noise level through tighter filtering more than compensates for the self-interference that it generates.

In a two way relaying system, the SNRs of different links are not necessarily equal as explained in the previous chapters. For instance, if the relay is much closer to one of S_1 and S_2, then we expect the SNR in the $S_1 \rightarrow R$ or $S_2 \rightarrow R$ link to be higher than that in the $S_2 \rightarrow S_1$ link. We next show in Figures 4.4 and 4.5 BER results for different asymmetric channel conditions, for both static fading and time-selective fading with a normalized fade rate of 0.03. As in Figure 4.3, the bandwidth of the LPF filter in the $R \rightarrow S_1$ path is set to that of MSK. Three different scenarios are considered -

1. All the links have the same SNR,

2. The two source-relay paths have higher SNRs, and

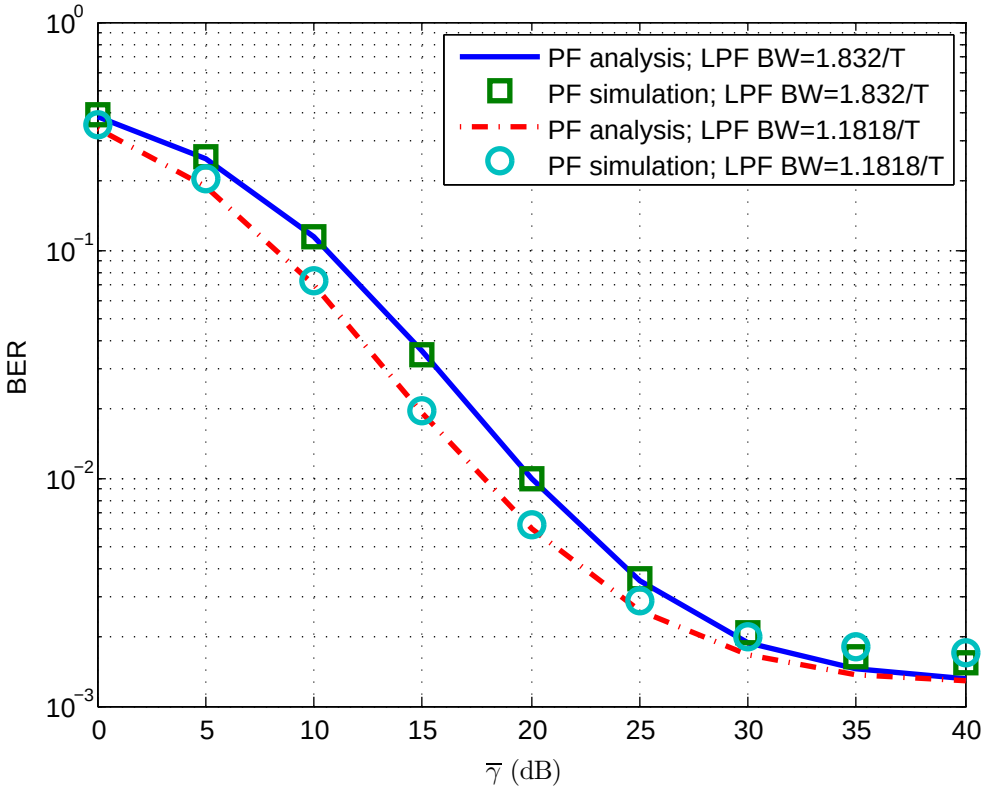

Figure 4.3: Effect of using the different LPF bandwidth, B_3, in Phase 3 of PF cooperative transmission; $f_d T = 0.03$.

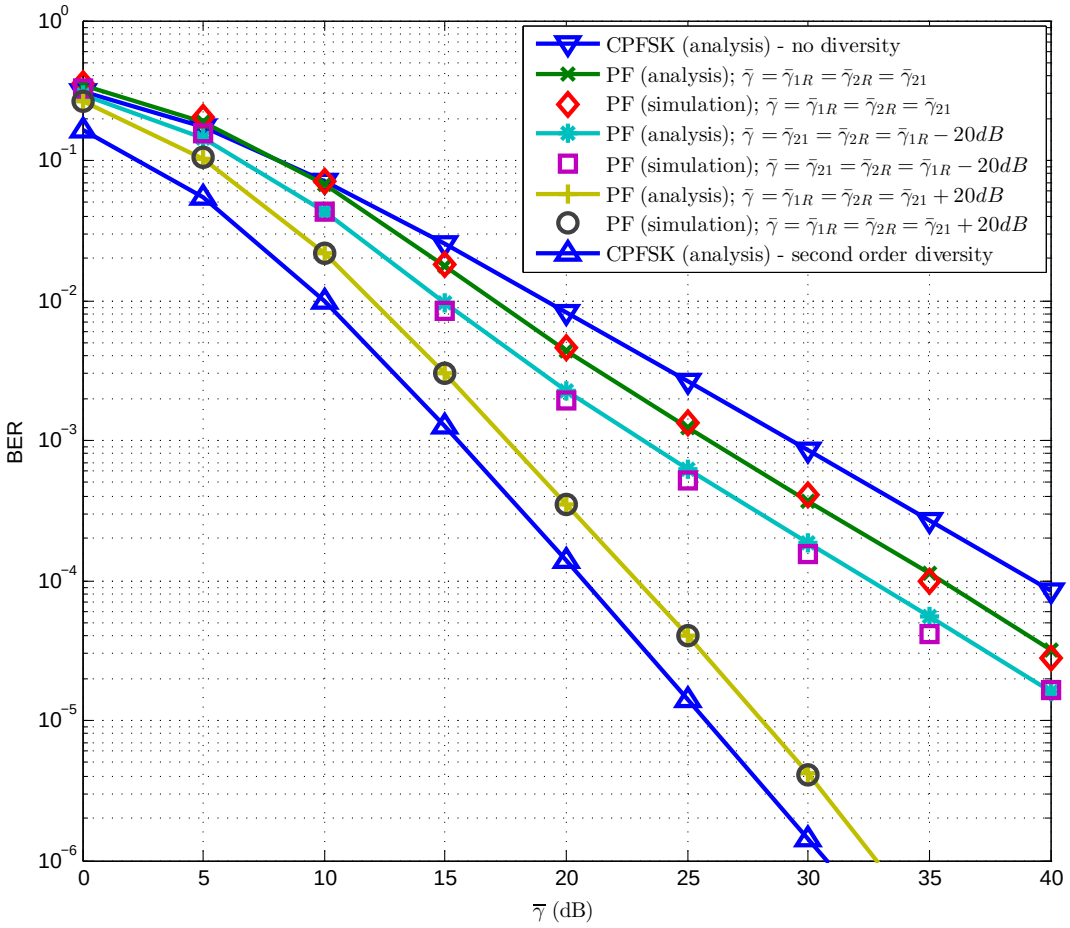

Figure 4.4: BER at S_1 for unequal SNR under static fading; $\bar{\gamma}_{1R}$, $\bar{\gamma}_{2R}$ and $\bar{\gamma}_{21}$ are the SNRs in the $S_1 \rightarrow R$, $S_2 \rightarrow R$ and $S_2 \rightarrow S_1$ links.

3. Only one of the source-relay paths is stronger.

Also included in Figures 4.4 and 4.5 are the BERs of MSK without diversity and with dual-receive diversity. From the figures, we can see that when the SNR in both the $S_1 \rightarrow R$ and $S_2 \rightarrow R$ links is 20 dB stronger than that in the $S_2 \rightarrow S_1$ link, the BER curve exhibits a very prominent second order diversity effect. In contrast, when all the three links are equally strong, the diversity effect disappears (the case when only the $S_1 \rightarrow R$ link has a higher SNR than the $S_2 \rightarrow S_1$ link falls in between these two cases).

Finally, we show in Figures 4.6 and 4.7 BER curves for the DF based 3-DPF and A4-DPF schemes. Also included in the figures are results for the proposed PF scheme. The bandwidth of all the receive LPFs is set to $1.1818/T$, the bandwidth of MSK. From Figure 4.6, we can see that the performance of PF is consistently 2 dB more energy efficient than

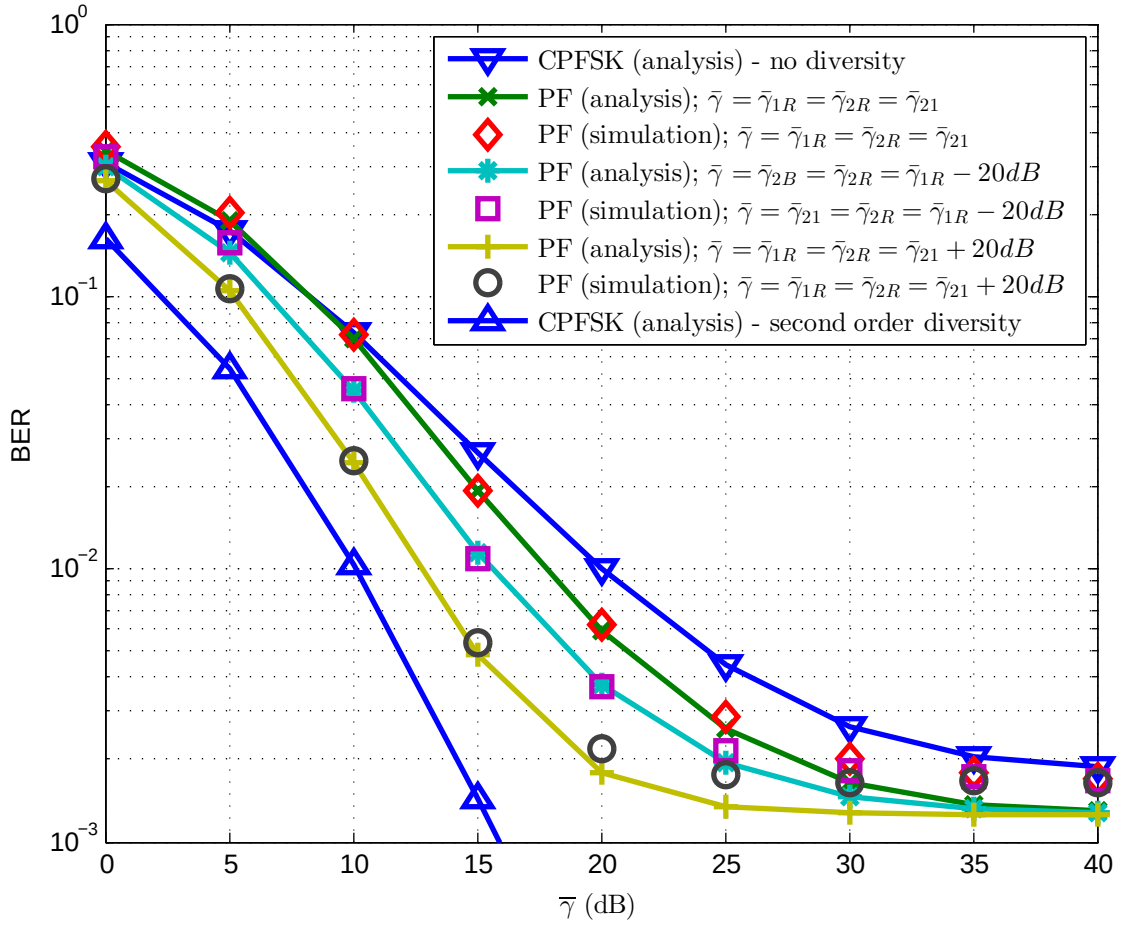

Figure 4.5: BER at S_1 for unequal SNR and a fade rate of $f_dT = 0.03$; $\bar{\gamma}_{1R}$, $\bar{\gamma}_{2R}$ and $\bar{\gamma}_{21}$ are the SNRs in the $S_1 \rightarrow R$, $S_2 \rightarrow R$ and $S_2 \rightarrow S_1$ links.

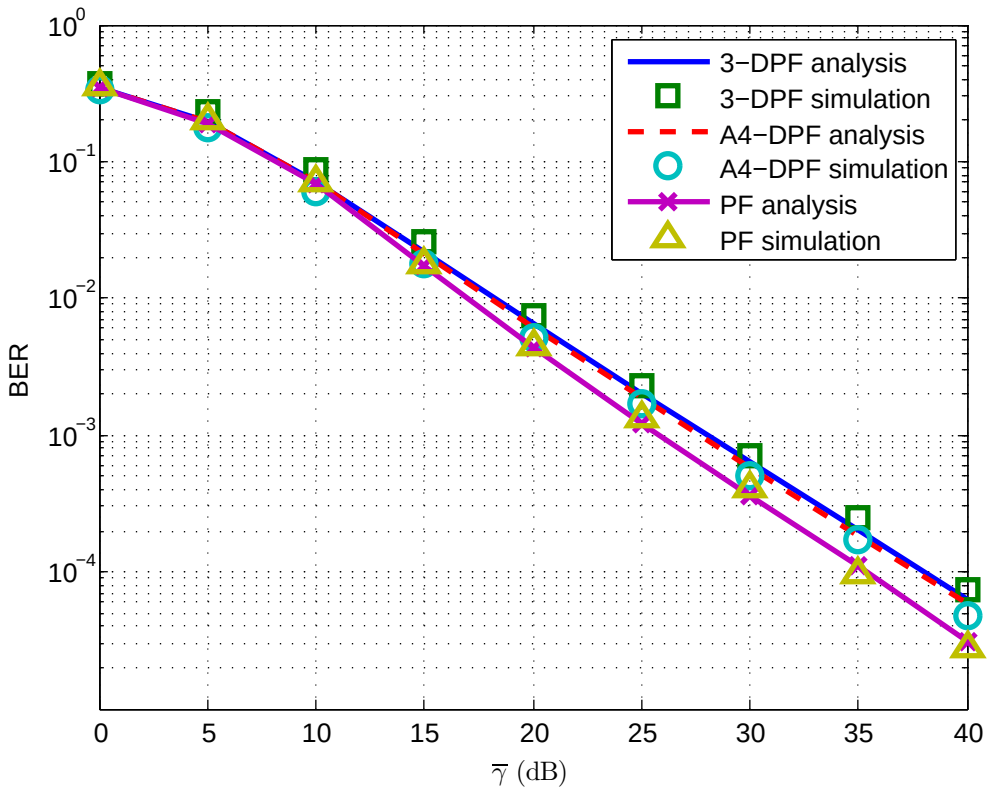

Figure 4.6: Performance of multi-level DPF and PF in static fading channel; $B_{12} = B_3 = 1.1818/T$.

the two multi-level DPF schemes when fading is static. With time-selective fading, the simulation results indicate PF and A4-DPF have somewhat similar performance and both are more power efficient than 3-DPF. Hence, it can be concluded that the proposed PF scheme not only offers a complexity advantage over multi-level DPF, it also provides a BER advantage.

4.7 Conclusions

We consider in this chapter the use of constant envelope modulation in three-phase two-way cooperative transmission. Specifically, CPFSK PF is proposed and its BER performance compared to one-way relaying and to two-way relaying based on decode-and-forward and multi-level re-modulation. As demonstrated in this chapter, the proposed technique allows us to maintain constant envelope signaling throughout the signaling chain. This property enables the relay to operate with highly power efficient power amplifiers without

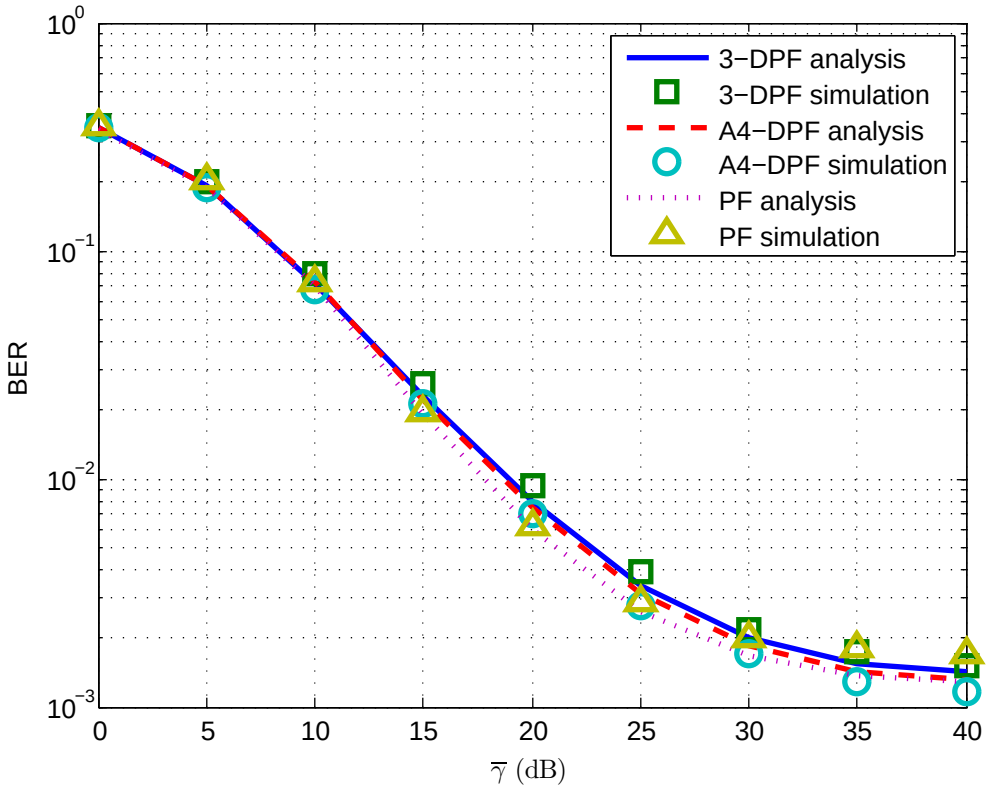

Figure 4.7: Performance of multi-level DPF and PF in a time-selective fading channel with an $f_dT = 0.03$; $B_{12} = B_3 = 1.1818/T$.

distortion, and does not require complicated signal processing at the relay like its decode-and-forward counterparts. Through analytical and simulation studies, we found that the BER of PF with discriminator detection in Rayleigh fading suffers only a moderate loss in energy efficiency (of 1.5 dB after energy normalization) when compared to its one-way relaying counterpart. We consider this loss as acceptable, considering that PF improves the transmission efficiency by 33% and it offers a way to avoid expensive linear power amplifiers and complicated signal processing at the relay. We also found that, in comparison with its decoded-and-forward counterparts, the proposed PF scheme offers a lower BER while at the same time relieves the relay from performing unnecessary demodulation and re-modulation tasks.

Appendix 4A Statistical Properties of Faded Signal

We discuss in this Appendix the statistical properties of the faded signal

$$y(t) = g(t)e^{j\theta(t)} + n(t) = a(t)e^{j\psi(t)}, \tag{4A.1}$$

where $g(t)$ and $n(t)$ are zero-mean complex Gaussian processes with variances (per dimension) of σ_g^2 and σ_n^2 respectively, $\theta(t)$ is the transmitted signal phase, which is treated as a deterministic parameter, and $a(t)$ and $\psi(t)$ are respectively the amplitude and phase of $y(t)$. Furthermore, the autocorrelation functions of $g(t)$ follows a Jakes spectrum, i.e.

$$R_g(\tau) = \frac{1}{2}\mathbb{E}[g^*(t)g(t+\tau)] = \sigma_g^2 J_0(2\pi f_d \tau), \tag{4A.2}$$

where f_d is the bandwidth (Doppler frequency) of $g(t)$. The noise term, $n(t)$, on the other hand, is band-limited white noise with an autocorrelation function of

$$R_n(\tau) = \frac{1}{2}\mathbb{E}[n^*(t)n(t+\tau)] = \sigma_n^2 sinc(B\tau), \tag{4A.3}$$

where $\sigma_n^2 = N_0 B$, N_0 being the power spectral density of $n(t)$, and B the bandwidth of $e^{j\theta(t)}$.

At any time instant, the joint pdf of a, its derivative $\dot{a}$, ψ, its derivative $\dot{\psi}$, given the data phase derivative $\dot{\theta}$, is [31, 74]

$$\begin{aligned} p(a,\dot{a},\psi,\dot{\psi}|\dot{\theta}) =& \frac{a^2}{4\pi^2\alpha^2\beta^2(1-\rho^2)} \exp\left\{-\frac{\dot{a}^2}{2\beta^2(1-\rho^2)}\right\} \\ & \times \exp\left\{-\frac{a^2}{2\beta^2(1-\rho^2)}\left[\left(\dot{\psi}^2 - \rho\frac{\beta}{\alpha}\right) + \frac{\beta^2}{\alpha^2}(1-\rho^2)\right]\right\}, \end{aligned} \tag{4A.4}$$

where

$$\begin{aligned}
\alpha^2 =& \frac{1}{2}\mathbb{E}\big[|y(t)|^2\big] = \sigma_g^2 + \sigma_n^2, \quad \beta^2 = \frac{1}{2}\mathbb{E}\big[|\dot{y}(t)|^2\big] = \sigma_g^2\,\dot{\theta}^2 + \lambda + \sigma_{\dot{n}}^2, \\
\lambda =& \frac{1}{2}\mathbb{E}\big[|\dot{g}(t)|^2\big] = 2\pi^2 f_d^2\,\sigma_g^2, \quad \sigma_{\dot{n}}^2 = \frac{1}{2}\mathbb{E}\big[|\dot{n}(t)|^2\big] = \pi^2 B^2 \sigma_n^2/3, \\
\chi^2 =& j\frac{1}{2}\mathbb{E}[y(t)\dot{y}^*(t)] = \sigma_g^2\,\dot{\theta}, \qquad \rho = \chi^2/(\alpha\beta) = \sigma_g^2\,\dot{\theta}/(\alpha\beta),
\end{aligned} \tag{4A.5}$$

with $\dot{g}(t)$, $\dot{n}(t)$, $\dot{y}(t)$ being the derivatives of $g(t)$, $n(t)$, $y(t)$ respectively. A useful marginal pdf of (4A.4) is the pdf of $\dot{\psi}$ given $\dot{\theta}$, which is found to be

$$p(\dot{\psi}|\dot{\theta}) = \frac{\beta^2(1-\rho^2)}{2\alpha^2}\left[\left(\dot{\psi} - \rho\frac{\beta}{\alpha}\right)^2 + \frac{\beta^2}{\alpha^2}(1-\rho^2)\right]^{-\frac{3}{2}} \tag{4A.6}$$

Another useful property is that the random vector

$$\mathbf{r} = \begin{bmatrix} y \\ \dot{y} \end{bmatrix} \tag{4A.7}$$

is zero mean complex Gaussian with a covariance matrix of

$$\mathbf{\Phi} = \frac{1}{2}\mathbb{E}\big[\mathbf{r}\mathbf{r}^H\big] = \begin{bmatrix} \alpha^2 & -j\chi^2 \\ j\chi^2 & \beta^2 \end{bmatrix} \tag{4A.8}$$

Consequently, the CF of the quadratic form

$$D = \mathbf{r}^H \mathbf{F}\,\mathbf{r} \tag{4A.9}$$

is

$$\Phi(s) = \|\mathbf{I} + 2s\mathbf{\Phi}\mathbf{F}\|^{-1} = \frac{p_1 p_2}{(s-p_1)(s-p_2)} \tag{4A.10}$$

where $\|\cdot\|$ denotes the determinant of a matrix, s is the transform domain parameter, and $p_1 < 0$ and $p_2 > 0$ are respectively the left and right plane poles of the CF.

Chapter 5

Conclusion and Future Work

In this thesis, we considered two multiplication based two-way relay protocols, the MF and PF relay protocols. These two protocols have been shown to work with both coherent and non-coherent modulation. The newly proposed relay protocols are insensitive to power amplifier non-linearity and are therefore suitable for low cost high power efficiency applications.

In Chapter 2, coherent modulation, i.e. MPSK, is used to develop the MF and PF relay protocols. These protocols are studied under both LPA and NLPA and show that they offer superior performance over the conventional AF two-way relay when the relay power amplifier has limited instantaneous power. Further, PSK PF relay protocol achieves lower BER than the AF counterpart. Both theoretical analysis and simulation were carried out to characterize the BER performance of the relay protocols. We also found that both MF and PF relays can achieve second order diversity.

When non-coherent modulations are used, we see that the MF and PF protocols have the main advantage of having simple self-interference cancellation operation at the receiver end. In Chapter 3, we applied both MF and PF protocols to DPSK modulation. The DPSK MF and PF relays were found to work under both static and fast fading. And a BER lower bound was derived for the static fading scenario. Based on this lower bound, we were able to show that the DPSK MF two-way relay can fully exploit the diversity order available to the system. Due to the lack of CSI at the receiver, the performance gain of PF over MF protocol depends on uplink channel conditions. And the PF relay should be used when the

relay is positioned in between the two user terminals to achieve best performance. Because of the omission of pilot symbols in the DPSK modulated relay network, scalability can be achieved easier compared to coherent relay network. This motivated us to generalized the DPSK MF relay, and through analysis on the BER, we determined that the proposed DPSK MF relay can fully utilize the diversity order available to the system.

In Chapter 4, the PF protocol was used with CPFSK modulation that achieves constant envelop relay transmitted signal. The combination of PF forwarding relay and CPFSK modulation led to a highly power efficient cooperative system. For comparison purpose, we correspondingly developed two DF two-way relay protocols for the CPFSK. The DF protocols allows self-interference cancellation before decision and can be combined with direct path signal for data detection. Exact BER results were obtained for the proposed protocols and were further verified by simulation.

The ideas reported in this thesis are new and has not been previously reported in the two-way relay literature. Future research work may include extending the MF and PF protocols to more spectrum efficient modulations such as the QAM. In the literature, star-QAM has been know as to work with power efficient power amplifiers. It may be a good modulation candidate to work with MF or PF protocols to improve data rate.

Bibliography

[1] A. Sendonaris, E. Erkip, and B. Aazhang, "User cooperation diversity — Part I: System description," *IEEE Transactions on Communications*, vol. 51, no. 11, pp. 1927–1938, Nov. 2003. 1

[2] R. Nabar, H. Bolcskei, and F. Kneubuhler, "Fading relay channels: performance limits and space-time signal design," *IEEE Journal on Selected Areas in Communications*, vol. 22, no. 6, pp. 1099–1109, Aug. 2004. 1, 2

[3] A. Nosratinia, T. Hunter, and A. Hedayat, "Cooperative communication in wireless networks," *IEEE Communications Magazine*, vol. 42, no. 10, pp. 74–80, Oct. 2004. 1

[4] J. Laneman, D. Tse, and G. Wornell, "Cooperative diversity in wireless networks: Efficient protocols and outage behavior," *IEEE Transactions on Information Theory*, vol. 50, no. 12, pp. 3062–3080, Dec. 2004. 1, 2

[5] T. Cover and A. Gamal, "Capacity theorems for the relay channel," *IEEE Transactions on Information Theory*, vol. 25, no. 5, pp. 572–584, Sep. 1979. 1

[6] C.-X. Wang, X. Hong, X. Ge, X. Cheng, G. Zhang, and J. Thompson, "Cooperative MIMO channel models: A survey," *IEEE Communications Magazine*, vol. 48, no. 2, pp. 80–87, Feb 2010. 1

[7] L. Xiao, T. Fuja, and J. Costello, D.J., "Mobile relaying: Coverage extension and throughput enhancement," *IEEE Transactions on Communications*, vol. 58, no. 9, pp. 2709–2717, September 2010. 1

[8] Y. Yang, H. Hu, J. Xu, and G. Mao, "Relay technologies for WiMax and LTE-advanced mobile systems," *IEEE Communications Magazine*, vol. 47, no. 10, pp. 100–105, October 2009. 1

[9] A. Ghosh, R. Ratasuk, B. Mondal, N. Mangalvedhe, and T. Thomas, "LTE-advanced: next-generation wireless broadband technology," *IEEE Transactions on Wireless Communications*, vol. 17, no. 3, pp. 10–22, June 2010. 1

[10] A. Ribeiro, X. Cai, and G. Giannakis, "Symbol error probabilities for general cooperative links," *IEEE Transactions on Wireless Communications*, vol. 4, no. 3, pp. 1264–1273, May 2005. 1, 2

[11] Y. Jing and H. Jafarkhani, "Single and multiple relay selection schemes and their achievable diversity orders," *IEEE Transactions on Wireless Communications*, vol. 8, no. 3, pp. 1414–1423, March 2009. 1

[12] Y. Zhao, R. Adve, and T. J. Lim, "Improving amplify-and-forward relay networks: optimal power allocation versus selection," *IEEE Transactions on Wireless Communications*, vol. 6, no. 8, pp. 3114–3123, August 2007. 2

[13] S. J. Kim, P. Mitran, and V. Tarokh, "Performance bounds for bidirectional coded cooperation protocols," *IEEE Transactions on Information Theory*, vol. 54, no. 11, pp. 5235–5241, Nov 2008. 2

[14] X. J. Zhang and Y. Gong, "Adaptive power allocation in two-way amplify-and-forward relay networks," in *Communications, 2009. ICC '09. IEEE International Conference on*, June 2009, pp. 1–5. 2

[15] Z. Yi and I.-M. Kim, "Optimum beamforming in the broadcasting phase of bidirectional cooperative communication with multiple decode-and-forward relays," *IEEE Transactions on Wireless Communications*, vol. 8, no. 12, pp. 5806–5812, December 2009. 2

[16] Q. Zhou, Y. Li, F. Lau, and B. Vucetic, "Decode-and-forward two-way relaying with network coding and opportunistic relay selection," *IEEE Transactions on Communications*, vol. 58, no. 11, pp. 3070–3076, November 2010. 2

[17] M. Chen and A. Yener, "Power allocation for multi-access two-way relaying," in *Proceedings IEEE International Conference Communications (ICC'09)*, Dresden, Germany, Jun. 2009. 2

[18] H. Guo, J. Ge, and H. Ding, "Symbol error probability of two-way amplify-and-forward relaying," *IEEE Communications Letters*, vol. 15, no. 1, pp. 22–24, January 2011. 5, 13

[19] K.-S. Hwang, Y.-C. Ko, and M.-S. Alouini, "Performance bounds for two-way amplify-and-forward relaying based on relay path selection," in *Vehicular Technology Conference, 2009. VTC Spring 2009. IEEE 69th*, April 2009, pp. 1–5. 5, 13

[20] J. Yang, P. Fan, T. Duong, and X. Lei, "Exact performance of two-way af relaying in nakagami-m fading environment," *IEEE Transactions on Wireless Communications*, vol. 10, no. 3, pp. 980–987, March 2011. 5, 13

[21] Q. Liu, W. Zhang, X. Ma, and G. Zhou, "Designing peak power constrained amplify-and-forward relay networks with cooperative diversity," *IEEE Transactions on Wireless Communications*, vol. 11, no. 5, pp. 1733–1743, May 2012. 5

[22] K. Ishibashi and H. Ochiai, "Analysis of instantaneous power distributions for non-regenerative and regenerative relaying signals," *IEEE Transactions on Wireless Communications*, vol. 11, no. 1, pp. 258–265, Jan. 2012. 5

[23] Z. Hadzi-Velkov, D. S. Michalopoulos, G. K. Karagiannidis, and R. Schober, "On the effect of outdated channel estimation in variable gain relaying: Error performance and PAPR," *IEEE Transactions on Wireless Communications*, vol. 12, no. 3, pp. 1084–1097, March 2013. 5

[24] S. H. Han and J. H. Lee, "An overview of peak-to-average power ratio reduction techniques for multicarrier transmission," *IEEE Wireless Communications Magazine*, vol. 12, no. 2, pp. 56–65, April 2005. 5, 12

[25] T. Jiang and Y. Wu, "An overview: Peak-to-average power ratio reduction techniques for ofdm signals," *IEEE Transactions on Broadcasting*, vol. 54, no. 2, pp. 257–268, June 2008. 5, 12

[26] T. Riihonen, S. Werner, F. Gregorio, R. Wichman, and J. Hamalainen, "BEP analysis of OFDM relay links with nonlinear power amplifiers," in *Wireless Communications and Networking Conference (WCNC), 2010 IEEE*, Apr. 2010. 6

[27] V. del Razo, T. Riihonen, F. Gregorio, S. Werner, and R. Wichman, "Nonlinear amplifier distortion in cooperative amplify-and-forward OFDM systems," in *Wireless Communications and Networking Conference, 2009. WCNC 2009. IEEE*, April 2009, pp. 1–5. 6

[28] C. Zhang, Y. Zhang, and Z. Gao, "Performances of amplify-and-forward based wireless relay networks with traveling-wave tube amplifiers," in *Wireless Communications Signal Processing (WCSP), 2013 International Conference on*, Oct 2013, pp. 1–5. 6

[29] C. Fernandes, D. da Costa, and A. de Almeida, "Performance analysis of cooperative amplify-and-forward orthogonal frequency division multiplexing systems with power amplifier non-linearity," *Communications, IET*, vol. 8, no. 18, pp. 3223–3233, 2014. 6

[30] K. Ishibashi, W.-Y. Shin, H. Ochiai, and V. Tarokh, "A peak power efficient cooperative diversity using star-QAM with coherent/noncoherent detection," *IEEE Transactions on Wireless Communications*, vol. 12, no. 5, pp. 2137–2147, May 2013. 6, 25

[31] Q. Yang and P. Ho, "Cooperative transmission with constant envelope modulations and phase-only forward relays," *IEEE Transactions on Wireless Communications*, vol. 10, no. 1, pp. 114–123, Jan. 2011. 6, 25, 72, 77, 78, 82, 85, 86, 94

[32] Z. Fang, J. Shi, and H. Shan, "Comparison of channel estimation schemes for MIMO two-way relaying systems," in *Cross Strait Quad-Regional Radio Science and Wireless Technology Conference (CSQRWC), 2011*, vol. 1, July 2011, pp. 719–722. 7, 35

[33] C. Chiong, Y. Rong, and Y. Xiang, "Channel estimation for two-way MIMO relay systems in frequency-selective fading environments," *IEEE Transactions on Wireless Communications*, vol. PP, no. 99, pp. 1–1, 2014. 7, 35

[34] J. Makhoul, "Linear prediction: A tutorial review," *Proceedings of the IEEE*, vol. 63, no. 4, pp. 561–580, April 1975. 10

[35] J. Cavers, "Amplifier linearization using a digital predistorter with fast adaptation and low memory requirements," *IEEE Transactions on Vehicular Technology*, vol. 39, no. 4, pp. 374–382, Nov. 1990. 11

[36] A. Saleh, "Frequency-independent and frequency-dependent nonlinear models of TWT amplifiers," *IEEE Transactions on Communications*, vol. 29, no. 11, pp. 1715–1720, Nov. 1981. 11

[37] A. Ghorbani and M. Sheikhan, "The effect of solid state power amplifiers (SSPAs) nonlinearities on MPSK and M-QAM signal transmission," in *Sixth International Conference on Digital Processing of Signals in Communications*, sep 1991, pp. 193 –197. 11

[38] C. Rapp, "Effects of hpa-nonlinearity on a 4-dpsk/ofdm-signal for a digital sound broadcasting signal," in *Proceedings of the Second European Conference on Satellite Communications*, oct 1991, pp. 179 – 184. 11

[39] E. Costa and S. Pupolin, "M-QAM-OFDM system performance in the presence of a nonlinear amplifier and phase noise," *IEEE Transactions on Communications*, vol. 50, no. 3, pp. 462–472, Mar 2002. 12, 20

[40] E. Al-Dalakta, A. Al-Dweik, A. Hazmi, C. Tsimenidis, and B. Sharif, "Efficient BER reduction technique for nonlinear OFDM transmission using distortion prediction," *IEEE Transactions on Vehicular Technology*, vol. 61, no. 5, pp. 2330–2336, Jun 2012. 12, 20

[41] H. Suzuki, T. V. A. Tran, I. Collings, G. Daniels, and M. Hedley, "Transmitter noise effect on the performance of a MIMO-OFDM hardware implementation achieving improved coverage," *Selected Areas in Communications, IEEE Journal on*, vol. 26, no. 6, pp. 867–876, August 2008. 12, 20

[42] J. Bussgang, "Cross correlation function of amplitude-distorted gaussian input signals," Technical report, Research Laboratory of Electronics, M.I.T., Cambridge, MA, Tech. Rep., Mar. 1952. 13

[43] D. Dardari, V. Tralli, and A. Vaccari, "A theoretical characterization of nonlinear distortion effects in OFDM systems," *IEEE Transactions on Communications*, vol. 48, no. 10, pp. 1755–1764, Oct 2000. 13

[44] A. Conti, D. Dardari, and V. Tralli, "An analytical framework for CDMA systems with a nonlinear amplifier and AWGN," *IEEE Transactions on Communications*, vol. 50, no. 7, pp. 1110–1120, Jul. 2002. 13

[45] J. G. Proakis, *Digital Communications*, 3rd ed. McGraw-Hill, 1995. 18

[46] M. Hasna and M.-S. Alouini, "Outage probability of multihop transmission over nakagami fading channels," *IEEE Communications Letters*, vol. 7, no. 5, pp. 216–218, May 2003. 27

[47] M. K. Simon and M.-S. Alouini, *Digital Communications over Fading Channels: A Unified Aproach to Performance Analysis*. John Wiley & Sons, 2000. 27, 39, 43, 48, 51, 57

[48] J. Salo, H. El-Sallabi, and P. Vainikainen, "The distribution of the product of independent Rayleigh random variables," *IEEE Transactions on Antennas and Propagation*, vol. 54, no. 2, pp. 639–643, Feb. 2006. 27, 38

[49] F. Yilmaz, O. Kucur, and M.-S. Alouini, "Exact capacity analysis of multihop transmission over amplify-and-forward relay fading channels," in *Personal Indoor and Mobile Radio Communications (PIMRC), 2010 IEEE 21st International Symposium on*, Sept 2010, pp. 2293–2298. 28

[50] M. Renzo, F. Graziosi, and F. Santucci, "A unified framework for performance analysis of CSI-assisted cooperative communications over fading channels," *IEEE Transactions on Communications*, vol. 57, no. 9, pp. 2551–2557, Sept. 2009. 28, 42

[51] P. Lahdekorpi, T. Isotalo, S. Khan, and J. Lempiainen, "Implementation aspects of RF repeaters in cellular networks," in *Personal Indoor and Mobile Radio Communications (PIMRC),*, Sept 2010, pp. 2511–2516. 34

[52] M. Patwary, P. Rapajic, and I. Oppermann, "Capacity and coverage increase with repeaters in UMTS urban cellular mobile communication environment," *IEEE Transactions on Communications*, vol. 53, no. 10, pp. 1620–1624, Oct 2005. 34

[53] K. Tsioumparakis, T. Doumi, and J. Gardiner, "Delay-spread considerations of same-frequency repeaters in wideband channels," *IEEE Transactions on Vehicular Technology*, vol. 46, no. 3, pp. 664–675, Aug 1997. 35

[54] Y. L. Luke, *The Special Functions and Their Approximations.* Academic Press, 1969, vol. 1. 38, 39, 52, 53

[55] I. Gradshteyn and I. Ryzhik, *Table of Integrals, Series, and Products*, 7th ed., A. Jeffery and D. Zwillinger, Eds. Academic Press, 2007. 40, 41, 42

[56] W. Guan and K. Liu, "Performance analysis of two-way relaying with non-coherent differential modulation," *IEEE Transactions on Wireless Communications*, vol. 10, no. 6, pp. 2004–2014, June 2011. 45, 53, 63

[57] S. Alabed, J. Paredes, and A. Gershman, "A simple distributed space-time coded strategy for two-way relay channels," *IEEE Transactions on Wireless Communications*, vol. 11, no. 4, pp. 1260–1265, April 2012. 45

[58] K. Zhu and A. Burr, "Two-way non-coherent physical-layer network coded differential distributed space-time block coding," in *Wireless Communications and Networking Conference (WCNC), 2013 IEEE*, April 2013, pp. 2416–2421. 45, 54

[59] T. Cui, F. Gao, and C. Tellambura, "Differential modulation for two-way wireless communications: a perspective of differential network coding at the physical layer," *IEEE Transactions on Communications*, vol. 57, no. 10, pp. 2977–2987, October 2009. 45, 63

[60] L. Song, G. Hong, B. Jiao, and M. Debbah, "Joint relay selection and analog network coding using differential modulation in two-way relay channels," *IEEE Transactions on Vehicular Technology*, vol. 59, no. 6, pp. 2932–2939, July 2010. 45, 53, 62

[61] Z. Fang, F. Liang, L. Li, and L. Jin, "Performance analysis and power allocation for two-way amplify-and-forward relaying with generalized differential modulation," *IEEE Transactions on Vehicular Technology*, vol. 63, no. 2, pp. 937–942, Feb 2014. 45, 46, 62, 68

[62] J. G. Proakis, *Digital Communications*, 4th ed. McGraw Hill, 2000. 51, 54, 73, 75

[63] A. P. andS. U. Pillai, *Probability, Random Variables and Stochastic Processes*, 4th ed. McGraw-Hill, 2002. 51

[64] J. Riordan, *An introduction to combinatorial analysis*, 1958. 59

[65] W. C. Jakes, Jr., Ed., *Microwave Mobile communications.* John Wiley & Sons, 1974. 63

[66] J. K. Cavers, *Mobile Channel Characteristics.* Kluwer Academic Publishers, 2002. 63

[67] R. Pawula, S. Rice, and J. Roberts, "Distribution of the phase angle between two vectors perturbed by gaussian noise," *IEEE Journal on Selected Areas in Communications*, vol. 30, no. 8, pp. 1828–1841, Aug 1982. 69

[68] R. Maw, P. Martin, and D. Taylor, "Cooperative relaying with CPFSK and distributed space-time trellis codes," *IEEE Communications Letters*, vol. 12, no. 5, pp. 356–358, May 2008. 72

[69] M. Valenti, D. Torrieri, and T. Ferrett, "Noncoherent physical-layer network coding using binary CPFSK modulation," in *Military Communications Conference, 2009. MILCOM 2009. IEEE*, Oct 2009, pp. 1–7. 72

[70] T. A. J. B. Anderson and C.-E. W. Sundberg, *Digital Phase Modulation.* New York: Plenum, 1986. 73

[71] A. V. Oppenheim and R. W. Schafer, *Discrete-Time Signal Processing*, 2nd ed. Prentice Hall, 1998. 80

[72] J. Max, "Envelope fluctuations in the output of a bandpass limiter," *IEEE Transactions on Communications*, vol. 18, no. 5, pp. 597–605, October 1970. 81

[73] R. Vaughan, N. Scott, and D. White, "The theory of bandpass sampling," *IEEE Transactions on Signal Processing*, vol. 39, no. 9, pp. 1973–1984, Sep 1991. 81

[74] S. Elnoubi, "Analysis of gmsk with discriminator detection in mobile radio channels," *IEEE Transactions on Vehicular Technology*, vol. 35, no. 2, pp. 71–76, May 1986. 85, 94

Appendix A

Simulation Parameters

Both of the MF and PF relays are simulation studied for the various modulations employed in this thesis. The purpose of simulation study is twofold. First, simulations are used to verify the analyses of the proposed relays, especially the BER performance. Secondly, when analytical results are not available, e.g. the BER performance of AF and MF under NLPA in Section 2.2.3 and 2.3.3, simulation is the only viable way to evaluate the system performance. In the following, important simulation parameters are summarized.

The number of trials is the number of transmitted symbols from a user node during the simulation for a given set of channel conditions and system configurations. The number of trials for each BER point simulated is at least 10^7. This is to ensure accurate modeling of the wireless channels as well as to collect enough error counts for reliable BER results. Furthermore, if the BER is expected to be small, on the order of 10^{-7}, then the number of trials is increased to at least 10 times the inverse of the BER order so that sufficient error counts are collected. For example, when the BER is expected to be 1×10^{-7}, then the number of trials is at least 10^8.

Two levels of simulations are performed — symbol level and waveform level. The symbol level simulation is conducted when the communication system can be represented by a discrete model, which typically corresponds to MF and PF relays with LPA in Chapter 2 and 3. However, when NLPA is employed in a MF or PF relay employing PSK or DPSK modulation, the non-linearity effect acts on the waveforms of the relay transmitted signals, and the symbol level discrete time model is no longer valid. In this case, waveform simulation

is needed to simulate the performance of the system. The SQRC pulse with unit energy and a roll-off factor of 0.5 is adopted and 8 samples per symbol is used to approximate the received waveform at the relay. Another application of waveform simulation is the CPFSK PF relay, because the CPFSK signals must be band limited to its 99% power bandwidth and the limiter discriminator extracts phase derivative by differentiating the continuous time signal. Further, to avoid aliasing, an oversampling factor of 16 is used when simulating the CPFSK waveforms.